Framework for Connected and Automated Bus Rapid Transit with Sectionalized Speed Guidance based on Deep Reinforcement Learning: Field Test in Sejong City

Seongjin Choi[a,*], Donghoun Lee[b,*], Sari Kim[c] and Sehyun Tak[b,**]

[a]Department of Civil Engineering, McGill University, 817 Sherbrooke Street West, Montreal, Quebec H3A 0C3, Canada
[b]Center for Connected and Automated Driving Research, The Korea Transport Institute, Sejong 30147, Korea
[c]R&D Division, NZERO, 126, Beolmal-ro, Dongan-gu, Anyang-si, Gyeonggi-do, 14057, Republic of Korea

ARTICLE INFO

Keywords:
Cooperative Intelligent Transportation System
Connected and Automated Vehicles
Bus Rapid Transit Speed Guidance
Deep Reinforcement Learning

ABSTRACT

Nowadays, Automated Vehicle (AV) technology is gaining attention as a candidate to improve the efficiency of Bus Rapid Transit (BRT) systems. However, there are still some challenges in AV technology including limited perception range and lack of cooperation capability in mixed traffic situations with drivers. The emerging Connected and Automated Vehicles (CAVs) and Cooperative Intelligent Transportation System (C-ITS) offer an unprecedented opportunity to solve such challenges. As a result, this study presents a framework for Connected and Automated BRT (CA-BRT), including a cloud-based architecture and a deep reinforcement learning system for Sectionalized Speed Guidance (SSG) system designed for CAVs.The proposed framework is field-tested in Sejong City in South Korea, where there are various road environments such as bus stops, overpasses, underground tunnels, intersections, and crosswalks. The driving performance of the proposed system is compared with different types of control scenarios, and the results from the field tests show that the proposed system improves the driving performance of the AVs in various aspects including driving safety, ride comfort, and energy efficiency with downstream information obtained from road infrastructures.

1. Introduction

Bus Rapid Transit (BRT) is defined as a "rapid mode of transportation that can combine the quality of rail transit and the flexibility of buses" (Thomas, 2001). This is achieved by providing a dedicated busways and iconic stations typically located at the center of the road (Basso et al., 2019). Since BRT contains features similar to Light-Rail Transit (LRT) and metro system, it is more reliable than conventional bus system, while requiring less investments for installation compared to LRT and metro system. This is why BRT systems have gained such popularity worldwide (Cervero, 2013).

Nowadays, Automated Vehicle (AV) technology is gaining attention as a candidate to improve the efficiency of BRT systems. An automated vehicle is defined as a vehicle that can drive without human intervention by using multiple subsystems installed in vehicle. AVs use perception sensors to detect objects and classify the detected objects, and internal computation resources to identify navigation paths based on collected data while obeying the relevant rules of the road (Campbell et al., 2010; Azad et al., 2019). In the last two decades, the AV technology has advanced at a breakneck pace, increasing concerns among researchers and professionals in related sectors about how AVs will influence and alter the future transportation system. Despite the fact that this technique has been proven in field tests, AV technology still has some challenges to be resolved: First, the limited perception range of in-vehicle sensors to identify various objects located at blind spots; and second, the lack of cooperation capability with other vehicles and infrastructure (Hobert et al., 2015). Such challenges are prevalent, especially when deploying actual system in real-world transportation system.

*Co-first authors: Dr. Seongjin Choi and Dr. Donghoun Lee contributed equally to this paper.
**Corresponding author
Email addresses: seongjin.choi@mcgill.ca (S. Choi); donghoun.lee@outlook.com (D. Lee); rizzysarizzy@gmail.com (S. Kim); sehyun.tak@outlook.com (S. Tak)
ORCID(s): 0000-0001-7140-537X (S. Choi); 0000-0002-3349-636X (D. Lee); 0000-0001-6804-3769 (S. Kim); 0000-0001-7140-537X (S. Tak)

The emerging technology based on V2X communication such as Connected Vehicle (CV) and cooperative intelligent transportation system (C-ITS) offer an unprecedented opportunity for AVs (Tak and Choi, 2022). These technologies allow the buses (vehicles) to have both cooperative perception and driving. Cooperative perception means that the ego vehicle can access to the data shared by other surrounding vehicles and by roadside infrastructures and cooperative driving means that the ego vehicle controls the longitudinal and lateral movements by integrating the data from both in-vehicle sensors, surrounding vehicles, and roadside infrastructure. This enables the ego vehicle to react to objects at the blind spot, which cannot be detected by in-vehicle sensors. Also, the computing load of the automated driving system can be reduced by using the processed data at edge device installed in road side and cloud. (Liu et al., 2019). Especially for BRT system, Connected Vehicle (CV) and C-ITS technologies have great potential to improve driving efficiency and safety. Acceptable range of acceleration of bus is more narrow compared to passenger vehicles for passenger comfort and safety. In this circumstance, Buses can reduce the hard acceleration and severe deceleration by responding to downstream traffic situation in advance with information from CV and C-ITS technologies. In addition, the importance of utilization of CV and C-ITS technologies increases even more when considering difficult control of heavy duty vehicles like buses and trucks due to large inertia, low power-to-weight ratio, and large uncertainties in vehicle parameters (Misener and Shladover, 2006).

Notwithstanding usefulness of the information from CV and C-ITS, only few studies proposed BRT system under V2X communication-based technology such as CAVs and C-ITS (Azad et al., 2019; Mudge et al., 2020), but most studies have focused mainly on the technology on a single bus without considering cooperation between vehicle and infrastructure. In some existing researches, BRT system utilizes the information from V2X communication to minimize acceleration and braking of the ego vehicle for high fuel efficiency. In other words, these approaches minimize stop-and-go driving patterns of the ego vehicle and replace it with slow-an-go driving patterns, since slow-and-go driving pattern shows much better fuel (energy) efficiency than stop-and-go driving patterns (Seredynski et al., 2013b). One of the common approaches proposed in the previous studies is to use Transit Signal Priority (TSP) — controlling traffic signal to give the priority of passing intersections to buses in BRT system. Such approach provides the buses with preferential treatment by adjusting the traffic signal temporarily, and offers the priority-related information to the buses through V2X communication or LTE communication (Seredynski et al., 2019). Although the TSP improves the overall efficiency (Dion et al., 2004), the inefficiency of other vehicles having lower priority is inevitable (Dion et al., 2005; Sunkari et al., 1995). An alternative way is to provide guided speed, or advisory speed, for the buses in BRT system. The idea is to use various information on the road such as traffic situation, traffic signal, and obstacles to provide the optimal speed profile to the buses for safe and efficient driving. Ideally, the ego vehicle can be informed of an optimal speed in advance to pass through the signalized intersection when the traffic light is green.

The speed guidance system, which provides the guided speed to ego vehicle has huge potential for safe and efficient operation of connected and automated bus-based BRT system because it can minimize the negative impact on other vehicles. However, as the information from infrastructures and vehicles diversify and the amount of data increases, the complexity of model for speed guidance system also increases. Especially, the use of V2X communication accelerates these increasing trend of data and it leads to the increases in computing time and load for the calculation of guided speed. To efficiently and speedily process the data, methods for data handling have been proposed in terms of system framework and algorithm.

In terms of algorithm, deep learning model is used because it can rapidly produce the output that requires a highly complex calculation process from various input sources. The majority of previous research on deep learning-based approaches have used traffic simulation models to investigate the benefits of their own systems. However, traffic simulation models use a lot of simplified assumptions, which might lead to unrealistic driving behavior. Also, the simulations do not account for realistic time delays or V2X communication architecture between the server infrastructure and the ego vehicle, and the speed of the ego vehicle is precisely matched with the guided speed provided by the system without any mechanical issues. As a result, it is necessary to field-test the system to properly validate the the deep learning-based approach.

In terms of system framework, cloud architecture along with edge computing is considered as an alternative. The cloud computing can process the large amounts of data collected from various devices by using distributed computing and highly scalable computing resources. However, when it comes to deploying actual system on real-world transportation system, designing and establishing such a cloud-based framework in V2X communication environment for speed guidance system is very challenging. Only a few studies presented C-ITS architecture (Lu et al., 2018a,b; Sjoberg et al., 2017), and there still remains a big research gap, particularly for public transportation system like BRT.

As a results, the main objective of this research is to propose a framework to assist the management services for public transportation system, especially for connected and automated vehicle-based BRT system. Such framework should offer supports for different types of services, such as handling V2X communication efficiently, providing mechanisms for the storage of information and data collected from various sensors, and computation resources to reduce the automated driving workloads. Consequently, this paper proposes a cloud-based architecture to handle such supports for various services.

To summarize, this study proposes a Cooperative Intelligent Transportation System (C-ITS) framework for Connected and Automated Bus Rapid Transit (CA-BRT). There are mainly three contributions as follows:

- This paper proposes a framework, which specifies what is the role of each system, how V2X and LTE communication is used for cooperative perception of vehicle and infrastructure, and how the collected data is used to control the buses in BRT system.
- This paper develops a cloud-based architecture to handle different types of tasks to be done by the Traffic Management Center (TMC) in C-ITS. The proposed architecture also includes detailed specifications on how cloud services are used for efficient message passing, data processing, and computing.
- This paper proposes a new speed guidance system based on deep reinforcement learning. This system considers driving safety and ride comfort as well as energy efficiency, to provide optimal guided speed for the buses.

The proposed system is field-tested in Sejong, South Korea, and we present a comparison analysis among various control scenarios including human-driven case, default automated driving, and two types of speed guidance system.

This paper is organized as follows. Section 2 presents literature reviews on related previous works. Section 3 provides detailed explanation on proposed C-ITS framework, including cloud-based architecture, and Sectionalized Speed Guidance System based on Deep Reinforcement Learning. Then, several comparative studies are to be conducted with respect to driving safety, ride comfort and energy efficiency based on the results obtained from the real-world experiments in Section 4. Section 5 further discusses the results and analyses in terms of spatial characteristics. Finally, Section 6 describes the conclusions and directions for future studies.

2. Literature Review

There have been enormous efforts to develop a novel control strategy for improving the efficiency of transit performance and Level Of Service (LOS) in urban areas, particularly in signalized intersections. One of the most commonly used approaches in the field of C-ITS is to adjust vehicle's speed by utilizing an optimal speed trajectory (or profile) based on upcoming traffic signal information via I2V communication. The subject vehicle can be informed of an optimal speed in advance to pass through the signalized intersection when the traffic light is green. Such application is called Optimal Speed Advisory (OSA), also known as Green Light Optimal Speed Advisory (GLOSA), which has often been used for reducing fuel consumption and average stop time behind a signalized intersection.

A previous study proposed the use of upcoming traffic signal information to be incorporated into a modified adaptive cruise control (Asadi and Vahidi, 2010), which considered a Model Predictive Control (MPC) framework to seek the optimal speed that can reduce the use of brakes and idling time at the signalized intersection. Although they assumed successful transmission of the C-ITS messages without any discussions regarding the communication mechanism, their approach was of great inspiration to the establishment of the GLOSA-related researches. Katsaros et al. (2011) was the first one to propose the GLOSA application based on a C-ITS message, such as Cooperative Awareness Message (CAM). The proposed GLOSA system determined the optimal speed using a single-segment approach that considers the information of single traffic signal ahead. Seredynski et al. (2013a) and Seredynski et al. (2013b) improved the previous single-segment approach by considering a concept of multi-segment GLOSA system based on the information of multiple signals in a sequence of vehicle's route. Both of them determined the set of optimal speeds in each segment by using Genetic Algorithm (GA)-based optimization. Another method using the GA-based optimization was also developed in Luo et al. (2017), which considered a multi-segment GLOSA system applied to hybrid electric vehicles. Similarly, Simchon and Rabinovici (2020) developed a dynamic GLOSA algorithm for electric vehicle based on a smoother relaxation procedure for the non-convex optimization problem associated with the discontinuity of traffic signals.

However, even though the previous approaches showed a considerable improvement in terms of operational efficiency, the optimal solutions from the previous GLOSA algorithms were hardly close to global optimum since they did not take into account downstream traffic conditions. Eckhoff et al. (2013) raised the question of whether the GLOSA system would be effective given a dense downstream traffic condition. Based on an assumption that the traffic signal information can be shared within a range of communication distance using C-ITS message such as Signal Phase and Timing (SPaT), they revealed that the GLOSA system was no longer beneficial in a dense traffic condition, which affects the vehicles each other. Therefore, it often makes the ego vehicles less able to follow their own optimal speed trajectories.

Unlike the previous researches that have not considered the impact of queue at signalized intersection, He et al. (2015) have incorporated the information on queue formation and dissipation status into their analytical model in order to determine the optimal speed profile on signalized arterial. Likewise, there have been various researches to propose a more advanced OSA or GLOSA model by considering the information on multiple downstream traffic signals and downstream traffic states. Wu et al. (2015) developed an analytical model to find a time-dependent optimal speed trajectory for electric vehicle in a given travel route by considering the effect of intersection queues every segment. Sun et al. (2018) and Sun et al. (2020) proposed an eco-driving control strategy to traverse multiple signalized intersections using a Dynamic Programming (DP)-based approach under the information uncertainty associated with the SPaT message or intersection queue. The performances of their proposed control strategies were verified by comparing it with a modified Intelligent Driver Model (IDM). Zeng and Wang (2018) also considered a DP-based fuel-efficient algorithm for finding an optimal speed trajectory along a given route based on a key idea that converts distance-related constraints, including speed limits and traffic signal locations, to input constraints and time-domain states such as traffic signal timing. Xin et al. (2018) imposed an speed reduction method based on a predictive IDM, which considered both an estimated time of downstream queue discharge at the signalized intersections and upcoming traffic signal information from the SPaT message. Another eco-driving strategy considering both vehicle queue information and SPaT message was proposed by Yang et al. (2020), which evaluated the performance of their algorithm in a network scale based on the Van Aerde's car-following model-based INTEGRATION traffic simulator (Rakha et al., 2010; Rakha and Van Aerde, 2015). Similar to this approach, Tang et al. (2018) incorporated a speed control strategy into a car-following model based on the Full Velocity Difference (FVD) model (Jiang et al., 2001).

Most of the previous studies have conducted to explore the benefits of their own systems primarily based on traffic simulation models, such as IDM, Van Aerde and FVD model. However, since numerous simplified assumptions are involved in the traffic simulation models, it may often result in unrealistic driving behaviors. For instance, even though the simulations simplified the time delay or latency of transmitting the information on the advisory speed, vehicles' speeds were exactly following the guided speed provided by the OSA or GLOSA system without any time-lags. Therefore, field testing is further required to validate the performance of the proposed system on real roads.

There have been a few studies to conduct a field test for assessing the optimal speed control strategy according to the proposed system. Xia et al. (2012) conducted a field operational test at a closed test intersection to demonstrate the effectiveness of their proposed eco-driving application utilizing the SPaT and MAP messages based on a LTE/4G network link using a cloud-based server, such as Amazon Web Services (AWS). Chen et al. (2016) dealt with the implementation issues related to the field application of Eco-Speed Control (ESC) system, which was designed to minimize the fuel consumption by providing a fuel-efficient speed trajectory using the information on surrounding vehicles and downstream traffic signal timing (Rakha et al., 2012). Almannaa et al. (2017) extended the previous study to verify the efficiency of the OSA by an extensive controlled-field testing. Later, Almannaa et al. (2019) proposed an Eco-Cooperative Adaptive Cruise Control (Eco-CACC) by incorporating the OSA algorithm into a CACC system. Their experimental results revealed that more significant improvements in saving fuel and travel time was observed in the case of automated Eco-CACC compared to manual driving without any OSAs and manual Eco-CACC. Unlike the previous studies that performed a controlled field experiment, Zhang et al. (2020) conducted real-world experiments using a electric passenger vehicle to evaluate the performance of their proposed GLOSA system that considered a queue length estimation as well as driver's tracking error between actual output speed and desired speed given by the OSA. However, since the speed trajectories given by the OSAs still have a negative effect of other following vehicles on maintaining their speeds, it may result in additional fuel consumption and delay. Consequently, the GLOSA system is more appropriate for dedicated lane-based BRT system, which requires a sufficiently large headway, rather than passenger vehicle.

Despite the benefits of imposing the GLOSA system, only a few studies have considered the GLOSA system to be applied to a transit bus. Seredynski et al. (2014) took into account into a transit bus-based GLOSA system, which considered dwell times at each bus station. Seredynski et al. (2019) improved the previous study by developing an integrated system that combined the GLOSA with TSP. Their simulation-based analyses showed that the GLOSA used alone had marginal impact on travel times compared to the integrated system. In contrast with the previous studies, Chen and Rakha (2022) conducted a controlled field test to verify the benefit of GLOSA system for buses (B-GLOSA), which was able to provide a smoother trajectories through signalized intersections, thus saving fuel and travel time. However, none of these previous studies have yet considered a real-world experiment to explore the effect of the GLOSA system on the transit bus. In addition, even though the benefits of automated function for following the optimal speed has been revealed, incorporating the GLOSA system into an Automated Driving System (ADS) have not yet been fully considered in the BRT system. Moreover, since most of the existing optimization algorithms used in the OSA or GLOSA system have used the MPC, GA or discrete DP approaches based solely on longitudinal kinematic models, it may not be appropriate for being used in the automated transit bus due to its driving automation capability. For instance, unlike the human-driven vehicle, the automated vehicle may be not able to follow a guided speed provided by the existing OSA system in driving conditions with instantaneous changes in road curvature, where its maximum allowable speed is lower than the guided speed due to the safety assurance of ADS. Nevertheless, since the existing studies on the OSA and GLOSA system have mainly focused on the human-driven vehicles to enhance their system performances in terms of fuel or energy efficiency, it is needed to further consider other system performances, such as driving safety and ride comfort, when incorporating the OSA or GLOSA system into the automated transit bus.

All the automated vehicles are required to specify a functional system boundary for their own ADSs. It is known as Operational Design Domain (ODD), which is one of the most crucial factors to capture the ADS's operational limitations on driving environments, such as location-dependent characteristics, weather conditions, the availability and placement of traffic management devices and operational surfacing (Koopman and Fratrik, 2019). A limited ODD often affects the maximum allowable speed for the automated vehicle. Therefore, the upper bound of the guided speed given by the OSA system is likely to be limited to operational or tactical constraints because the automated transit bus should be safely operated to perform a given Dynamic Driving Task (DDT). However, most of the previous OSA and GlOSA systems have considered that there were no any ODD constraints in vehicle speed control to follow the guided speed. Consequently, they are still necessary to further consider the ODD constraints when determining the guided speed for the automated transit bus.

Even though there have been considerable progress in forming a common understanding towards the ODD, such as SAE J3016, BSI PAS 1883 and ISO 34503, most of the existing approaches in defining the ODD for the ADS have still specified its functional boundary based on a combination of system requirements predetermined by their own ADSs (Thorn et al., 2018). As a result, they have mainly focused on identifying a geo-fenced area by determining whether the ADSs are operating within or outside of those pre-defined ODDs (Fraade-Blanar et al., 2018; Fruehling et al., 2019; Kim et al., 2020a). However, the ADS failure may be often observed from inconceivable events even in the geo-fenced area since the conventional methods of specifying the ODD are designed based solely on the known knowns (Sun et al., 2021). Therefore, it needs to further consider the dynamic changes in the driving environments by incorporating the risk of ADS operation into the identification of ODD (Lee et al., 2020).

In addition, since the ODD is defined by various elements with pre-specified driving conditions, it is critical for the ADS to monitor the current driving conditions. However, there has been still lack of considerations for a framework of Connected and Automated Bus Rapid Transit (CA-BRT) system to monitor and assess the current driving environment in real-time. Moreover, a more advanced algorithm is also required for providing the optimal guided speed by rapidly processing massive amounts of information associated with the CA-BRT system due to a variety of elements involved in the ODD. With these backgrounds, recent advances in the field of Deep Reinforcement Learning (DRL) have been made on combining the optimal speed control with the automated driving system (Sallab et al., 2017; Buechel and Knoll, 2018; Kim et al., 2020b; Du et al., 2022). Nonetheless, their simulation-based evaluation studies are of doubtful validity in the context of real-world application because they have not yet fully considered the applicability of the proposed systems in a real-world driving environment. Furthermore, in order to conduct a performance analysis in a real-world experiment, it is still necessary to consider an integrated C-ITS framework to deploy the DRL-based speed guidance system for the CA-BRT service.

Over the past two decades, a variety of C-ITS systems under V2X communication environments have been developed and deployed by numerous research projects in Europe and USA, such as CVIS, SAFESPOT, DRIVE C2X, Compass 4D, Eco-AT, SCOOP@F, C-ITS Corridor, Safety Pilot Model Deployment (SPMD), Connected Vehicle Pilot Deployment Program, Smart City Challenge and Ohio Smart Corridor. However, since the message sets used in the previous C-ITS systems have mostly been prepared for the advent of connected vehicles in the first deployment phases, they cannot be directly utilized for the automated vehicles (Naranjo et al., 2020), particularly when dealing with real-time processing for massive traffic data. Furthermore, although the existing systems have covered a wide range of C-ITS services, they still have limitations on an integrated use of resources associated with an automated BRT service due to the absence of an integration architecture for the legacy ITS/C-ITS and next-generation system. Consequently, an integrated system architecture is needed for the CA-BRT system to collect, process and provide a comprehensive traffic information. Therefore, this study aims to develop a novel C-ITS framework for the CA-BRT system to uprate driving safety, ride comfort and energy efficiency, which enables to use a DRL-based speed guidance system. The following section describes more explanations on the proposed framework in detail.

3. Methodology

The main focus of this paper is to propose an advanced integrated C-ITS framework for the CA-BRT system introduced in Section 3.1. The proposed framework also contains C-ITS message sets for V2X communication (see Appendix A for more details) as well as a cloud-based architecture to deal with extensive traffic data and C-ITS messages collected from various sources (see Section 3.2 for more details). By utilizing the proposed C-ITS framework, we develop a novel DRL-based speed guidance system, which is called *Sectionalized Speed Guidance (SSG)* system (see Section 3.3 for details). It provides a guided speed for each section for optimal driving of connected and automated bus by further considering driving risks given ODD constraints. Finally, the proposed system is field-tested in Sejong, South Korea, and Section 3.4 shows the details of the field tests including detailed description on the testing site and comparison models.

3.1. C-ITS Framework for Connected and Automated Bus Rapid Transit with Sectionalized Speed Guidance

Figure 1 shows the C-ITS framework for CA-BRT with SSG. The proposed system framework consist of four main sub-systems: (i) Road Monitoring System, (ii) Traffic Management Center System, (iii) Communication System, and (iv) Connected and Automated Bus System.

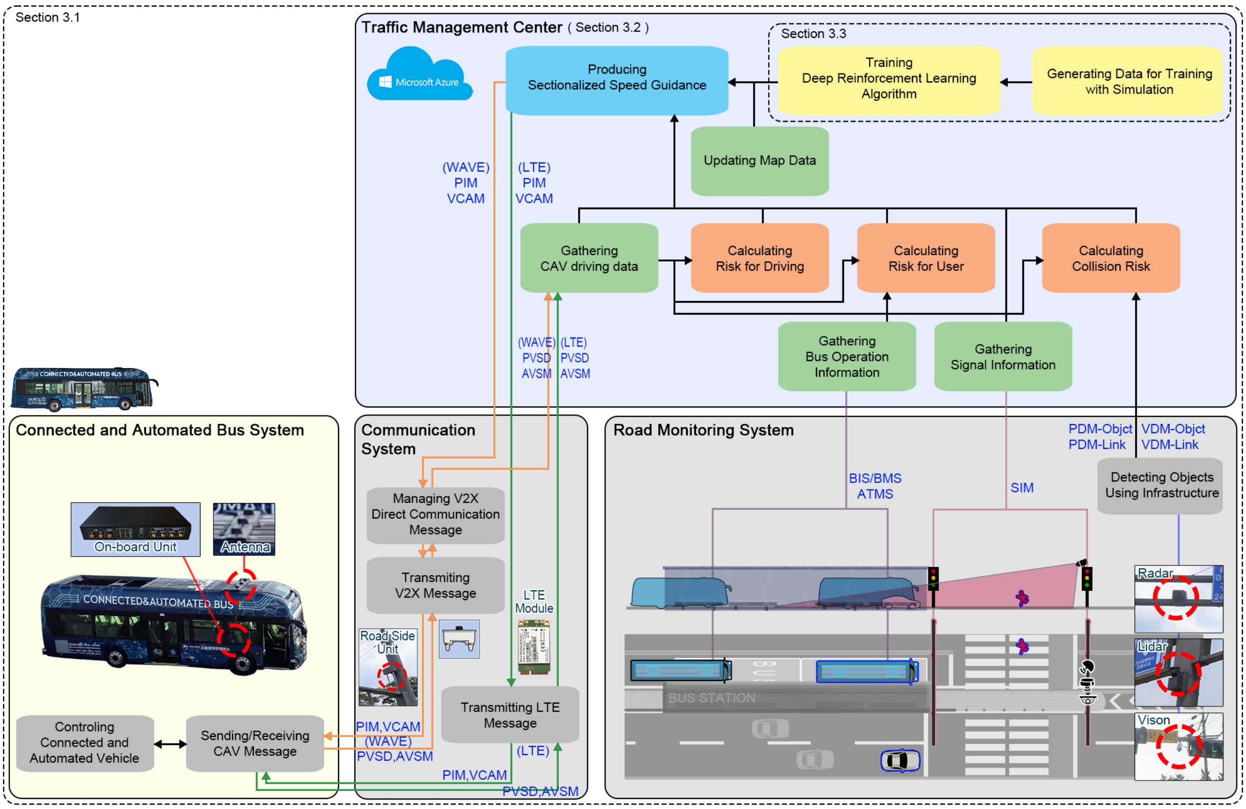

Figure 1: C-ITS Framework for Connected and Automated Bus Rapid Transit with Sectionalized Speed Guidance

The Road Monitoring System serves the function of detecting various objects on the road such as vehicles, motorcycles, bicycles, and pedestrians. The sensors include radar, lidar, and vision sensors, as shown in the bottom right of Figure 1. The sensors and edge processors, which are installed on the roadsides, predict the location of various objects by detecting the objects on the roads with deep learning (Tak et al., 2021). The prediction process is implemented at every 0.1 seconds with 3 seconds prediction horizon. The prediction horizon is set by considering the delay incurred in collecting, processing, and transmitting data. Subsequently, the detection and prediction information is matched to lane-level road links which are defined in High-Definition Map (HDMap) of a study site. Data defined in HDMap format enhances the information compatibility between CAV, road infrastructure, and traffic management center.

The information from the sensors and edge devices are converted into two messages: Pedestrian Detection Message (PDM) and Vehicle Detection Message (VDM). The PDM contains information on the detected and predicted pedestrians such as location, speed, and number of pedestrians. The VDM contains information on the detected and predicted vehicles near intersection and bus station such as trajectory, speed, and density. Then, these messages are sent to the Traffic Management Center (TMC) at 0.1-second intervals. (Refer to Appendix A.1 and Appendix A.2 for more information about the messages). The Road Monitoring System also collects signal information from the signal control devices installed on roads and converts it to Signal Information Message (SIM) message to transmit the signal information to TMC at every 0.1 seconds. The SIM format is basically based on the SAE J2735 and combined to the HDMap format to improve the interoperability of other messages such as PDM and VDM (SAE J2735).

The Traffic Management Center (TMC) generates a optimal guided speed for each road section based on information of traffic situation collected from the Road Monitoring System and vehicle information collected from CAV through the communication System. In this study, we implemented a Cloud-based TMC using Microsoft Azure, and detailed explanations on the architecture, data flows and algorithm are presented in Section 3.2. The operation of the TMC progresses through four main modules: (i) data gathering, (ii) risk calculation, (iii) deep reinforcement learning, and (iv) sectionlized speed guidance production, which corresponds to boxes colored in (i) green, (ii) orange, (iii) yellow, and (iv) blue in the top right of Figure 1, respectively. In the data gathering module, three types of data are collected. The first type is the driving and detection data of the CAV. This data includes the information detected by the in-vehicle sensors, the information on surrounding vehicles, the sensor status information and information about the vehicle dynamics, such as the acceleration, speed, and steering of the ego vehicle. These information are represented in two message types: Probe Vehicle Safety Data (PVSD) and Automated vehicle Safety Message (AVSM). Detailed information on these message types are specified in Appendix A.3 and Appendix A.4, respectively. The second type is the data obtained from the existing legacy intelligent transportation systems (ITSs), such as the Bus Information System (BIS), Bus Management System (BMS), and Advanced Traffic Management System (ATMS). This includes information on the buses on bus location, bus-stop congestion, and traffic volume. The information from the existing legacy ITS is used to improve the driving efficiency of CAV in response to various traffic conditions in the downstream site. Especially, the TMC can take advantage of using the existing legacy ITS without incurring a large additional cost of installation through the cloud server (Tak et al., 2016b). The third type is PDM and VDM collected from the Road Monitoring system. The PDM consists of *PDM-objects* containing location of detected objects, and *PDM-links* which is a lane-level aggregated version of PDM-objects. Similarly, the VDM consists of *VDM-object* containing information on detected vehicles including location and speed, and *VDM-link* which is a lane-level aggregated version of VDM-object. In this study, the PDM-link and VDM-link data are mainly used, which can be easily matched to the route of the ego vehicle.

In the risk calculation module, various types of data collected from the vehicle and the Road Monitoring System are combined to calculate three types of risks: (i) driving risk, (ii) user risk, and (iii) collision risk. First, the driving risk is calculated according to the driving stability of each road section with data collected from the in-vehicle sensors of AV. Then, the calculated driving risk is used as a base data in calculating the optimal guided speed, which serves to minimize the driving risk arising from the limited driving ability of AV. For example, a road section with a speed limit of 50 km/h, where the ODD confirms the feasibility of driving, may contain a section where a large longitudinal acceleration occurs. In this case, the safety performance of the ego vehicle can be increased by providing a guided speed of 40 km/h. Second, the user risk is the passenger-centric factors influencing the comfort and safety. It arises from the abrupt movement of CAV such as severe lateral deceleration and hard acceleration near the bus station and intersection, which is calculated based on the data collected from the legacy ITS. Lastly, the collision risk with nearby pedestrians and vehicles at the intersection is calculated based on the object detection data from Road Monitoring System. Particularly, jaywalking pedestrians and vehicles at blind spot of CAV are hard to detect by only using in-vehicle sensors. Therefore, the collision risk is calculated continuously based on the PDM and VDM, which contains both current and predicted locations of each object.

In the deep reinforcement learning module of the TMC, it trains the deep reinforcement learning algorithm with simulation data in various scenarios. The main role of this model is to generate various training scenarios using collected data from CAV and Road Monitoring System. With this process, the proposed speed guidance system can improve the ability to respond to various situations on the road in terms of energy efficiency and safety. For example, when a vehicle approaches a signalized intersection, the acceleration behavior is minimized if the red light is expected at the intersection, and the speed is reduced to an appropriate range if the green light is expected so that the vehicle can pass through the intersection without stopping. Detailed information of this process is provided in Section 3.3

In the sectionalized speed guidance production module, a set of optimal guided speeds for each road section is generated by integrating data from risk calculation module and deep reinforcement learning module. The generated guided speed at each road section serves as an upper bound of longitudinal speed at the corresponding road section. This module is designed to improve the overall performance of CAV, such as driving safety, ride comfort and energy efficiency, by providing the optimal advisory speed for each road section. The CAV updates its maximum speed of each road section according to the guided speed, and drives with the guided speed until dangerous situation is detected by in-vehicle sensors. When generating the optimal guided speed for each road section, driving safety related aspects are given the highest priority and other aspects, such as ride comfort and energy efficiency, are considered within the condition that the safety aspect is satisfied. On the other hand, if any dangerous situation is detected only considering the information from in-vehicle sensors, the CAV reduces its speed that is less than guided speed, to ensure its driving safety. With redundant speed control strategy, it copes with unexpected error and failure of road infrastructure, vehicle system, and traffic management center. Detailed information of this process is provided in Section 3.2.

The Communication System serves the function of transferring information related to the guided speed for each road section from the Traffic Management Center to CAV and transferring information of CAV such as location, speed, and sensor status to traffic management center. The Communication System consist of two parts: (i) V2X direct communication and (ii) LTE communication. For the V2X direct communication, WAVE communication is used and the emergent information is handled through the V2X direct communication. For this purpose, five Road Side Units (RSUs) capable of WAVE communication are installed, and are located mainly around the intersection to prepare for urgent situations in which the signal control is constantly changing. Beyond the WAVE communication area, the necessary information is transmitted to the CAV using LTE communication. As shown in the bottom center of Figure 1, with these two types of communication method, Path Indentification Message (PIM) and Vechile Control Advisory Message (VCAM) are sent to the CAV from the Traffic Management Center. The PIM is a message containing the route of CAV from the start to end of its operation, which is defined as a link sequence in units of lanes with the HDMap format. The PIM is mainly transferred through the LTE communication by considering the data volume and transmission time. The VCAM contains information on the guided speed trajectories for road sections, which are defined in the PIM. Basically, the VCAM provides the guided speed to CAV only for links used in PIM because proving guided speed for all road links that CAV can may drive is inefficient due to computation time and communication burden(Refer to Appendix A.5 and Appendix A.6 for more information about the messages). In addition, it can flexibly react to changes in route while driving according to the user requests and different routes for each CAV. The VCAMs are sent to the vehicles every second with both V2X direct communication and LTE communication. However, considering that the communication delay of LTE is greater than that of WAVE, the system attempts to mainly use information from the V2X communication, particularly in urgent situations such as near intersections and crosswalks.

The Connected and Automated Bus System controls vehicle dynamics based on the guided speeds received from Traffic Management Center through the Communication System. Figure 2 shows the CAV that is used in this study and its sensor configuration. Lidar, radar and camera sensors are used to detect the vehicle's surrounding environment such as vehicles, obstacles, pedestrians, and road infrastructure, as shown in the figure. To ensure robust cognitive performance, the front and rear object detection are combined with the radar and lidar sensors. Especially, the camera sensors are used to identify the left and right lanes and the type of the object in front. Information about the surrounding vehicles and road environment are collected through the lidar sensor. As shown in Figure 2 (b), the information collected from the sensors are processed through the Robot Operating System (ROS) installed in the vehicle. In addition, the WAVE and LTE communication data collected through the On-Board Unit (OBU) are also sent to the ROS after preprocessing such as changing their formats and merging data from the WAVE and LTE communication.

The Connected and Automated Bus System controls the longitudinal and lateral movement of the subject vehicle by considering conditions of CAV with various information including in-vehicle sensor data, driving state data, and the communication data. In-vehicle system for automated driving involved in the Connected and Automated Bus

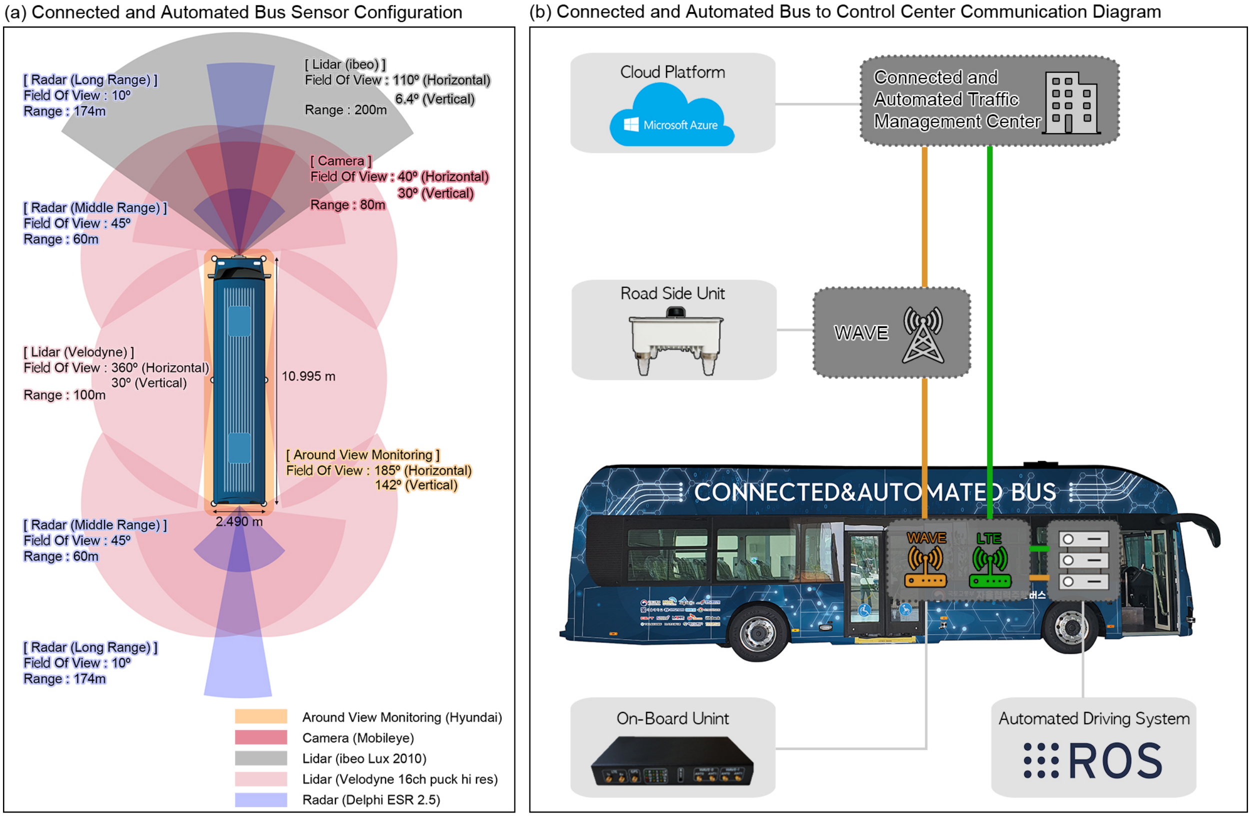

Figure 2: Connected and Automated Bus (a) Sensor Configuration and (b) Communication Diagram

System consists of localization, perception, motion planning and motion control module. The motion control module is composed of lateral and longitudinal controller. The lateral controller is designed to track a desired yaw rate with delay based on a simple second-order model for system dynamics, which formulates the tracking error and sliding surface using Lyapunov function. For more details on the lateral controller, the readers can refer to Jo (2022).

On the other hand, the longitudinal controller is composed of upper-level and lower-level controller. The upper-level controller adopts a MPC scheme based on a first-order delay model, which seeks a desired acceleration. The desired acceleration is used for an input to the lower-level controller. The lower-level controller is designed to compute throttle and brake control commands by considering the changes in environmental disturbances and model uncertainties. To deal with these issues, an adaptive sliding mode control is involved in the lower-level controller, instead of using parameter estimators. More detailed descriptions on the longitudinal controller are provided in Jo et al. (2022).

When the vehicle is at i-th section, the optimal guided speed generated in TMC is used for determining a target speed by utilizing it as an input to the upper-level longitudinal controller as follows:

$$v_{target}(t) = \min(v_{GS,i}(t), v_{ref}(t)), \tag{1}$$

where $v_{target}(t)$ is the target speed of CAV applied to upper-level controller which generates the desired acceleration, $v_{GS,i}(t)$ is the optimal guided speed of i-th section, and $v_{ref}(t)$ is the reference speed only considering vehicle dynamics and in-vehicle sensors. $v_{GS,i}(t)$ generated by the proposed algorithm in the TMC is used for an input to the upper-level controller of longitudinal motion control module to determine $v_{target}(t)$, as shown in Figure 3.

It is worth noting that this study only considers longitudinal collision avoidance since the proposed framework is applied to the dedicated lane-based BRT system, which physically separates the transit bus(ego vehicle) from other vehicles on the road. As described in equation (1), the CAV ultimately follows the target speed. When the target speed is set up to the reference speed($v_{ref}(t) \le v_{GS,i}(t)$), the CAV can react to a potential rear-end collision event

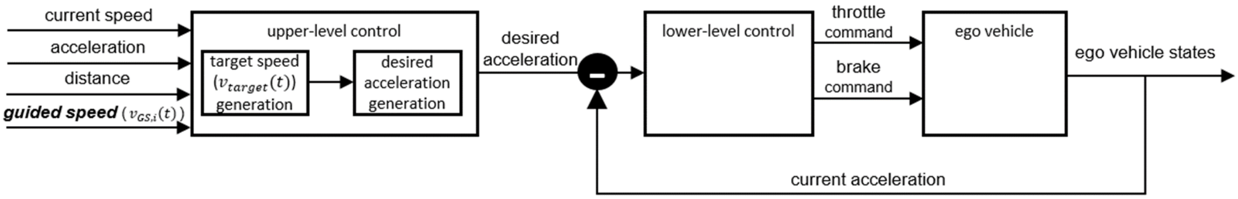

Figure 3: Longitudinal Control Scheme

since the reference speed is determined by considering the driving safety against collisions with moving objects or obstacles in the vehicle motion planning module of the in-vehicle system for automated driving (Jo, 2022). In other words, the CAV ensures its driving safety by detecting any potential collisions based solely on the information from in-vehicle sensors, such as lidar, radar and camera. On the other hand, when the target speed is set up to the guided speed ($v_{GS,i}(t) \leq v_{ref}(t)$), it is trivial to guarantee the driving safety against potential rear-end collision events since the target speed is less than or equal to the reference speed. Detailed descriptions on computing the guided speed are provided in Section 3.3.

3.2. Architecture of Cloud-based Traffic Management Center for Speed Guidance System

As mentioned in Section 3.1, we implemented a cloud-based TMC. The cloud-based TMC proposed in this study can manage the data flows and message processing function efficiently using various cloud services. Detailed description on each cloud service product used in this study is as follows:

- **Message Queue Service** is a message processing service that can receive and deliver data in real-time or in batch with elastic scalability and high throughput(Microsoft Azure Documentation (a);Amazon (a);Google Cloud Self-Paced Labs;IBM Cloud Documentation (a)). Major cloud vendors provide Message Queue Service under the name of Azure Eventhub, AWS EventBridge, Google cloud Pub/Sub, IBM cloud MQ. In this study, we use Eventhubs to send and receive messages from various sources such as traffic signal information and CAV driving information.

- **Real-time Data Processing** is a streaming engine that provides serverless, fast, and cost-effective data analysis and process of massive volumes of streaming data(Microsoft Azure Documentation (d);Amazon (b);Google Cloud Documentation (a);IBM Cloud Documentation (b)). There are Azure Stream Analytics, AWS Kinesis, Google Cloud Daraflow, IBM cloud streams in major cloud vendors' Real-time Data Processing services. In this study, we use Stream Analytics to process the real-time data and to save it into Cosmos DB(multi-model database).

- **Multi-model Database** is a database management system designed to handle different types of data models such as document, graph, relational, and key-value models(Microsoft Azure Documentation (c);IBM Cloud (b)). Well-known multi-model databases from cloud vendors are Azure Cosmos DB and IBM cloud Db2. In this study, we use Cosmos DB to store the real-time state from the messages. Function apps(serverless computing service) use the real-time states of different messages to calculate the sectionalized speed guidance.

- **Serverless Computing Service** is a solution that allows users to write and deploy codes on cloud (Microsoft Azure;Amazon (d);Google Cloud Documentation (b);IBM Cloud Education). Function as a service(FaaS) is one of the most popular serverless architecture. A function runs when a certain event is triggered. Examples of serverless architecture services from public cloud vendors includes Azure Function App, AWS Lambda, Google Cloud Functions, and IBM cloud functions. In this study, we use Azure Function app to calculate risks on the road and generate appropriate messages at current circumstances.

- **Object Storage** is a database where unstructured object data can be stored(Microsoft Azure Documentation (b);Amazon (c);Google Cloud Documentation (c);IBM Cloud (a)). Unstructured object data can be any type including binary, text, or image. Major public cloud providers offer object storage services such as Azure Blob storage, AWS S3, Google Cloud Storage, IBM cloud Object storage. In this stduy, we use Azure Blob Storage to store the trained model parameters from Deep Reinforcement Learning Module.

Figure 4 shows the overall architecture of cloud-based Traffic Management Center, which is composed of four modules: PIM Generation Module, Real-time Data Processing Module, VCAM Generation Module, and Deep Reinforcement Learning Module. First, the PIM Generation Module generates PIM for each CAV bus on the road during the scheduled operation time. Second, the Real-time Data Processing Module processes various real-time messages and save the messages in Multi-model database. This module corresponds to the *data gathering* module colored in green in Figure 1 in Section 3.1. Third, the VCAM Generation Module processes the messages uploaded on Multi-model database to generate VCAM which contains the optimal SSG calculated by using deep reinforcement learning. This module corresponds to the *risk calculation* and *speed guidance determination* module colored in orange and blue

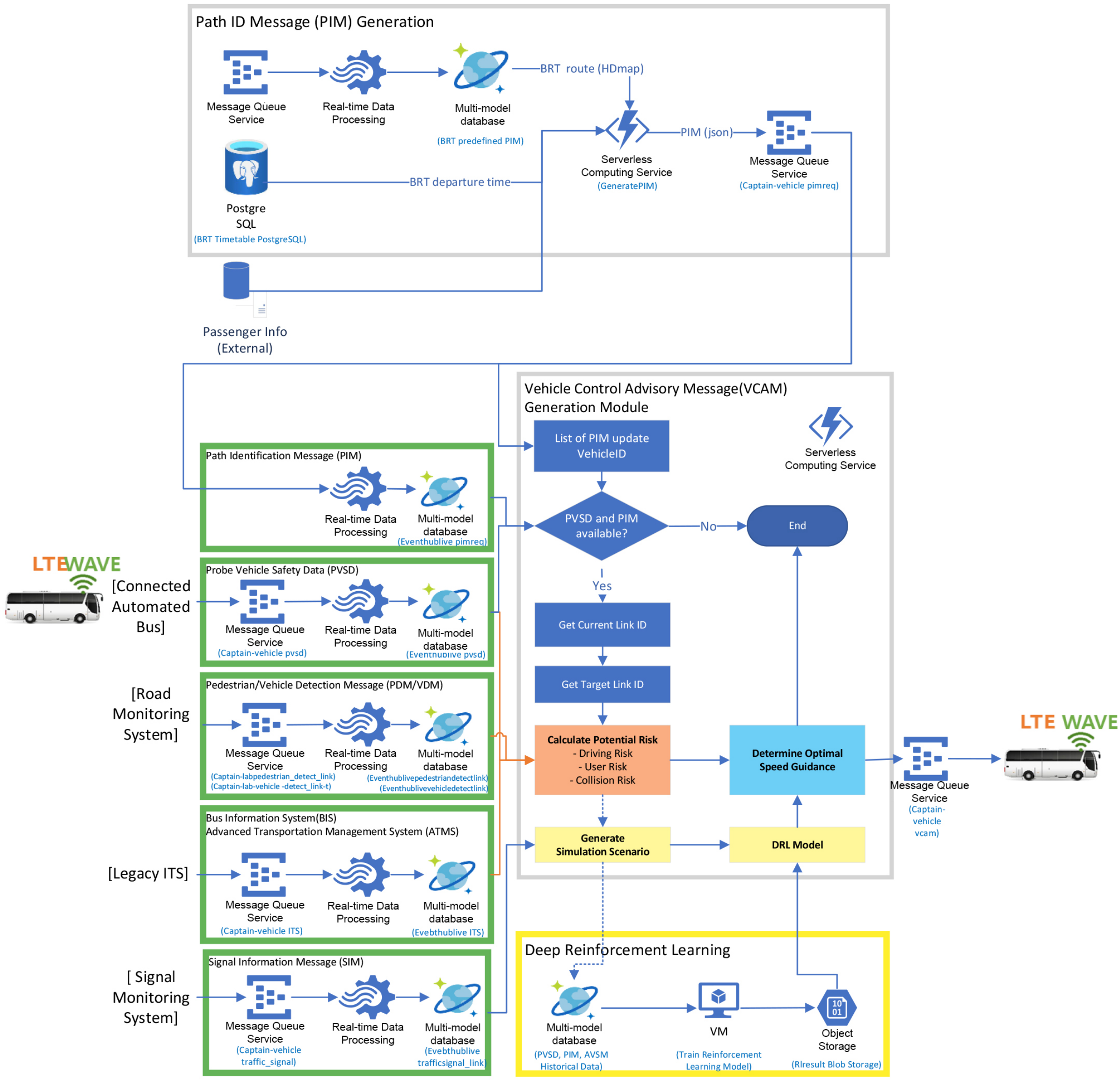

Figure 4: Architecture of Sectionalized Speed Guidance System for Connected and Automated Vehicle in Cloud Platform

in Figure 1 in Section 3.1. Finally, the Deep Reinforcement Learning (DRL) Module trains the deep reinforcement learning algorithm based on various scenarios from real roads. This module corresponds to the *deep reinforcement learning* module colored in yellow in Figure 1 in Section 3.1

In the PIM Generation Module, we use the bus timetable from PostgreSQL database which contains pre-defined departure time and bus route. The Serverless Computing Service in the PIM Generation Module checks the timetable every 20 seconds, and is triggered if there exist buses that have to depart at present time. If the Serverless Computing Service is triggered, the Serverless Computing Service uses the pre-defined bus route stored in Multi-model database to construct the PIM for the departing bus, and sends the PIM to the PIM Message Queue Service.

The Real-time Data Processing Module processes real-time messages, and saves the messages in Multi-model database for use in other modules. There are fix types of real-time messages used in this framework, as well as legacy ITS data: PIM, PVSD, PDM, VDM and SIM. All messages are transmitted to the Message Queue Service from the source, processed in Real-time data processing, and stored in the Multi-model database. The legacy ITS data is stored in the PostgreSQL database. In practice, synchronizing the timestamps in different messages is very challenging task. As a result, in this study, processing the real-time data and storing it in Multi-model database allow other modules to use synchronized and up-to-date messages from different message sources.

In the VCAM Generation Module, we use processed real-time data to calculate optimal guided speed, and generate the VCAM. The main role of VCAM is to give CAV guided speeds of the target links in front of the vehicle, as well as other information like potential risk of collision, pedestrian/vehicle detection information in front. At every generation cycle, the module checks if there exists any vehicles that have PIM and PVSD uploaded on the Multi-model database, and VCAM generation is triggered for those vehicles. First, the module checks the current Link ID in PVSD, and matches it to the PIM, and then determines the target links for Speed Guidance. The target links are defined to be lane-level HDMap links within 400m range, but if there is only one link in 400m range, the next link in the PIM is added to the target links. Then, the target links are divided into 25m segments, which serves as an unit in the VCAM. Next, the module calculates the integrated risks of driving risk, user risk, and collision risk discussed in Section 3.1. The calculated integrated risks are sent to "*Determine Optimal Speed Guidance*" function and generates a **base speed guidance profile** with pre-defined rules. Then, considering the calculated risks, the module generates simulation scenario for DRL Model and triggers DRL Model to inference the optimal guided speed for the given condition. The simulation scenario is also used to train DRL Model later. In "*Determine Optimal Speed Guidance*" function, we combine the base speed guidance profile and output of DRL Model to determine final speed profile. This is converted into the VCAM format and sent to the Message Queue Service, which is connected to the OBU of Connected Automated Bus through Communication System in Figure 1.

In the Deep Reinforcement Learning Module, DRL Model is trained based on the simulation scenarios collected from the VCAM Generation Module. The parameters of the trained model are saved with binary file and stored in the Object Storage. Detailed descriptions on the reinforcement learning model and the simulation set-ups are presented in Section 3.3

3.3. Sectionalized Speed Guidance based on Deep Reinforcement Learning

3.3.1. Reinforcement Learning Algorithm

Reinforcement Learning (RL) is a learning framework that optimizes sequential decision-makings of an *agent* interacting with an *environment* to maximize potential benefits. At a certain time step t, the agent observes the current state ($s_t \in S$) from the environment. From the current state, the agent calculates the action ($a_t \in A$) based on the policy $\pi(a_t|s_t)$. The environment gives a reward $r_t(s,a)$, which is feedback to the agent that represents how good the action was at the current state. The objective of RL is to maximize *expected cumulative reward* $G_t = \sum_{k=0}^{\infty} \gamma^k r_{t+k}(s,a)$, where γ^k represents the k^{th} discount factor.

The current state-of-the-art RL algorithms include Deep Deterministic Policy Gradient (DDPG) (Lillicrap et al., 2015), Trust Region Policy Gradient (TRPO) (Schulman et al., 2015), Proximal Policy Gradient (PPO) (Schulman et al., 2017), and Soft Actor-Critic (SAC) (Haarnoja et al., 2018). Among the current state-of-the-art models, we selected PPO for our system.[1] The PPO is a model-free, on-policy, actor-critic and policy-gradient method. It is a practical and computation-efficient modification of the TRPO, which updates the policy by taking the largest step possible while satisfying Kullback–Leibler (KL)-divergence constraint (or Trust Region constraint) on how close the

[1] At the very beginning of this research, we tested four different RL algorithms for model selection. The results showed that all algorithms could successfully generate an optimal policy for the given task, and among all, PPO had the best performance compared to other models in terms of model convergence and training time. We do not include the results of these tests because selecting an RL model is not the scope of this study.

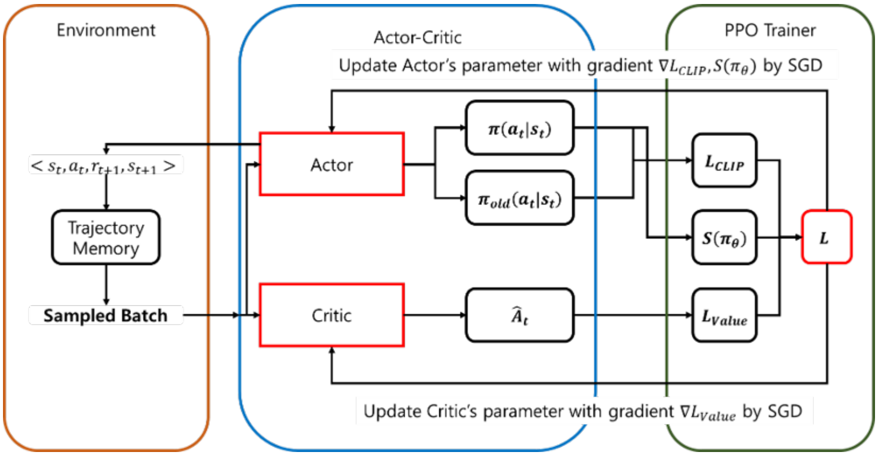

Figure 5: Learning framework of Proximal Policy Optimization

new and old policy are allowed to be. The TRPO usually requires a complex computation, whereas the PPO simplifies the computation by using the first-order optimization.

Figure 5 shows the specific learning framework in the PPO algorithm. The PPO has two sub-modules called Actor and Critic. Usually, the Actor generates a policy (or policy distribution) based on the current state, and the Critic calculates the expected value of the current state. In the PPO, *advantage function* ($A_t(s,a) = Q(s,a) - V(s)$), is used instead of expected reward because it reduces the variance of the estimation. The PPO is updated by using following objective function:

$$\max L = \hat{E}_t[L_{CLIP} - c_1 L_{Value} + c_2 S(\pi_\theta(s_t))], \tag{2}$$

where L is the objective function, L_{CLIP} is the clipped surrogate loss, $L_{Value} = (A_t - \hat{A}_t)^2$ is the value (advantage) estimation loss, $S(\pi_\theta(s_t)) = E[\pi_\theta(s_t) \log \pi_\theta(s_t)]$ is the action entropy loss, and π_θ is θ-parameterized policy. L_{CLIP} is an approximation of TRPO loss by using clipping function:

$$L^{CLIP}(\theta) = \hat{E}_t\left[\min\left(r_t(\theta)\hat{A}_t, clip(r_t(\theta), 1-\epsilon, 1+\epsilon)\hat{A}_t\right)\right], \tag{3}$$

where $\hat{A}_t$ represents the estimated advantage at time t, ϵ describes the hyperparameter for the limit of the range within which the update is allowed, and $r_t(\theta)$ indicates the importance sampling ratio which can be expressed as follows.

$$r_t(\theta) = \frac{\pi_\theta(a_t|s_t)}{\pi_{\theta_{old}}(a_t|s_t)}, \tag{4}$$

where $\pi_\theta(a_t|s_t)$ and $\pi_{\theta_{old}}(a_t|s_t)$ are θ-parameterized new and old policies, respectively.

3.3.2. Training and Inferencing Framework

As shown in Figure 6, when training DRL model, we use *base speed guidance profile* as input to represent the simplified version of various real-world scenarios. Also, in training phase, we slightly randomize the given base speed guidance profile to train more robust DRL model. In the inference phase, we use the parameters learned from training phase, and here, the base speed guidance profile as well as the real-time vehicle driving state is used as input (state) of DRL module. Based on the DRL inference, we generate the VCAM containing the information on the optimal guided speed at each section, which is sent to the CAV via V2X or LTE communication.

We first generate the base speed guidance profile based on the integrated risks including driving risk, user risk, and collision risk defined in Section 3.1. This base speed guidance profile is used as one of the variables in the state

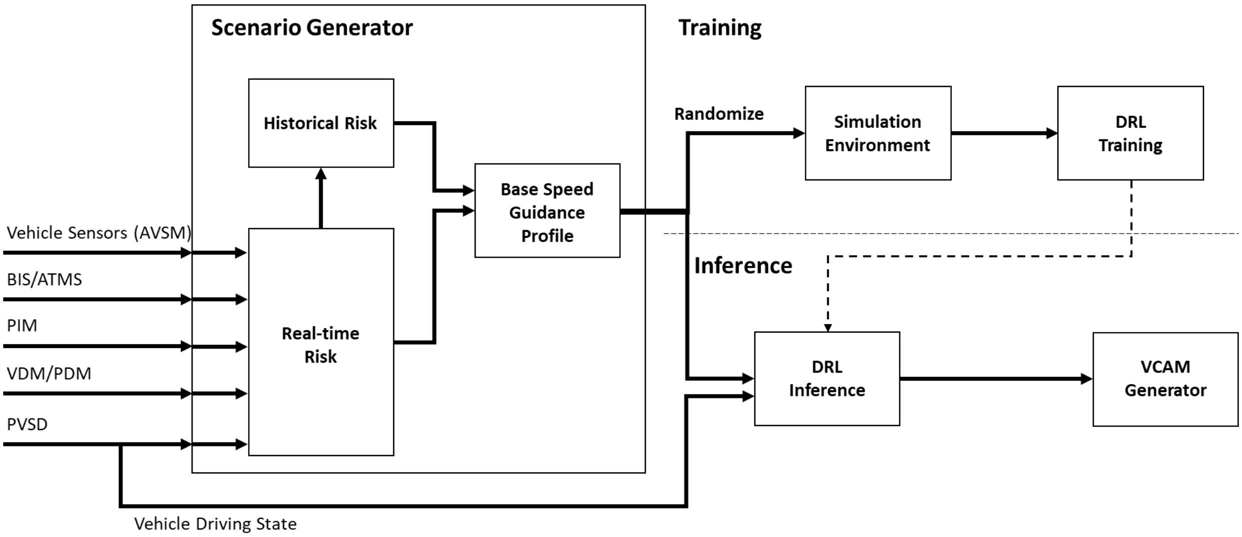

Figure 6: Data flow for training and inference of DRL module

definition in Section 3.3.3. The driving risk is calculated according to the driving stability of the ego vehicle at each road section. Especially, as mentioned in an example, we use historical driving data to identify the sections which show high driving risk, and reduce the guided speed at those sections. Next, the user risk represents the passenger-centric factors influencing the comfort and safety of on-board passengers and waiting passengers at bus stops. Similar to driving risk, we use historical driving data to identify the sections which show more frequent occurrences of severe lateral deceleration and hard acceleration and reduce the guided speed at those sections considering the number of passengers on the ego vehicle. Also, note that our system is based on ride-reservation, so that we have access to the number of passengers at each station and we estimate the dwell time by using this data. Finally, the collision risk represents the risk between ego vehicle and surrounding agents such as other buses, passenger vehicles, and pedestrians. These surrounding agents are detected based on the Road Monitoring System where the PDM and VDM are used to determine the base speed guidance profile. Especially, when there exist any jaywalking pedestrians the guided speed of the corresponding section is reduced to 15 km/hr so that the vehicle can stop as soon as these pedestrians are detected by in-vehicle sensors. Also, when preceding vehicle is detected, the speed of corresponding section is reduced to guarantee safe stopping behind the preceding vehicle even though the preceding vehicle is not detected by the in-vehicle sensors.

3.3.3. States, Action, and Rewards

States — At time-step t, the state of the speed guidance system can be defined by the information from the ego CAV and the information from infrastructures. The information from the ego CAV includes the position ($x(t)$), speed ($v(t)$), and acceleration ($a(t)$) of the ego CAV. The information on the CAV (BRT bus) position, speed and acceleration could be obtained from Probe Vehicle Safety Data (PVSD) received by V2X communication. The detailed specification of PVSD can be found in Appendix A.3. The exact values associated with the speed, and acceleration of CAV can be found in "wheel" and "accel" field in "snapshot(list)-chassis" field. The position data can be found in "offsetOfVehicle" at "snapshot(list)-currentBusDrivingInfo-cavCurrentProvidedInfo-linkInfo". This value represents the distance between the ego vehicle and the start location of the current section. We can sum up the lengths of previous links to get the location of the ego vehicle. The information from the infrastructures can come from various sources. Also, there are almost infinite possibilities in real-world driving scenario. As a result, we first aggregate the data from infrastructure and generate "base speed guidance profile" as discussed in Section 3.3.2. Especially, we use the data from AVSM, PVSD, VDM/PDM, BIS/ATMS to generate the base speed guidance profile as shown in Figure 6 The specification of traffic signal data can be found in "Signal Phase And Timing Message (SPaT)" in Appendix A.7. We use "next-event" and "event-after-next" fields in "regional-regExtValue-captain-states(list)" to get the remaining time to closest green signal. In Figure 7, green lines represents the data flow from the ego vehicle and near-by infrastructures to get the current state. The state can be represented as follows:

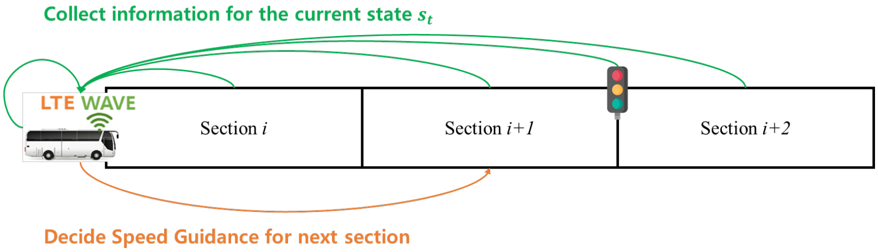

Figure 7: Graphical illustration on how the states are collected and how the action is applied

$$s(t) = \left[x(t), v(t), a(t), \left(d^{ns,1} t^{ns,1}_{g,start}, t^{ns-1}_{g,end}\right), \left(d^{ns,2}, t^{ns,2}_{g,start}, t^{ns-2}_{g,end}\right), \left(v_{base,i}, \cdots, v_{base,i+k}\right)\right], \tag{5}$$

where $d^{ns,1}$ and $d^{ns,2}$ represent the distance to the nearest/second-nearest traffic signal, respectively, $t^{ns,1}_{g,start}$ and $t^{ns,2}_{g,start}$ represent the time remaining to the closest start time of the green signal (0 if already green) at each traffic signal, $t^{ns,1}_{g,end}$ and $t^{ns,2}_{g,end}$ represent the time remaining to the closest end time of the green signal, and $v_{base,i}$ represents the base speed guidance profile at section i. We use speed values from the current and the next k sections, typically set to 3.

Action — Based on the current state (s_t), the policy (π) decides an action. The action is defined as the guided speed (GS) for the next section. Figure 7 shows that when the ego CAV enters the Section i, the ego CAV collects the current state, and the proposed algorithm decides the GS for the next section (Section $i+1$). The reason why we decide the GS for the next section is because of the communication processing time during the data processes from the CAV to cloud server. When the event that the ego CAV entered Section i is detected by the cloud server, a Message Queue Service is triggered and runs the RL inference module. Then, the optimal GS is sent to the CAV. From our field tests, the time from triggering to receiving took around 0.5 to 2 seconds. As a result, if the action is to decide the GS for the current section, there can be a time-lag in the decision, which can reduce the performance of optimal action calculated by the RL module. In this study, we use a discrete action space for GS. When the maximum GS (v^{max}_{GS}) and minimum GS (v^{min}_{GS}) are given, we discretize the speed limit value by (Δv_{GS}).

Rewards — The reward function can be regarded as a training signal to encourage or discourage certain behavior. The reward function in this study is composed of four sub-functions, and is defined as a linear combination of the four sub-functions as follows:

$$\begin{aligned} R &= R_{CAV} + \alpha_{GS} R_{GS} \\ &= \sum_{t=t_i}^{t_{i+1}} \left[\alpha_{speed} R_{speed}(t) + \alpha_{acc} R_{acc}(t) + \alpha_{power} R_{power}(t)\right] + \alpha_{GS} R_{GS}, \end{aligned} \tag{6}$$

where R_{CAV} is the reward from the performances of CAV and R_{GS} is the reward from the determined guided speed. R_{CAV} can be further divided into R_{speed}, R_{acc}, and R_{power}. t_i refers to the time the ego CAV enters Section i, and t_{i+1} refers to the time the ego CAV enters Section $i+1$ (leaves Section i). R_{CAV} is calculated by accumulating R_{speed}, R_{acc}, and R_{power} throughout the time that CAV is located in Section i.

R_{speed} is designed to maximize the operational efficiency, which is similar to the previous studies on the OSA and GLOSA system. R_{speed} is calculated by the difference between the current vehicle speed and GS as shown in Equation 7:

$$R_{speed}(t) = \begin{cases} -\frac{|v(t)-v_{GS,i}|}{v_{max}} & , if\, v(t) \le v_{GS,i} \\ -\frac{|v(t)-v_{GS,i}|}{v_{max}} - 1 & , otherwise \end{cases}, \tag{7}$$

where $v(t)$ is the speed of the CAV, $v_{GS,i}$ is the GS of Section i, and v_{max} is the maximum (desired) speed of the vehicle. We further penalize the GS exceeding case by giving the negative reward.

R_{acc} is designed to enhance driving safety, which penalizes when the vehicle has abrupt acceleration or deceleration as shown in Equation 8:

$$R_{acc}(t) = -\left(\frac{a(t)}{a_{max}}\right)^2, \tag{8}$$

where $a(t)$ is the acceleration of the CAV, and a_{max} is the max acceleration rate of the CAV. In this study, a_{max} is assumed to be 5 m/s^2.

R_{power} is designed to maximize the energy efficiency. R_{power} is based on the instantaneous mechanical power needed at the wheels to make the vehicle move or brake as shown in Equation 9 (Basso et al., 2019). The power can be further estimated to fuel consumption or energy consumption depending on the types of the vehicle (fossil-fueled vehicle, EV, HEV) (Ben-Chaim et al., 2013; Basso et al., 2019). In this study, we use the mechanical power equation for simplicity and generaizability. Also, we ignore negative power (which is often referred to as "regeneration mode") to prevent the agent getting positive reward while decelerating (braking).

$$R_{power}(t) = -\max\left(0, Mv(t)a(t) + MgC_r v(t) + 0.5\rho AC_a (v(t))^3\right), \tag{9}$$

where M denotes the mass of the vehicle, g represents the gravitational acceleration, C_r describes the rolling resistance coefficient, C_a indicates the aerodynamic drag coefficient, ρ represents the air density, and A refers to the cross-sectional area of the vehicle.

Finally, R_{GS} is designed to keep up with the transition from the current to following section for ride comfort, which penalizes sudden changes in GS as follows:

$$R_{GS} = -|v_{GS,i} - v_{GS,i+1}|, \tag{10}$$

where $v_{GS,i}$ is the GS of the current section, and $v_{GS,i+1}$ is the GS of the next section (which is the action).

3.3.4. Simulation Set-up and Training

We developed a simulation environment to train the RL module and to determine the optimal GS at inference step. The geometry of the simulation environment is designed to resemble the actual road geometry where the field tests are conducted. The simulation environment contains identical values for length of each section, locations or traffic signals, and signal timings. Based on the simulation scenario generated in the VCAM Generation Module in TMC, the simulation environment is initialized with actual initial position, speed of the ego vehicle and signal phase and timing. In the simulation, we used Intelligent Driver Model (IDM) (Kesting et al., 2010) as the baseline car-following model. The equation for calculating the acceleration of the ego vehicle is shown in Equation 11:

$$\begin{aligned} a(t) &= a\left(1 - \left(\frac{v(t)}{v_0}\right)^\delta - \left(\frac{s^*(v(t), \Delta v(t))}{s(t)}\right)^2\right), \\ s^*(v(t), \Delta v(t)) &= s_0 + v(t)T + \frac{v(t)\Delta v(t)}{2\sqrt{ab}} \end{aligned} \tag{11}$$

where a is the maximum vehicle acceleration, b is the comfortable braking deceleration, v_0 is desired speed, and s_* is the desired gap. In the original definition of IDM, $s(t)$ is the spacing between the front vehicle and $\Delta v(t)$ is the relative speed. In this study, when the traffic signal is in red, $s(t)$ refers to the distance to the signal, and $\Delta v(t)$ is $-v(t)$. We used the GS value ($v_{GS,i}$) for the section that the ego CAV is located in as the desired speed, v_0.

There are several parameters to be defined for the reward setting. Table 1 shows the hyper-parameters used in the training. The learning procedure is implemented with Python 3.7 and Pytorch 1.8.0, and the reinforcement learning framework is embedded into the simulation.

Table 1
Hyperparameters used for training deep reinforcement learning algorithm

Hyperparameter	Value
Learning Rate	0.0003
Reward Discount Factor(γ)	0.99
Clip range (ϵ)	0.2
Coefficient for Value Loss (c_1)	0.5
Coefficient for Entropy Loss (c_2)	0.1
Maximum GS (v_{GS}^{max})	45 km/h
Minimum GS (v_{GS}^{min})	15 km/h
Maximum acceleration (a_{max})	5 m/s^2
GS Discretization Unit (Δv_{GS})	5 km/h
Speed Reward Coefficient (α_{speed})	1
Acceleration Reward Coefficient (α_{acc})	1
Power Reward Coefficient (α_{power})	0.01
GS Reward Coefficient (α_{GS})	1

If simulation scenario is not specified, at each scenario generation, we set the initial position of the ego vehicle as the start location of the simulation environment and we set the initial speed as the maximum speed of the ego vehicle. Also, we randomly select the *global traffic signal offset* —time difference from the green-signal start-time of the first signal— to generate different signal timings at each roll-out. This will eventually make the RL model to be robust to the traffic signal phase and timing.

We set the each reward coefficients ($\alpha_{speed}, \alpha_{jerk}, \alpha_{GS}$) as 1, except for power reward coefficient (α_{power}). We tested different values for α_{power}. Figure 8 shows the performance ratio of each setting compared to *Non-control case* (example runs for each case are presented in Appendix B). PPO0 represents $\alpha_{power} = 0.001$, PPO1 represents $\alpha_{power} = 0.003$, PPO2 represents $\alpha_{power} = 0.005$, and $\alpha_{power} = 0.01$. Examples of simulation runs are presented in Appendix B. In Figure 8, we had three evaluation criteria, performance ratio of speed, power, and jerk. The performance ratio of speed is higher-the-better, while the performance ratios of power and jerk are lower-the-better. As a result of Figure 8, we selected settings of PPO3 for the use in the case study because both performances of power and jerk is improved while the performance of speed maintained at an adequate level.

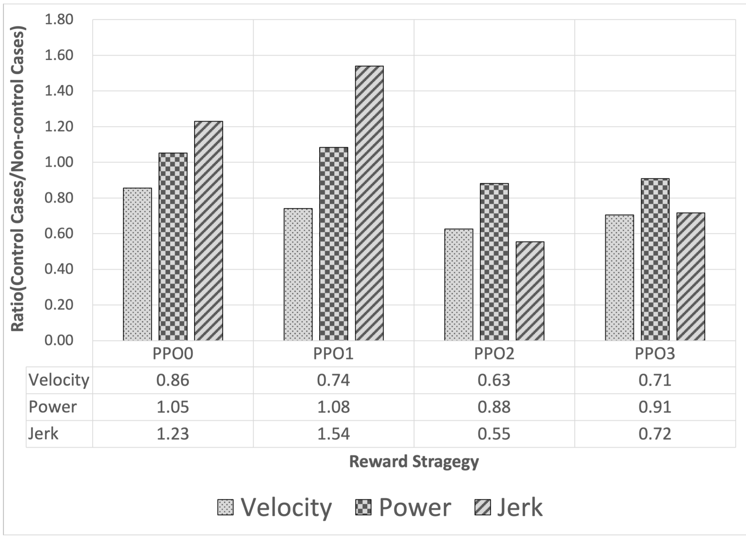

Figure 8: Simulation results with different $alpha_{power}$; PPO0 represents $\alpha_{power} = 0.001$, PPO1 represents $\alpha_{power} = 0.003$, PPO2 represents $\alpha_{power} = 0.005$, and $\alpha_{power} = 0.01$. The performance ratio of velocity is higher-the-better, while the performance ratios of power and jerk are lower-the-better

3.4. Case Study for Evaluation: Field Test in Sejong City

3.4.1. Site

This research conducted a case study based on real-world experiments in a study site, which is part of BRT roadway located in Sejong City, South Korea, as represented by the red line in Figure 9 (a). The data used in this study obtained from an approximately 4-km-long BRT roadway. The data were collected with 1millisecond-interval based on three test drives per one day for 10 days: 10:00 a.m., 2:00 p.m., and 4:00 p.m.; on November 17 to 19 and 23 to 25, December 6, 9, 13, and 14, 2021.

A detailed view of the study site is described in Figure 9 (b). The study site is composed of 24 lane-level links defined in the HDMap. The links have different geometric characteristics and features, which influences the performance of the tested system, as depicted in Table 2. The geometric characteristics of each link can be categorized into five groups: *overpass*, *straight road*, *signalized intersection*, *curved road* and *underground tunnel*. There are three overpasses in the study site; two bridges cross over a river and the other one is an upper-level road that crosses over an intersection. The bridges have BRT lanes in the middle of road and other lanes along the side of the road for other types of vehicles such as passenger vehicles and trucks. The BRT lanes in two bridges are physically separated by the traffic barriers such as curbstones and road safety poles. The upper-level overpass having two-lane two-way road is designed only for the BRT buses, and other types of vehicles are not legally allowed for driving.

There are thirteen straight road links in the study site and 32% of study site is straight road. The length of the straight road links vary from 1.58m to 197.86m and most of the straight roads are physically separated from the road for other types of vehicles.

There are two signalized intersections. The signalized intersections are the only sections which are not physically separated from road for other vehicles by using the traffic barriers. Instead, yellow colored road surface and white dotted lane marking demarcate the BRT lane and other lanes (See Link A2207G003373 in Figure 9 (b)). In the signalized intersection, BRT bus drives only in a straight forward direction without left or right turns.

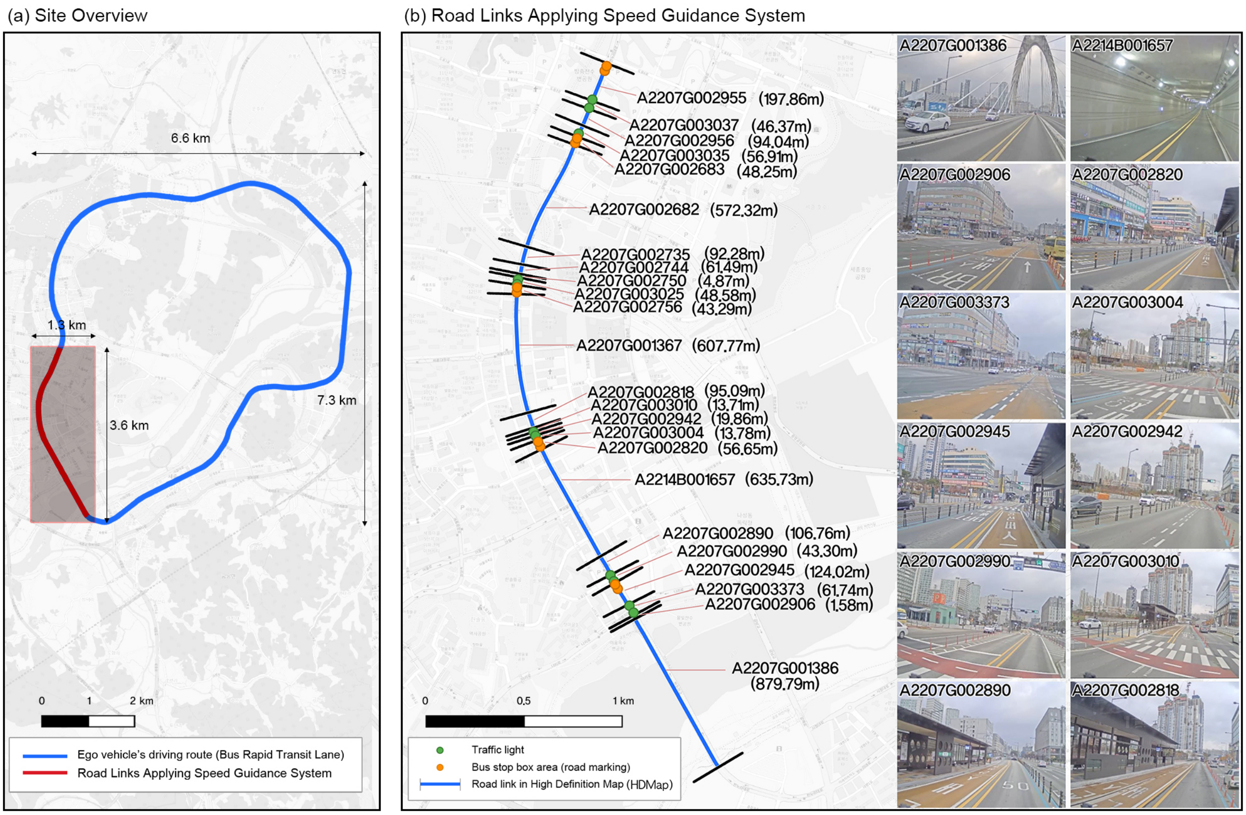

Figure 9: Detailed view of road links applying speed guidance system:(a) site overview and (b) road links applying speed guidance system (enlarged area marked by the red box in a)

There are six curved road links that account for 26% of study site. The minimum and maximum lengths of curved road links are 43.29m (A2207G002756) and 607.77m (A2207G001367), respectively. The fifteenth link (A2207G003025) shows the minimum curve radius with approximately 257m, and the thirteenth link (A2207G001367) has maximum curve radius with approximately 1,866m.

There are two long underground tunnels in the study site. One (A2214B001657) is a 635.73m-long straight road, and the other (A2207G001367) is a 607.77m-long curved road. The Underground tunnel consists of three parts: entry, underground, and exit. In the entry part and exit part, there are downhill and uphill slopes for going into the underground and going back to the ground-level road without any roofs. The underground part consists of a flat ground. Compared to the entry and exit parts, the underground part suffers from the high latency and high delay of V2X communication and low accuracy of GPS data.

Along with the geometric characteristics, there are key functional features related to operation performance of CA-BRT such as *bus station*, *crosswalk*, *traffic barrier*, *RSU for V2X communication*, *traffic signal controller*, *sensors for Road Monitoring System*, and *legacy ITS*. There are five bus stations in the study site. The length of each bus station is approximately 30m, and each bus station has two bus stops. Since there are not any detour lanes in each bus station, congestion near the bus station is often observed when any of the bus stops is occupied by preceding transit bus for boarding or alighting passengers. In this situation, an ego vehicle approaching the bus station is inevitably enforced to reduce its longitudinal speed to prevent possible rear-end collision, which may have an negative influence on ride comfort and energy efficiency due to the deceleration maneuvers.

There are eleven crosswalks in the study site. Three crosswalks are located on the intersections, and the rest of them are located right after the bus stations. The crosswalks near bus station have a layout in which it is difficult to detect pedestrians entering the crosswalk through human vision or cognitive devices of CAV because the distance between the bus stop facility and crosswalk is too close (See Link A2207G002945 in Figure 9 (b)).

The traffic barriers are installed in almost all roads of study site, expect for signalized intersections, to physically separate the BRT lanes from lanes for other types of vehicles such as passenger vehicles and truck. It has an important role for safe driving of CAVs because the driving of the CAVs can be hindered by irregular arrangement of traffic barriers in some cases. There are three types of traffic barriers installed in the study site: road safety pole, curbstone and road fence. The road safety poles are installed in the straight road and curved road along BRT lanes due to easy installation and high visibility at night. The curbstones are installed in the important sections for vehicle safety such as a place where an dedicated BRT lane and other lanes for passenger vehicles must be clearly separated for avoiding driver's confusion. In the study site, the curbstones are usually installed in the entry and exit of underground tunnels and the entry and exit of overpasses. The road safety fences are installed near underground tunnels and bus stations for safety of pedestrians and vehicles.

The RSUs for V2X communication are an important equipment for transmitting the information from TMC to CAVs in real-time. Eleven RSUs are installed in the important place where the information is transmitted quickly and accurately for safety reasons such as signalized intersections, bus stations and underground tunnels. The installation distance of RSUs is at least 160m and at most 400m. The shaded region of V2X communication is reinforced by the LTE communication for seamless connectivity.

There are eleven traffic signal controllers in the study site to provide signal information to CAV through V2X communication in real-time. The traffic signal controller is located near crosswalks or intersections to control the digital traffic signal and to extract its information in order to send the information to RSUs.

The sensors for Road Monitoring System are installed to reinforce the limited perception range of in-vehicle sensors of CAVs, particularly in the signalized intersections and bus stations. Three types of sensors are installed such as vision, lidar and radar sensors near RSUs to more robustly transmit the information. The information from the vision and lidar sensors are mainly used to detect the individual objects such as vehicles and pedestrians near intersections, crosswalks, and bus station. The information from the radar sensors are mainly used for monitoring traffic situation such congestion and incident. Especially, the importance of information from radar sensors increases in adverse weather conditions such as heavy rain and heavy snow.

Lastly, the legacy ITSs are installed throughout the BRT route in the study site. The ATMS produces the traffic information such as speed and flow for whole BRT lanes every 30 seconds. The BIS-related information such as approximate location of bus and passenger number are also collected from the entire BRT route every 30 seconds. The TMC uses the information from the ATMS and BIS to supplement limited monitoring region covered by the sensors of Road Monitoring System. With these information from the legacy ITS, the CAVs can react to more various traffic situations in a wide region compared to the cases using information only from the Road Monitoring System.

Table 2
Key features of each link in the study site

LinkID	Index	Length	Geometry	Features
A2207G001386	1	879.79m	Overpass	- Long straight bridge except for the entrance of the section - Curbstone along the BRT lanes - Road safety poles (at the end of the link, 30m) - Abrupt changes in the width of the BRT lane
A2207G002096	2	1.58m	Straight	- Stop line for following signalized intersection at the end of the link
A2207G003373	3	61.74m	Signalized intersection	- 8-lane 2-way road and 4-lane 2-way road intersection including mixed traffic lanes - Demarcated BRT lanes by a dotted guideline - BRT roads are not physically separated from the lane for passenger vehicles - Crosswalk and traffic lights(at the end of the link) - RSU for V2X communication and traffic signal controller (for BRT) at the beginning of the link
A2207G002945	4	124.02m	Curved	- Bus station having two bus stops at the end of the link - Road safety poles along the BRT lanes - Protruding curbstone near the entrance of a bus station
A2207G002990	5	43.30m	Straight	- Crosswalk and Traffic lights at the beginning of the link - Road safety poles along the BRT lanes - RSU for V2X communication and traffic signal controller (for BRT) at the beginning of the link
A2207G002890	6	106.76m	Curved	- Crosswalk and traffic lights at the beginning of the link
A2214B001657	7	635.73m	Underground tunnel, Straight	- Downhill slope leading to an underground tunnel at the beginning of the link (150m, no roofs) - Underground tunnel in the middle of the link (325m) - Uphill slope at the end of the link (160m, no roofs) - High latency and high delay of V2X communication - Low accuracy of GPS data - Two RSUs for V2X communication and two traffic signal controllers in the middle of the link
A2207G002820	8	56.65m	Straight	- Bus station having two bus stops at the end of the link - Bus station located right after an uphill section
A2207G003004	9	13.78m	Straight	- Crosswalk - RSU for V2X communication and traffic signal controller (for BRT) at the beginning of the link
A2207G002942	10	19.86m	Straight	- Road between the crosswalks and traffic lights
A2207G003010	11	13.71m	Straight	- Crosswalk - Traffic lights at the beginning of the link
A2207G002818	12	95.09m	Straight	- Road fences along the right side of BRT lane
A2207G001367	13	607.77m	Underground tunnel, Curved	- Downhill slope leading to an underground tunnel at the beginning of the link (140m, no roofs) - Underground tunnel in the middle of the link (337m) - Uphill slope at the end of the link (130m, no roofs) - High latency and high delay of V2X communication - Low accuracy of GPS data - RSU for V2X communication and traffic signal controller in the middle of the link
A2207G002756	14	43.29m	Curved	- Bus station having two bus stops at the end of the link - Bus station located at the beginning of the link
A2207G003025	15	48.58m	Curved	- Two crosswalks which is located at the beginning and at the end of the link respectively - Traffic lights at the beginning of the link - Three vision sensors for monitoring the individual vehicle near intersection and bus station - Two radar sensors for traffic and incident monitoring - RSU for V2X communication and traffic signal controller (for BRT) at the beginning of the link
A2207G002750	16	4.83m	Straight	- A link between crosswalk and overpass
A2207G002744	17	61.49m	Overpass	- Short straight bridge - Road safety poles along the BRT lanes
A2207G002735	18	92.28m	Curved	- Road separator along the BRT lanes
A2207G002682	19	572.32m	Overpass	- Long curved lane having relatively small radius of curvature - Three vision sensors for monitoring the individual vehicle near intersection under the overpass - Four radar sensors for traffic and incident monitoring - RSU for V2X communication and traffic signal controller in the middle of the link
A2207G002683	20	48.25m	Straight	- Bus station having two bus stops at the end of the link
A2207G003035	21	56.91m	Straight	- Two crosswalks which is located at the beginning and at the end of the link respectively - Traffic lights at the beginning of the link - Four vision sensors for monitoring the individual vehicle near intersection and bus station - Two radar sensors for traffic and incident monitoring - RSU for V2X communication and traffic signal controller (for BRT) at the end of the link
A2207G002956	22	94.04m	Straight	- A link between crosswalks
A2207G003037	23	46.27m	Signalized intersection	- 8-lane 2-way road and 6-lane 2-way road intersection including mixed traffic lanes - Demarcated BRT lanes by a dotted guideline - BRT roads are not physically separated from the lane for passenger vehicles - Two crosswalks and traffic lights located at the beginning and at the end of the link respectively - Two vision sensors for monitoring the individual vehicle near intersection - One lidar sensor and four radar sensors for traffic, incident, and pedestrian monitoring - RSU for V2X communication and traffic signal controller (for BRT) at the beginning of the link
A2207G002955	24	197.86m	Straight	- Bus station having two bus stops at the end of the link - A vision sensor for pedestrian monitoring - Two vision sensors for monitoring the individual vehicle near intersection and bus station - One lidar sensor and one radar sensor for traffic, incident, and pedestrian monitoring - RSU for V2X communication and traffic signal controller (for BRT) at the end of the link

3.4.2. Field Test Settings for Comparative Analysis

In the case study, we tested the ego vehicle with four different settings: Driver, Automated vehicle (AV), Uniform-segment-Speed-Guidance-based Connected and Automated Vehicle (USG-CAV), and Sectionalized-Speed-Guidance-based Connected and Automated Vehicle (SSG-CAV). Driver serves as a reference of the performance in current public transit system, and AV serves as a reference of the performance when automated driving technology is solely applied to public transit system without V2X communication. Both USG-CAV and SSG-CAV uses the same framework proposed in this study, but the unit for guided speed is different. USG-CAV uses 25m segment defined in VCAM as the unit for guided speed, while SSG-CAV uses sections, i.e. multiple segments with similar characteristics combined, as the unit for guided speed.

- Driver
  The ego vehicle is controlled by human driver.
- AV
  The ego vehicle is controlled by the default automated driving logic in Jo et al. (2022); Jo (2022).
- USG-CAV
  The sections are divided into *uniformly-distanced* segments. USG-CAV uses 25m segment defined in VCAM as the unit for guided speed as shown in Figure 10 (a). The guided speed is set as the maximum speed of the ego vehicle at each segment. Otherwise, the ego vehicle is controlled by the default automated driving logic in Jo et al. (2022); Jo (2022).
- SSG-CAV
  The sections are divided into sections considering the characteristics of the roadway. SSG-CAV uses sections (multiple segments combined) with similar characteristics as the unit for guided speed as shown in Figure 10 (b).

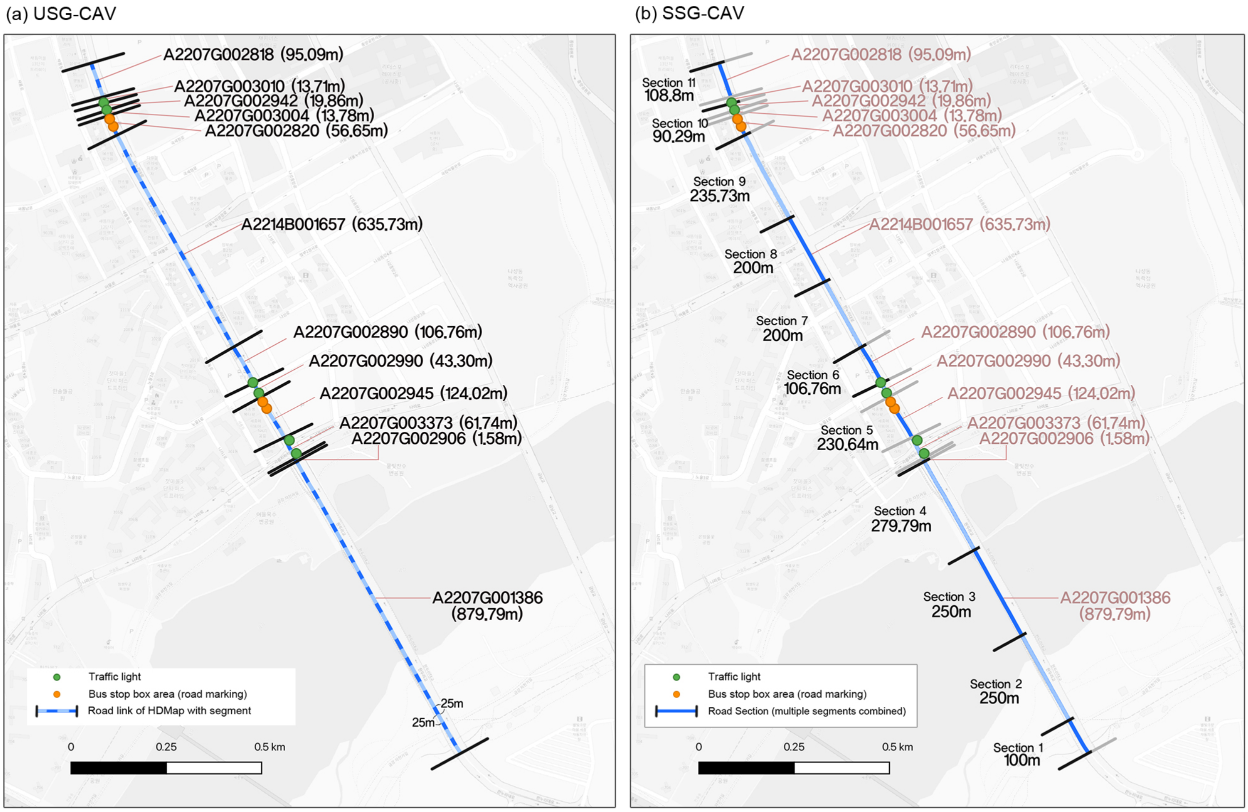

Figure 10: Segments and Sections for Speed Guidance

The guided speed is set as the maximum speed of the ego vehicle at each segment. Otherwise, the ego vehicle is controlled by the default automated driving logic in Jo et al. (2022); Jo (2022).

4. Results

Based on the datasets obtained from the real-world field tests with respect to the four comparison models, we present the characteristics of each model using several numerical studies in terms of driving safety, ride comfort and energy efficiency. The following subsection describes what criteria are used for measuring the performances of each model.

4.1. Evaluation Metrics

This study assesses the performances of the comparison models based on several evaluation metrics in terms of safety, comfort and efficiency. From the safety perspective, we consider several evaluation metrics for longitudinal and lateral safety driving performance measures. It is natural to characterize the driving safety based on historical crash or conflict data. However, real safety-related measures derived from those accident data are hardly utilized due to some limitations; i) accidents or incidents are rare events (Theofilatos et al., 2016), ii) not all of those events are reported (Laureshyn, 2010), iii) limited information on the failure mechanism are provided (Tarko, 2018). To deal with these issues, the concept of *surrogate safety measure*, which is an alternative or a complement to the reactive approaches (Johnsson et al., 2021), is adopted in this research to conduct numerical study regarding safe driving performance.

One of the surrogate safety measures used in the current study is ***longitudinal severe deceleration***, which is often used as a proxy measurement to identify a hazardous event associated with longitudinal driving behavior (Lee and Yeo, 2015; Tak et al., 2015; Lee and Yeo, 2016; Lee et al., 2017, 2019a,b). Another safety-critical driving event can be easily observed in ***longitudinal hard acceleration*** maneuvers (Palacio et al., 2009; Eboli et al., 2016; Feng et al., 2021). Since the vehicle dynamics of transit bus is totally different from those of light vehicles, both severe deceleration and hard acceleration rates should be considered in a conservative manner. According to the criteria on the risky driving behaviors of transit bus with respect to the longitudinal deceleration and acceleration rates investigated by the Korea Transportation Safety Authority (TS),[2] the severe deceleration and hard acceleration rates are herein set to -2.5 $\mathrm{m/s^2}$ and 1 $\mathrm{m/s^2}$, respectively. Furthermore, this study adopts ***Lateral Position Variation*** (LPV) (Tak and Choi, 2022), which is also known as lane offset or lateral offset (Chu et al., 2018; Das et al., 2019), for capturing the unstable steering control of the transit bus. The LPV is calculated as follows:

$$LPV = \min\left(\left|y_{left}^{dist} - \frac{l_{width}^{sub}}{2}\right|, \left|y_{right}^{dist} - \frac{l_{width}^{sub}}{2}\right|\right), \tag{12}$$

where y_{left}^{dist} indicates the distance from the vehicle center to the left lane in the vehicle-moving direction, y_{right}^{dist} represents the distance from the vehicle center to the right lane in the vehicle-moving direction, and l_{width}^{sub} describes the width of the ego vehicle. The LPV is used for monitoring whether the transit bus drives excessively to the left or right from the centerline. This study considers the LPV as the surrogate measure to monitor the safety performance of lateral driving behavior. The minimum allowable value for the LPV is set to 0.01 m though it may vary with given geometric conditions, such as road grade and curvature.

To explore the characteristics of the proposed system from the comfortable driving perspective, we use ***lateral severe deceleration*** and ***lateral hard acceleration*** as the surrogate measures to identify uncomfortable events (Nguyen et al., 2019; Bakhshi et al., 2021). Even though there have been different criteria for identifying the uncomfortable events by using the surrogate measures, it is well known that they are certain ranges of lateral deceleration and acceleration rates for determining the discomfort, particularly in the transit bus (Bae et al., 2019). The previous study reported that -0.9 $\mathrm{m/s^2}$ of lateral deceleration rates and 0.9 $\mathrm{m/s^2}$ of lateral acceleration rates are the lateral ride discomfort threshold values for public transportation. Since the transit bus is required to consider both seated and standing passengers, the threshold values are much less than those of light vehicles. More conservative threshold values of the lateral deceleration and acceleration are considered in this study to guarantee the ride comfort of passengers. The lateral severe deceleration and lateral hard acceleration rates are herein set to -0.5 $\mathrm{m/s^2}$ and 0.5 $\mathrm{m/s^2}$, respectively.

[2] http://etas.ts2020.kr/etas/frtl0401/pop/goList.do

In terms of efficiency measures, we employ ***vehicle speed*** and ***energy consumption***. These are conventional metrics to measure operational efficiency in previous studies on the OSA and GLOSA system. More specifically, the transit bus's speed can be categorized into twofold: instantaneous speed and average operation speed. The former indicates the instantaneous bus travel speed. The latter represents the average bus speed along the BRT rout, which is often used for monitoring the overall LOS of bus transit (Weng et al., 2013). Both measures are considered in this study to evaluate the effectiveness of imposing the proposed system. In addition, the vehicle speed trajectory is also discussed to explore the detailed characteristics on the performance of the proposed system.

Based on the surrogate measures of safety, comfort and efficiency associated with the connected and automated BRT service, we conduct a comparison study to evaluate and verify the performance of the proposed system. The following subsection provides the detailed descriptions on a real-world experiment for the comparison study.

4.2. Safe Driving Performance

4.2.1. Longitudinal Acceleration

Figure 11 shows the results for longitudinal acceleration among the driving test results of Driver, AV, USG-CAV, and SSG-CAV. In addition, it presents the characteristics analysis and the performance in terms of driving safety for

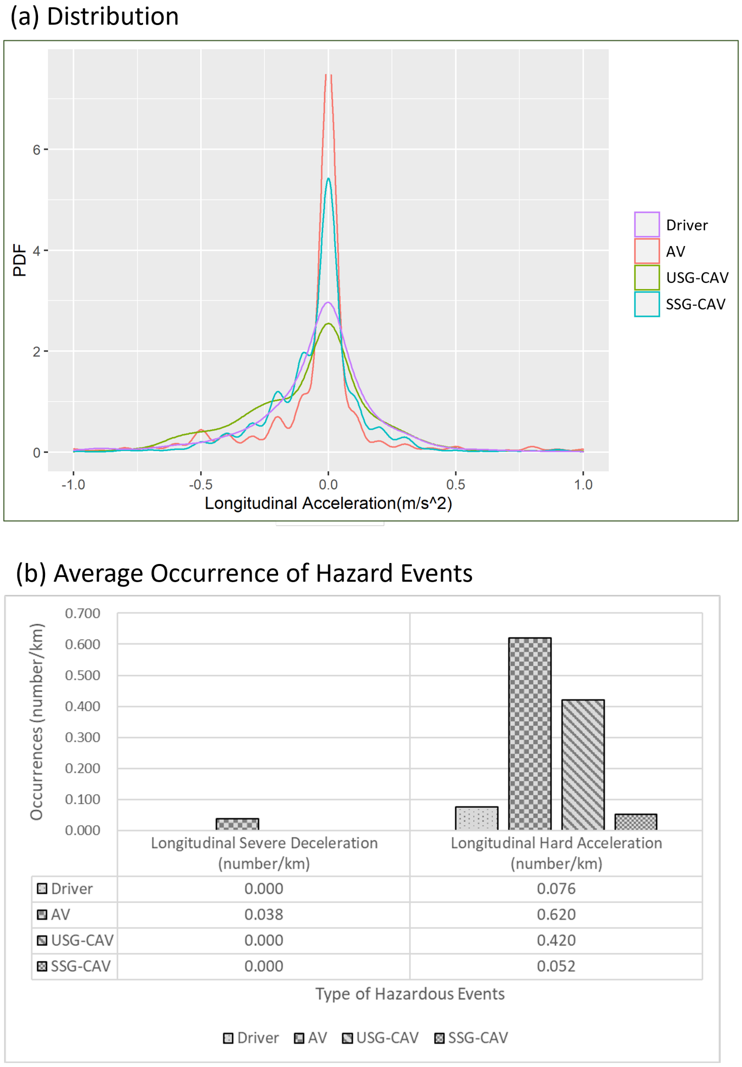

Figure 11: (a) Distribution and (b) Occurrences of Hazardous Events of Longitudinal Acceleration

the longitudinal movements of the four driving types. The four driving types show different characteristics, as shown in the distributions of longitudinal acceleration of Figure 11 (a). In the case of Driver, which serves as the reference in this study, the mean acceleration is $-0.042m/s^2$ with a standard deviation of $0.275m/s^2$, which is relatively dispersed compared with the other driving types. In other words, although the highest frequency is exhibited around $0m/s^2$, which declines as the acceleration value increases or decreases, similar to the other distributions, the degree of decline is relatively gradual. Among the four driving types, AV exhibits the highest frequency of values concentrated on 0, with a mean of $-0.023m/s^2$ and a standard deviation of $0.356m/s^2$. Moreover, it exhibits the steepest frequency decline as the acceleration value increases or decreases. However, despite its shape, the standard deviation of this distribution is larger than that of Driver. This discrepancy can be attributed to the fact that the values are less than $-0.5m/s^2$ and greater than $0.5m/s^2$, which are far away from 0, exhibit higher frequencies in the case of AV compared with the other distributions. The different results obtained in one distribution are understood to be due to the behavioral characteristics of AV. In the case of AV, the movement of longitudinal acceleration close to 0 is shown before the severe deceleration or hard acceleration situation occurs. Because of this, if a dangerous situation or a situation that requires acceleration occurs, relatively severe deceleration or harder acceleration is applied.

In the case of USG-CAV, downstream information is received in advance through speed guidance system and used to control the vehicle. Therefore, the longitudinal accelerations are concentrated less on 0 compared with those of AV. Consequently, USG-CAV exhibits a mean acceleration of $-0.041m/s^2$ and a marginally lower standard deviation of $0.329m/s^2$ than that of AV. However, despite their similarity, the cause of the deviation differs. In the case of USG-CAV, the standard deviation is large because its tendency to be concentrated at 0 is the lowest among the four driving types. In other words, it uses a broader range of longitudinal acceleration than AV to control the vehicle because it can early respond to the downstream information compared with AV. Finally, SSG-CAV exhibits a mean acceleration of $-0.040m/s^2$ with a standard deviation of $0.204m/s^2$, which is the lowest among the four driving types. The distribution SSG-CAV has the second-highest concentration on 0, after AV. However, in contrast to AV, the number of values below $-0.5m/s^2$ and above $0.5m/s^2$ is the least among the four driving types. Since the information on downstream situations allows the SSG-CAV to proactively react to the future traffic state (Tak et al., 2016a), the SSG-CAV could respond more effectively to the situations where severe deceleration and hard acceleration occurred, based on the guided speed that reflects the downstream situations compared with AV. Because of the effective response to the downstream, a clear difference was observed in the distribution of longitudinal acceleration between USG-CAV and SSG-CAV. SSG-CAV responded effectively to the downstream situations by guiding the speed based on the road information for a longer section compared with USG-CAV. Consequently, the deceleration phase from $-0.2m/s^2$ to $-0.8m/s^2$ and the acceleration phase from $0.2m/s^2$ to $0.7m/s^2$ could be replaced with an acceleration of $-0.2m/s^2$ to $0.2m/s^2$.

As shown in the distribution of longitudinal acceleration, the analysis results in terms of driving safety varied with the driving type because of the different longitudinal movements. Figure 11 (b) quantifies the performance in terms of driving safety through the number of occurrences of longitudinal severe deceleration. The performance in terms of driving safety is also quantified using the number of occurrences of longitudinal hard acceleration. As shown in the figure, AV exhibits the highest number of occurrences of longitudinal severe deceleration, i.e., $0.038/km$. In other words, AV performs worst in terms of the longitudinal safety. In contrast, Driver, USG-CAV, and SSG-CAV were almost free of hazardous events in terms of longitudinal severe deceleration. On comparing AV with USG-CAV and SSG-CAV, it is observed that the vehicle's safety performance can be improved significantly by utilizing guided speed reflecting the downstream information in the vehicle control in advance.

The differences between the driving types were more distinct in terms of longitudinal hard acceleration when compared with longitudinal severe deceleration. AV exhibited the highest number of occurrences, $0.620number/km$, followed by USG-CAV, Driver, and finally SSG-CAV. Importantly, the SSG-CAV proposed in this study provides the highest driving safety when compared to the reference of the Driver. SSG-CAV can avoid hard acceleration because it gradually accelerates the vehicle in advance based on the traffic signal changes and the congestion information around the bus stop. Furthermore, in the case of AV, if the signal is red when the vehicle approaches the signal intersection and suddenly turns into green as it approaches the stop line, hard acceleration may occur owing to the sudden change from stop mode to acceleration mode. However, the proposed SSG-CAV can overcome this drawback by predicting the signal change in advance. Consequently, it minimizes the deceleration as the vehicle approaches the stop line and responds to the signal change in advance through mild acceleration.

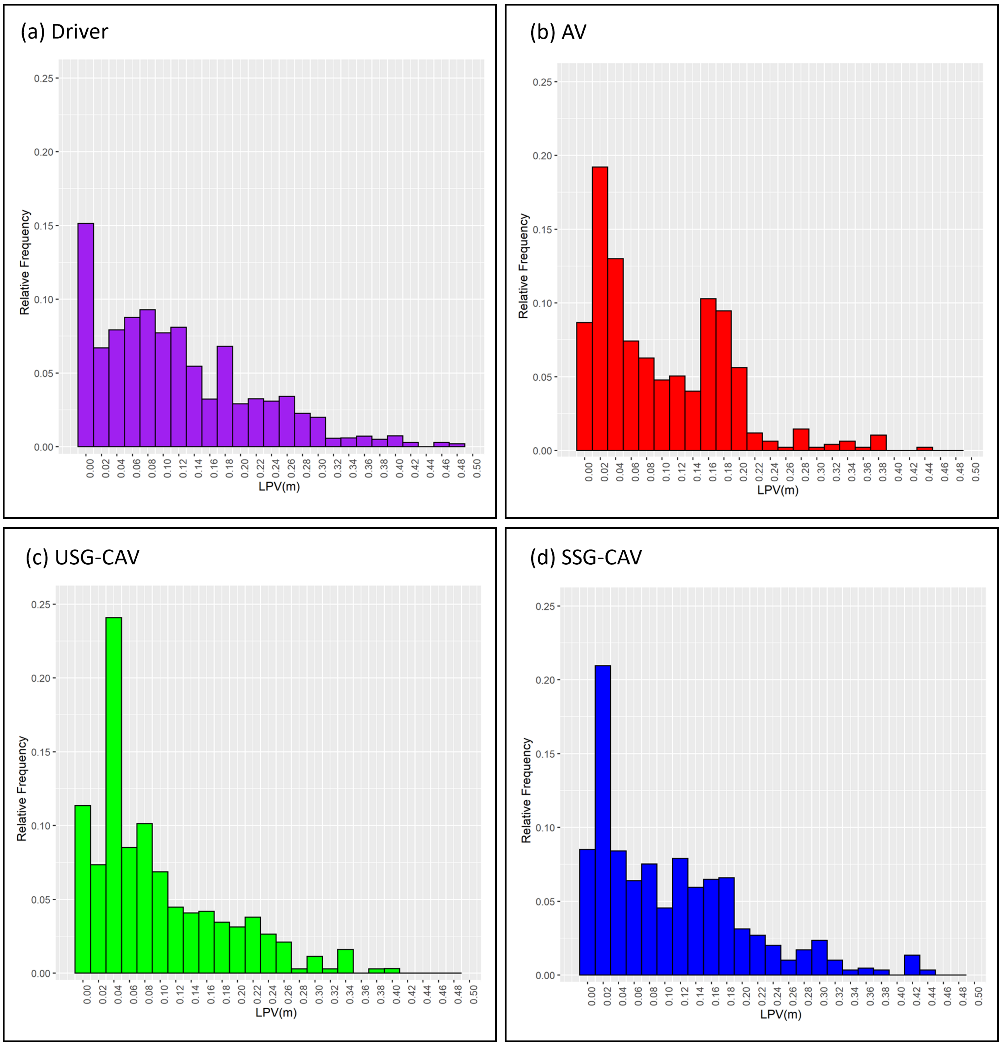

Figure 12: Distribution of Lateral Position Variation (LPV)

4.2.2. Lateral Position Variation

Figure 12 shows the results of the LPV, which is related to the stability of longitudinal control of the vehicle. It is a dangerous state when the LPV gets closer to 0, which represents that the ego vehicle is on one side of the lane. Otherwise, it is a safe state when the LPV is far away from 0, which suggests that the ego vehicle follows the center line. As shown in the distribution of LPV of Figure 12 (a), the four driving types show similar trends, in which the mode section appears between 0 and 0.04, and the frequency decreases gradually as the LPV increases beyond 0.4. All four driving types have a mode section between 0 and 0.4 because the road on which the vehicle traveled is not sufficiently wide for the bus. Moreover, the entrance and exit sections of the overpass and underground bridges could narrow abruptly, and the road's linearity could change rapidly. In this case, the vehicle describes a path biased to one side of the lane.

The overall change in LPV is similar in the four driving types. However, the degree of change in LPV frequency differs according to the increase in LPV value. Driver's LPV shows the most gradually decreasing distribution with a mode between 0 and 0.01. In the case of Driver, the mode section occurs at the lowest LPV among the four driving types, indicating that Driver is the driving type with the riskiest mode section. The LPV of AV has a mode between 0.01 and 0.03. Although the frequency decreases gradually as the LPV increases, the second-highest frequency section is found in the LPV section of 0.15 to 0.19. The characteristics of the second-highest frequency in AV is that certain sections (Link ID : A2207G001386, A2207G002820) account for 87% of the occurrences, indicating a decline in driving stability of AV in certain sections. Because of these two distinct mode sections of AV, the frequency of a stable LPV section of 0.20 or higher accounts for the smallest proportion in AV, among the four driving types. In USG-CAV and SSG-CAV, the mode section shows a more stable distribution than in AV. In particular, SSG-CAV shows the distribution characteristics of a gentle slope after the mode section compared with AV and USG-CAV, resulting in a higher mean and standard deviation. However, the mean and the standard deviation are marginally lower in SSG-CAV than in Driver. In other words, through the speed guidance for each road section, the performance in terms of LPV can be improved more in SSG-CAV than in AV. In short, using speed guidance SSG-CAV can achieve performance comparable to that of Driver.

Figure 13 shows the analysis results of the stability and risk of LPV based on the driving data. Figure 13 (a) shows the percentage of LPV over $0.3m$ for each driving type. A value close to 100% indicates a high frequency of driving close to the center line; a value approaching 0% indicates fewer cases of driving close to the center line. In other words, it shows how often the vehicle traveled stably on the center line of the lane for each driving type. As shown, the percentage of driving with an LPV of over 0.3 is 6.63% for Driver, which is the highest. Among AV, USG-CAV, and SSG-CAV, which is driven automatically, AV shows the lowest value (2.91%), and SSG-CAV shows the highest value (6.19%). Among the automated driving types, SSG-CAV shows the highest frequency of driving close to the center line of the lane. The value of SSG-CAV is similar to that of Driver. In other words, if the proposed system is applied to automated driving, it can prevent longitudinal and lateral severe deceleration and hard acceleration by providing sectionalized speeds, thereby improving the stability of lateral control.

Figure 13 (b) shows the occurrence frequency of hazard events arising with an LPV of $0.01m$ or less for each driving type. A situation, in which the distance from the left or right lane is less than or equal to $0.01m$, indicates that the vehicle is driving extremely close to the adjoining lane. This situation is considered as a dangerous condition comparable to crossing over the lane. As depicted in Figure 13 (b), the highest count of occurrences for the hazard events could be observed in Driver, which is $1.646/km$. AV and USG-CAV showed similar values with $0.668/km$ and $0.697/km$, respectively, resulting in the second and third-highest number of hazardous events, after Driver. SSG-CAV showed the lowest occurrence frequency ($0.239/km$) among the four driving types. Similar to the analysis results of Figure 13 (a), the vehicle's lateral driving safety has also been improved by providing an appropriate guided speed for each section. However, in contrast to the results from Figure 13 (a), Driver showed the lowest driving safety among

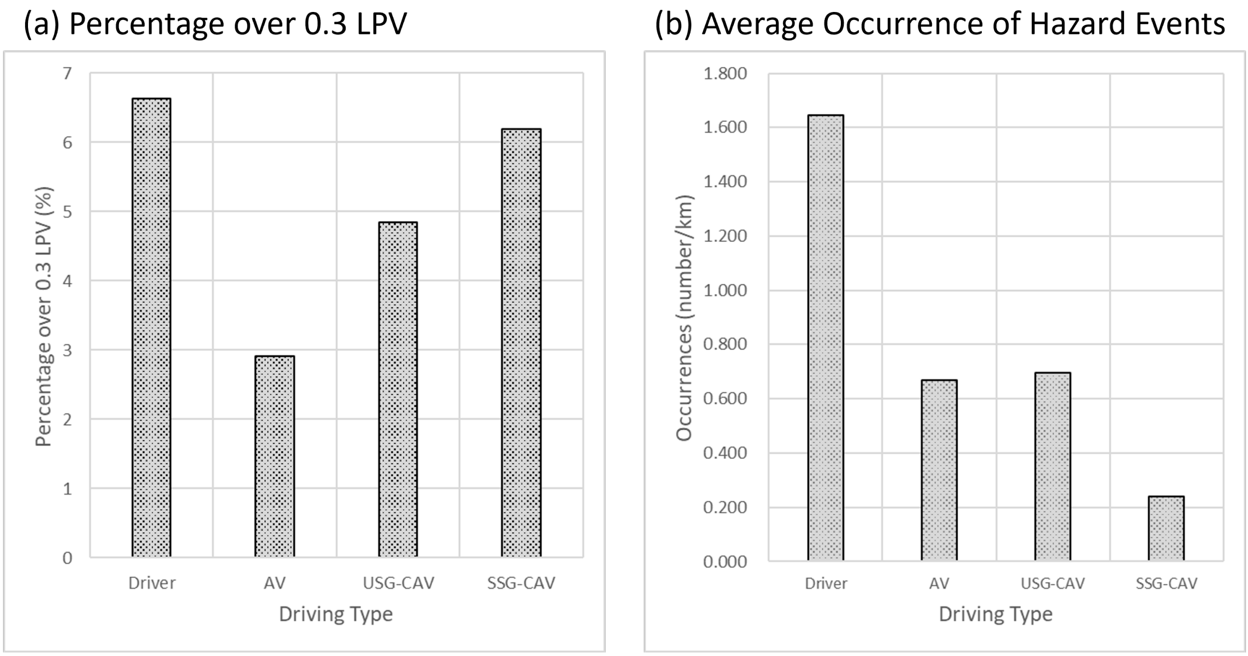

Figure 13: Analysis Results of LPV in terms of (a) percentage over 0.3 LPV and (b) Average Occurrence of Hazard Events

the four driving types. This discrepancy in behavior is the result of the driver responding actively to the topographic characteristics of the site, rather than the result of the driver's poor driving safety. The test site consists of a road section that is too narrow for the bus to travel and road facilities on the right side. In this case, to avoid a collision with the road facilities on the right side, the driver may intentionally drive extremely close to the road center line. The driver may even violate the road center line in situations where no vehicle is approaching from the opposite side.

4.3. Comfortable Driving Performance

4.3.1. Lateral Acceleration

Figure 14 shows the results for lateral acceleration, which can be used to analyze the characteristics of the vehicle's lateral movement and performance for ride comfort. As shown in the distribution of lateral acceleration of Figure 14 (a), the four driving types show similar characteristics overall: the mode is observed around 0, following which, the frequency decreases as the lateral acceleration increases or decreases. However, the increasing and decreasing patterns differ between the four driving types in the section where the lateral acceleration rate is greater or less than $0m/s^2$. In the case of Driver, which serves as the reference in this study, a shape similar to a normal distribution with a mean of $-0.0165m/s^2$ and a standard deviation of 0.126 is observed. In the range where the lateral acceleration

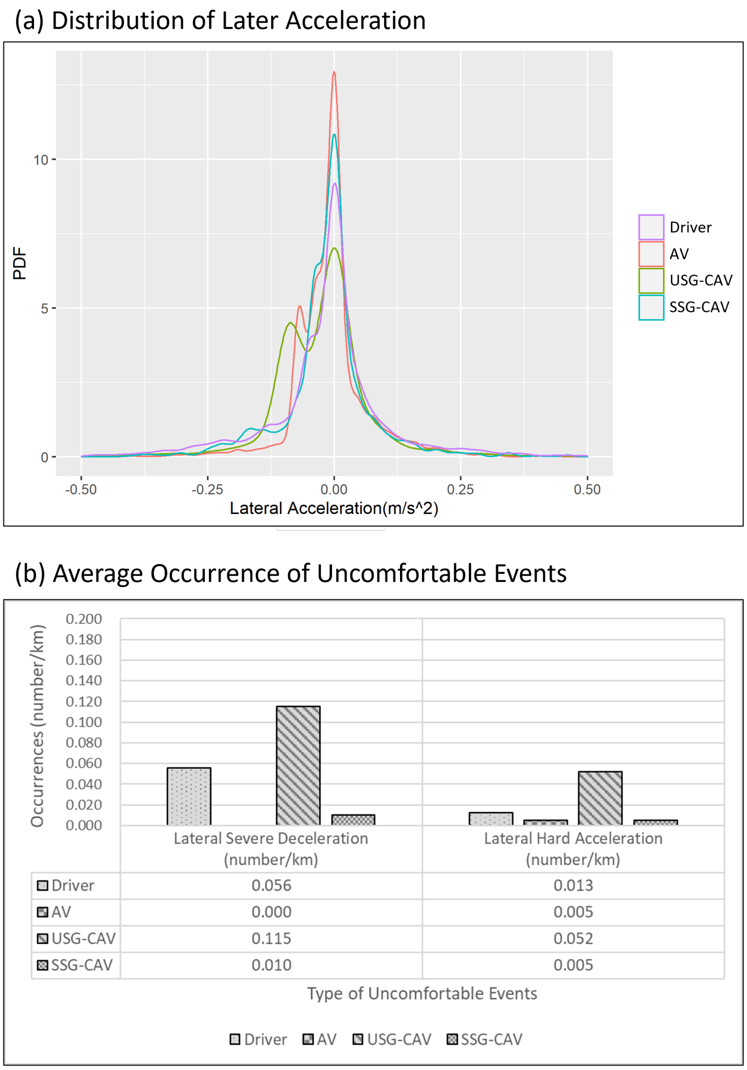

Figure 14: (a) Distribution and (b) Occurrences of Uncomfortable Events of Lateral Acceleration

rate is greater than $0m/s^2$, the other three driving types (AV, USG-CAV, SSG-CAV) have distributions similar to that of Driver. However, when the lateral acceleration is smaller than 0, their characteristics differ. AV and USG-CAV exhibit a sudden increase in frequency around $-0.06m/s^2$ and $-0.10m/s^2$, respectively, and then decreases sharply afterward, in contrast to Driver. This difference in behavior can be attributed to the fact that the topographic conditions cause a degradation in the lateral control performance of the vehicle, resulting in a sudden concentration of lateral acceleration on a particular value. Conversely, SSG-CAV has a distribution shape similar to that of the Driver and shows the exhibits a gradual decline in frequency as the lateral acceleration decreases.

Figure 14 (b) is a graph of results to estimate the ride comfort for lateral movement on the BRT bus. In the figure, the Lateral Severe Deceleration shows the number of occurrences of lateral deceleration less than $-0.5m/s^2$, and the Lateral Hard Acceleration shows the number of occurrences of lateral acceleration greater than $0.5m/s^2$. As shown in the figure, the four driving types show different behaviors in terms of Lateral Severe Deceleration and Lateral Hard Acceleration. In the results of Lateral Severe Deceleration, USG-CAV shows the highest frequency, i.e., $0.115/km$, of uncomfortable occurrences of lateral severe deceleration, followed by Driver, SSG-CAV, and finally AV. The same ranking is found in the case of uncomfortable occurrences of lateral hard acceleration: USG-CAV shows the highest frequency with $0.052/km$, followed by Driver, SSG-CAV, and finally AV. Taking the results of Driver as reference for evaluating the performance of the respective driving types, the ride comfort for lateral movement is observed to be higher in the cases of AV and SSG-CAV and lower in the case of USG-CAV. These differences are shown between AV, USG-CAV, and SSG-CAV because of the difference in guided speed provided for each section. In other words, the subject vehicle's speed is controlled according to the guided speed provided when a section changes to another section, which is accompanied by the change in lateral acceleration. Consequently, uncomfortable lateral acceleration occurs more frequently in USG-CAV than in SSG-CAV because the length of the sections where a guided speed is provided is short, resulting in several situations where the speed must be changed.

4.4. Efficient Driving Performance

4.4.1. Vehicle Speed and Energy Consumption

Figure 15 shows instantaneous speed distributions of four driving types based on the field testing in the study site, where the instantaneous speeds are measured with $0.1 - second$ intervals. To show the speed distribution when the vehicle is traveling, the situations where the speed is $0m/s$ in the stopped state are excluded from the histograms. As shown in the figure, the four driving types show different distributions. Driver exhibits a mode of $11.75m/s$, which is the highest one among those of the four driving types, and the distribution is concentrated around the mode. Consequently, the mean of the distribution is $9.668m/s$, which is the highest among those of the four driving types, and the variance is 2.42, which is a relatively large value. Furthermore, the maximum speed of Driver is $13.75m/s(49.5km/h)$, which is the closest value to the speed limit of the section, i.e., $13.89m/s(50km/h)$. The range of speeds extends from 0 to $13.75m/s$ depending on the situation, and the speed approaches the maximum when necessary.

The preferred speed in AV is concentrated in a small range. As shown, AV shows a relative frequency of 0.1 or higher at $6.75m/s$, $9.25m/s$, and $11.75m/s$, and shows a pattern, in which the frequency decreases sharply for the speed around the section. Because of these characteristics of the distribution, the mean of the distribution is $7.56m/s$, which is lower than that of Driver. In contrast, the standard deviation of AV's speed distribution shows the highest one among the four driving types, which corresponds to $2.915m/s$. The maximum speed of AV is $12.25m/s(44.1km/h)$, which is slightly less than that of Driver. Combining these characteristics, it can be inferred that AV has a preferred driving speed depending on the situation. Moreover, the standard deviation increases due to the increases in the gap between the preferred speeds. Furthermore, considering that the speed limit in the test section is $13.89m/s(50km/h)$, AV drives at a maximum speed that is approximately 10% lower than the speed limit.

Among the four driving types, USG-CAV exhibits the most concentrated speed distribution in the mode section. The mode section is found at $7.75m/s$ with a mean of $7.404m/s$ and a standard deviation of 2.029. USG-CAV shows the lowest mean speed and standard deviation among the four driving types. The maximum speed is $10.75m/s(38.7km/h)$, which is 22.6% lower than the speed limit of the section and also the lowest value among the four driving types. The low values of USG-CAV are low and their concentrated in a certain section can be attributed to the fact that the unit length of the speed guidance is short in USG-CAV. In other words, the guided speed changes before the vehicle's achieves the guided speed provided by the management center. For example, it is assumed that the current speed is $30km/h$, and the management center has sent a guided speed of $40km/h$ to the automated vehicle. Furthermore, when the vehicle's speed has reached around $35km/h$, the vehicle has already traveled through the section for which the guided speed was provided. At this point, the automated vehicle receives a guided speed for the next section. Here, if

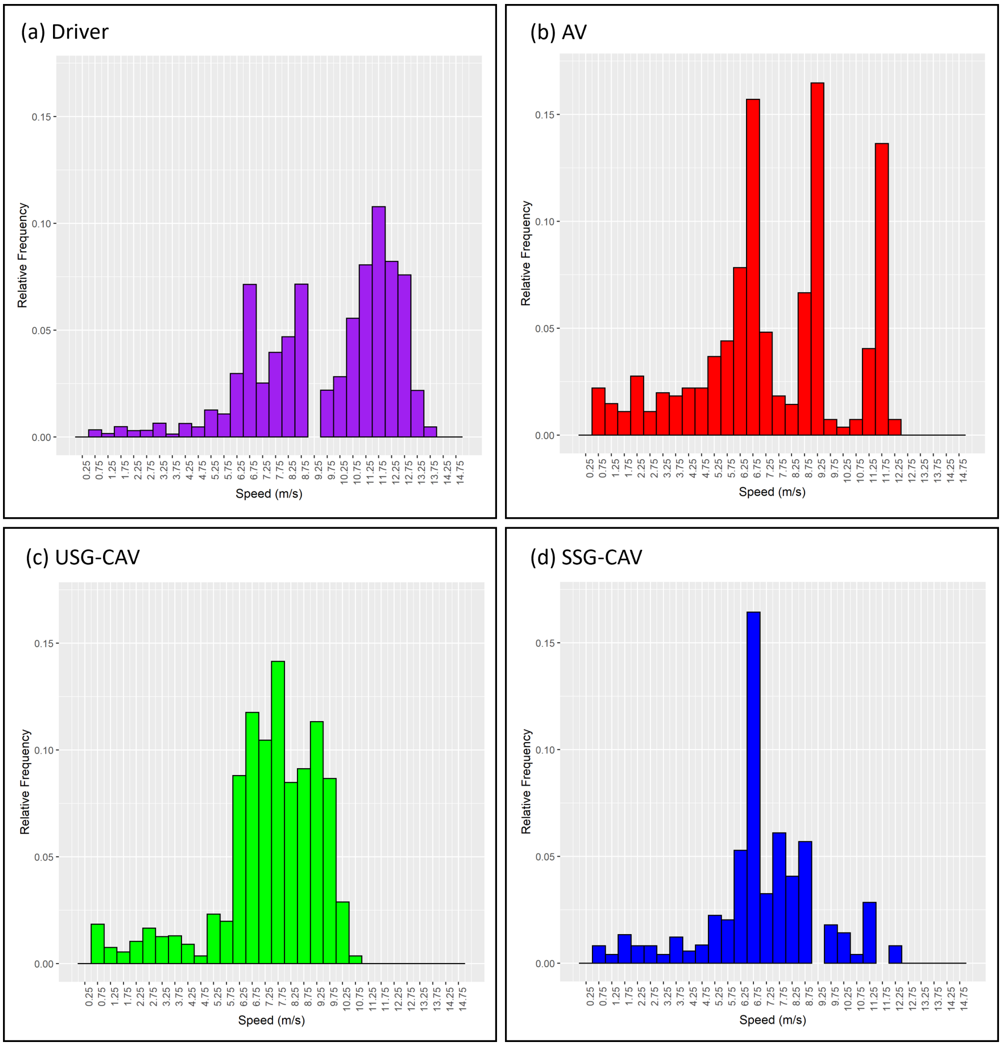

Figure 15: Instantaneous Speed Distribution of (a) Driver, (b) AV, (c) USG-CAV, and (D) SSG-CAV

$30km/h$ is received as the guided speed, the vehicle is controlled to reduce the speed again. In other words, because the length of the section for which the guided speed is provided is short, the vehicle's actual speed converges to the mid-level of the changes in the guided speed. Consequently, the speeds of USG-CAV are concentrated in a certain domain, and the maximum speed is low, as shown in the figure.

In contrast, SSG-CAV provides guided speeds for longer sections. Thus, it exhibits a distribution that overcomes the drawbacks of USG-CAV and AV. In contrast to AV, in which speeds were concentrated at three specific values, and USG-CAV, in which the distribution was concentrated on a certain domain, SSG-CAV exhibited the highest frequency at $6.75m/s$. However, the distribution of speeds is relatively wide before and after the highest frequency section. In other words, a marginally wider range of speed is used for control when compared with the other automated driving types. This result is related to the results of longitudinal acceleration and lateral acceleration analyzed earlier. In other words, because the distribution of the preferred speeds is very narrow for AV and USG-CAV, severe braking is likelier in a situation that requires stopping, such as case of congestion. In the case of SSG-CAV, however, the distribution of the preferred speeds is wide and relatively homogeneous, which enables a smoother response to stopping situations. The speed distribution of SSG-CAV has a mean of 8.39 m/s and a maximum value of $12.25m/s(44.1km/h)$, which is relatively high. Furthermore, when compared with USG-CAV, the increase in speed is clearly observed owing to the sufficient length of the section, in which a guided speed is provided, which allows the vehicle sufficient time to achieve

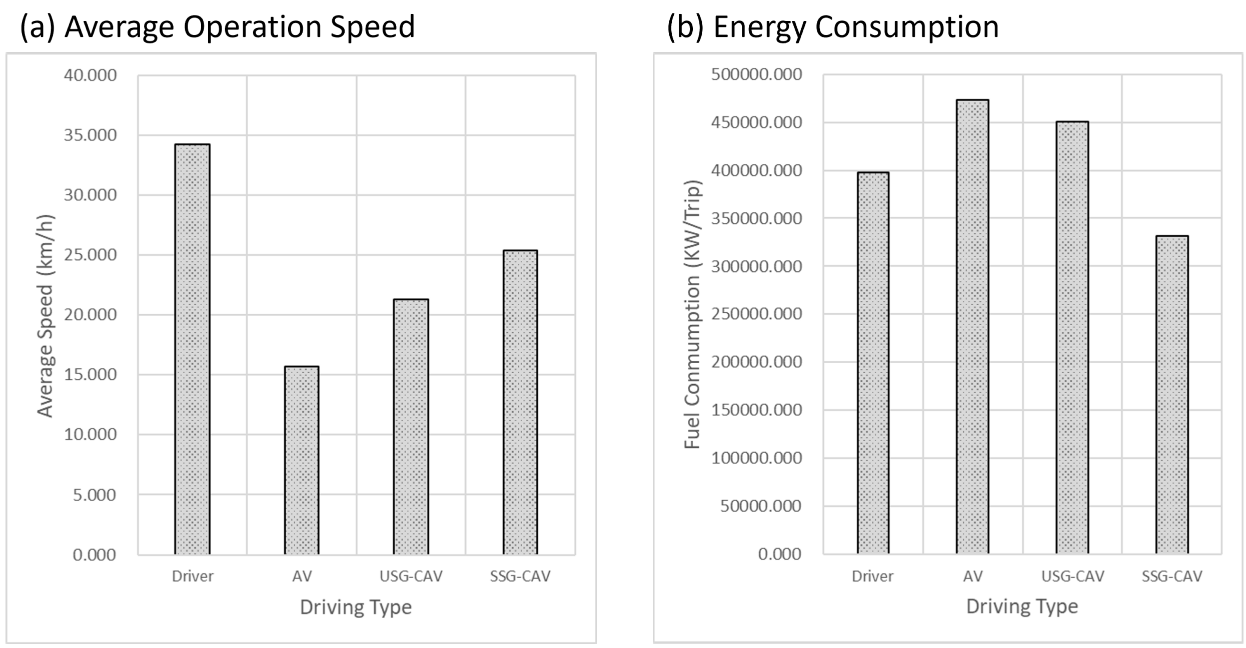

Figure 16: (a) Average Operation Speed and (b) Energy Consumption

the guided speed.

Figure 16 shows the average operation speed and average energy consumption, which demonstrates the vehicle's traveling efficiency. The average operation speed was calculated by dividing the length of the test section by the time required for traversing it. The average speed in Figure 16 (a) reflects the delay caused by the road elements, such as stopping at the signal, and the delay in providing public transportation services, such as stopping to allow the passengers to board or alight. As shown in the figure, Driver showed the highest average operation speed, followed by SSG-CAV, USG-CAV, and finally AV. As shown in the figure, the driver showed the highest average operation speed, followed by SSG-CAV, USG-CAV, and finally, AV. In general, the operation speed of the current AV is lower than that of the driver due to the limited driving capability of the AV system, and these results are observed in the previous research on AVs (Le Vine et al., 2015; Ainsalu et al., 2018; Salonen and Haavisto, 2019; Paddeu et al., 2020; Litman, 2020; Fujiwara et al., 2022). One of the primary purposes of SSG-CAV is to improve the operation speed of AV by providing the guided speed for each road section. As shown in the figure, by utilizing the guided speed for vehicle control, the proposed SSG-CAV increases the operation speed compared to other driving modes except for the driver. The differences in average operation speed are significantly affected by the vehicle's driving speed, as previously determined in Figure 15. The automated driving types(SSG-CAV, USG-CAV, and AV) show differences from the average values of the instantaneous speeds shown in Figure 15. For instance, AV and USG-CAV exhibit similar average instantaneous speeds. However, their average operation speeds clearly differ. This difference can be attributed to the fact that USG-CAV received the signal-related information near the intersection. Subsequently, it used this information in controlling the vehicle, thereby minimizing the stops caused by signals that may occur near the intersection. As a result, an increase in the average operation speed is observed in SSG-CAV by minimizing the unnecessary stops with guided speed from the Traffic Management Center.

Figure 16 (b) shows the energy efficiency for the four driving types. SSG-CAV consumes the lowest amount of energy, followed by Driver, USG-CAV, and then AV. SSG-CAV exhibits the lowest energy consumption because the Traffic Management Center provides the optimal guided speed based on the the signal information around the intersection and the congestion information near the bus stop in real-time. Consequently, unnecessary acceleration is inhibited when stopping is expected, and unnecessary deceleration is inhibited when the vehicle is expected to pass uninterrupted at the signals. In addition, the situation at the intersection is determined in advance based on the signal information, and the vehicle is controlled to minimize the stops at the intersection through controls, such as speed reduction. This minimizes the occurrence of unnecessary deceleration, acceleration, and stopping, thereby resulting

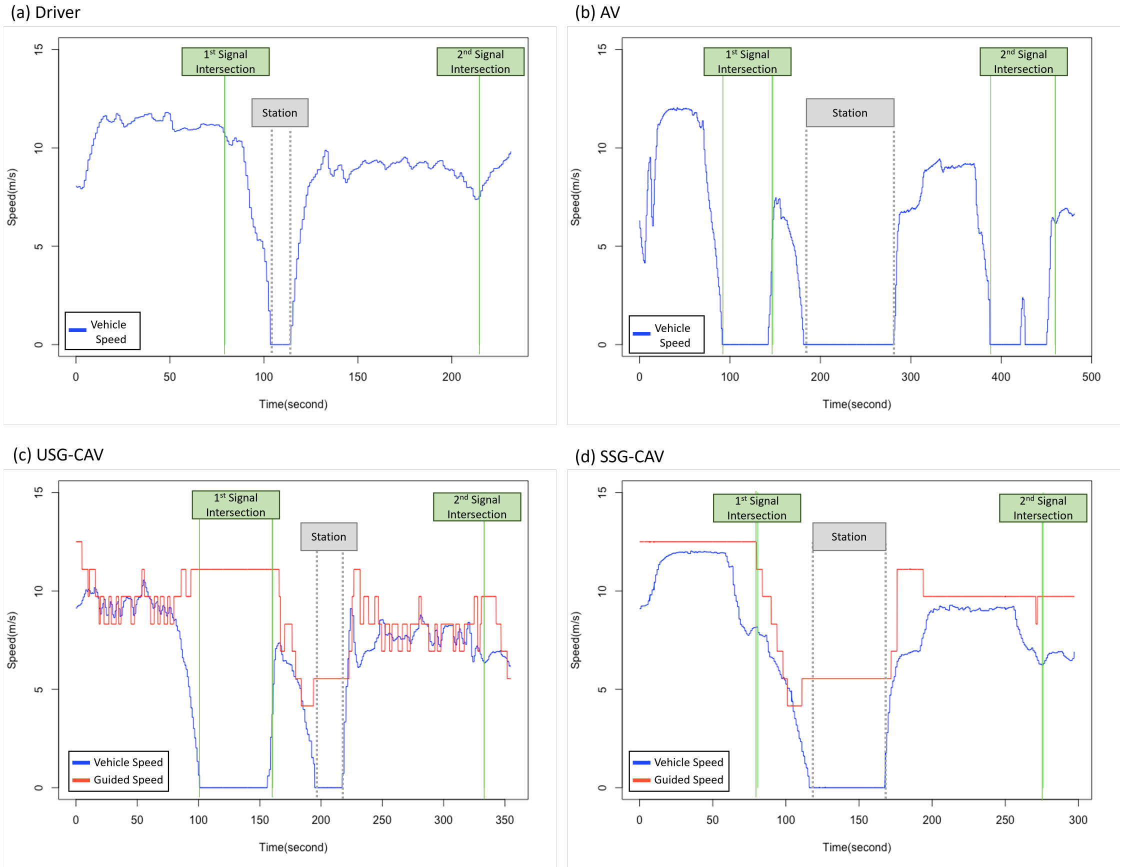

Figure 17: Speed Profile of (a) Driver, (b) AV, (c) USG-CAV, and (d) SSG-CAV

in the lowest energy consumption among the four driving types. USG-CAV can also respond in advance to the traffic situation occurring downstream to achieve lower energy consumption, compared with AV. However, because of the relatively short lengths of the sections where guided speeds are provided, it exhibits more frequent speed changes compared with SSG-CAV. Consequently, it consumes more energy than SSG-CAV. Comprehensive analysis shows that only SSG-CAV achieves lower energy consumption when compared with Driver.

Figure 17 shows speed trajectories for the driving data examples of the four driving types. In the case of Driver, which serves as the reference, the vehicle passed through the 1^{st} signal intersection without stopping and then stopped at a bus stop to allow passengers to board or alight. Afterward, the vehicle decelerated lightly to pass through the 2^{nd} signal intersection without stopping and then accelerated. In the case of AV, the vehicle entered the test section and traveled in a similar manner as Driver. However, it stopped at the 1^{st} signal intersection for the red signal owing to the low speed at the initial entering section. Afterward, the vehicle stopped at a bus stop to allow passengers to board or alight and then departed, exhibiting speed changes similar to that of Driver. However, it stopped at the 2^{nd} signal intersection for the red signal.

Figure 17 (c) and (d) show the cases of USG-CAV and SSG-CAV. In the figures, the red line indicates the guided speed provided by the Traffic Management Center, and the blue line represents the vehicle's driving speed. As shown in the figures, the length of the section where guided speeds were provided was shorter in USG-CAV than in SSG-CAV. Thus, the provided guided speed was changed frequently. USG-CAV controls its driving speed continuously to follow the guided speed. However, the result is that it follows the average of the frequently changing guided speed. Consequently, the vehicle stopped at the 1^{st} signal intersection for the red signal, following which, it stopped at a bus stop to allow passengers to board or alight, and then departed. At the 2^{nd} signal intersection, USG-CAV maintained a higher guided speed than that of AV. Based on this control, the vehicle received a green signal and passed through the 2^{nd} signal intersection without stopping. In SSG-CAV where the length of the section, in which information is provided, was longer, the provided guided speed does not change more frequently than in USG-CAV. Consequently, the vehicle follows the profile of the guided speeds provided by the traffic management center. Owing to the effect of the guided speed, SSG-CAV can pass through both the 1^{st} and 2^{nd} signal intersections without stopping. Furthermore, it can prevent dangerous situations, such as accidents and severe deceleration, that may occur around bus stops by obtaining the congestion information occurring around the bus stops and reducing the speed in advance.

5. Discussion

In the previous section, several numerical studies were performed to explore the characteristics of the proposed system based on various performance metrics. The most remarkable safety performance could be observed in the SSG-CAV showing less number of hazard events than others. However, it is still necessary to identify spatial distribution of road sections with a high driving risk in each driving type in order to analyze safety performances of individual driving types varying with spatial features. Therefore, a more detailed spatial analysis on the safety performances of each driving type is further conducted as follows.

Figure 18 shows the spatial distribution of *safety hazard score* in each driving type. The safety hazard score is calculated by summing the numbers of hazard event occurrences caused by longitudinal severe deceleration, hard acceleration and LPV every 10-m-segment along the route. For simplicity, the maximum value of the safety hazard score is herein set to 50. This indicates that it is more likely to show a high driving risk in a road section when the safety hazard score gets closer to its maximum value.

As depicted in Figure 18, the four driving types show critical road sections placed at different locations along the BRT route. It is also easily found that the number of road sections with a high value of safety hazard score is different depending on the driving type. We observe that there is only one road section with the maximum safety hazard score in the Driver, as shown in Figure 18 (a). Except for the road section with a red circle marked by the number 1, the Driver shows relatively low values of safety hazard score in other road sections along the route.

On the other hand, we find that the AV have more road sections with a high driving risk compared to other driving types, as shown in Figure 18 (b). There are four road sections with a high driving risk in the AV, where the safety hazard scores in the road sections with red circles marked by the number 1 to 3 reached the maximum, while the safety hazard score in the road section with the red circle marked by the number 4 showed 44. One can also observe that the USG-CAV has two road sections with the maximum safety hazard score, as shown in Figure 18 (c). The USG-CAV has less number of road sections with a high driving risk than those of the AV. However, the spatial distribution of the safety hazard scores in the rest of road sections along the BRT route describes that the USG-CAV show relatively high values of safety hazard scores compared to other driving types.

It is notable that the SSG-CAV has only one road section with the maximum safety hazard score in the BRT route, as shown in Figure 18 (d). Moreover, except for the road section with a red circle marked by the number 1, relatively low values of safety hazard score in the rest of road sections along the route are observed in the SSG-CAV, which is similar to the trends in the spatial distribution of the safety hazard scores in the Driver. This suggests that the SSG-CAV can secure the driving safety in a relatively wide range of road sections compared to the AV and SSG-CAV, which is consistent with the previous research findings from the result analyses on the longitudinal acceleration and LPV. Hence, the proposed system has a great potential to deal with the limitations associated with the conventional AV system in terms of longitudinal severe deceleration, hard acceleration or lateral instability.

To identify the causal factors of affecting the safety hazard score of each driving type, several features of the four critical road sections in the study site are provided in Figure 19. Figure 19 (a) describes the road section 1 where all the driving type show the maximum value of safety hazard score. The road section 1 represents the entrance to a bus station, where a curbstone is sticking out into the BRT lane as highlighted with the red dashed circle in Figure 19 (a). Since the curbstone interrupts the lane-following task, it enforces the approaching vehicle to adjust its lateral position rapidly for following the centerline of the BRT lane and avoiding collision with the curbstone. This leads to an decrease in the value of LPV, which results in a high value of safety hazard score. For instance, some extreme cases of the field testing in the road section showed two typical types of dangerous situations such as *go over-the-line* and *touch-the-line* events (Tak et al., 2022), which may lead to a head-on collision between two transit buses. Since both Driver and the others show the maximum value of safety hazard score due to the curbstone, irrespective of driving type, it is required to reconstruct the curbstone for dealing with the road geometry-related issue.

On the other hand, Figure 19 (b) presents the road section 2 where the AV and USG-CAV show the maximum value of safety hazard score. The road section 2 describes the entrance to a signalized intersection right after the north end

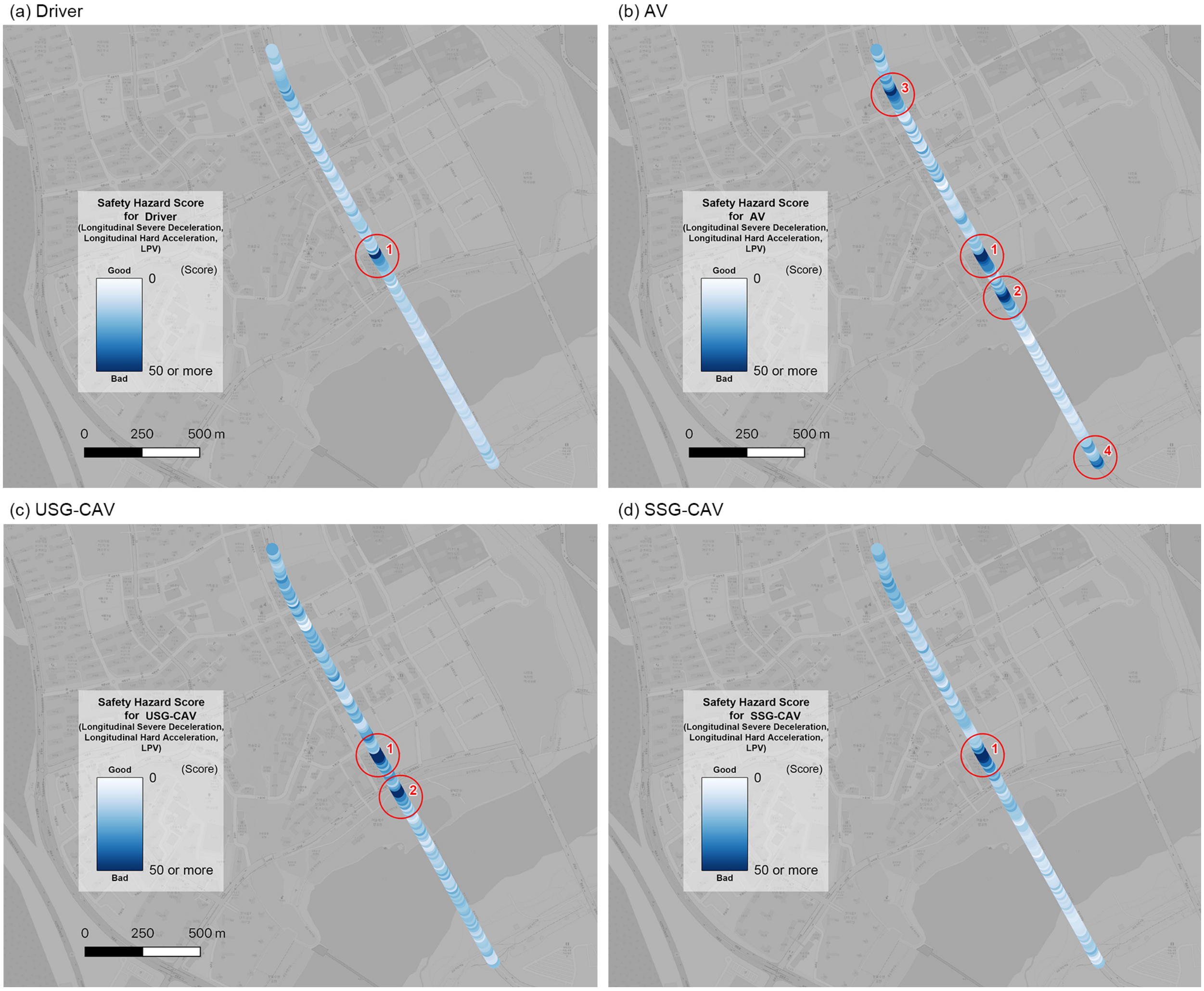

Figure 18: Spatial Distribution of Safety Hazard Score in (a) Driver, (b) AV, (c) USG-CAV and (d) SSG-CAV

of bridge. The value of LPV decrease due to the variation in the lane width caused by the change in the geometrical structure of curbside, such as the curbstone and road safety pole, as highlighted with the upper-left corner in Figure 19 (b). Moreover, the longitudinal severe deceleration events are frequently observed in the cases of reaction to the sudden change in traffic signal. For instance, the AV approaches to the upcoming intersection with its desired speed to pass through the signalized intersection in the green light phase, but the severe braking is inevitably applied for stopping behind the stop line for the intersection when the signal suddenly changes to red. Such events can be also found in the case of USG-CAV. The USG-CAV shows the maximum safety hazard score in the road section 2 since it cannot proactively respond to the change in the signal information due to the short length of the uniformly-distanced segments for determining its guided speed at the downstream site. The vehicles traveling upstream site may still be exposed to a potential collision situation because the detailed information is insufficient to predict the collision risk arising from downstream site (Lee et al., 2019b). In contrast to the AV and USG-CAV, the Driver and SSG-CAV consider the deceleration maneuver in a proactive manner. Particularly in the SSG-CAV, the guided speed is robust in the presence of time-varying environmental disturbances, such as dynamic changes in the road and traffic conditions, based on incorporating the driving risk into the ODD. Consequently, the safety hazard score of the SSG-CAV in the road section 2 is much lower than those of AV and USG-CAV.

Figure 19 (c) shows the characteristics of road geometric and traffic conditions with respect to the road section 3, where only the AV shows the maximum value of safety hazard score. The road section 3 describes the entrance to a

BRT station right after the end of an underground road, where the transit bus often suffers from the bus-stop congestion and is required for slowing down right after coming out of the underground road. Even though the in-vehicle sensors enable the AV to take an evasive action for a possible rear-end collision near the BRT station, there are not sufficient time to adjust the vehicle's speed with a mild deceleration due to the limited vertical angular field-of-view in case of the large changes in road grade such as the road section 3. Therefore, since the AV faces with a number of harsh braking events in the corresponding road section, it shows a higher value of safety hazard score compared to other ones.

Similar trends are also observed in the road section 4 where only the AV shows a high value of safety hazard score. As depicted in Figure 19 (d), the road section 4 describes the entrance of bridge. The value of LPV decreases due to large variations in road curvature when the AV travels at the entrance to the bridge, which results in a high value of safety hazard score. Since the AV system is operated reactively in the changes in road curvature, it requires to respond to the sudden changes in driving conditions, often resulting in poor driving outcomes. This suggests that the AV system needs to be precisely specify the ODD for safely performing its DDT (Colwell et al., 2018). Hence, it is necessary to uprate the safety performance of the existing AV system by considering additional elements associated with driving risks in the given ODD.

A numerical analysis is further conducted to discuss similarity of spatial characteristics with respect to safety hazard scores in a pair of two driving types every 10-m-segment along the BRT route. Taking the safety hazard score of Driver as a reference point, spatial trends in safety hazard scores with respect to two different driving types are depicted in Figure 20. The x-axis and y-axis in the subfigures indicate the distance along the route and safety hazard score, respectively. The correlation coefficient in each subfigure represents the Pearson correlation coefficient, which is one of the most widely used measurements for a linear relationship between two variables.

As shown in Figure 20 (a), overall, it can be seen that the safety hazard scores of AV are greater than those of Driver. This indicates that the AV has more road sections with high driving risks compared to the Driver. The average safety hazard scores of the AV and Driver were 20.005 and 16.565, respectively. Such results suggest that the existing AV

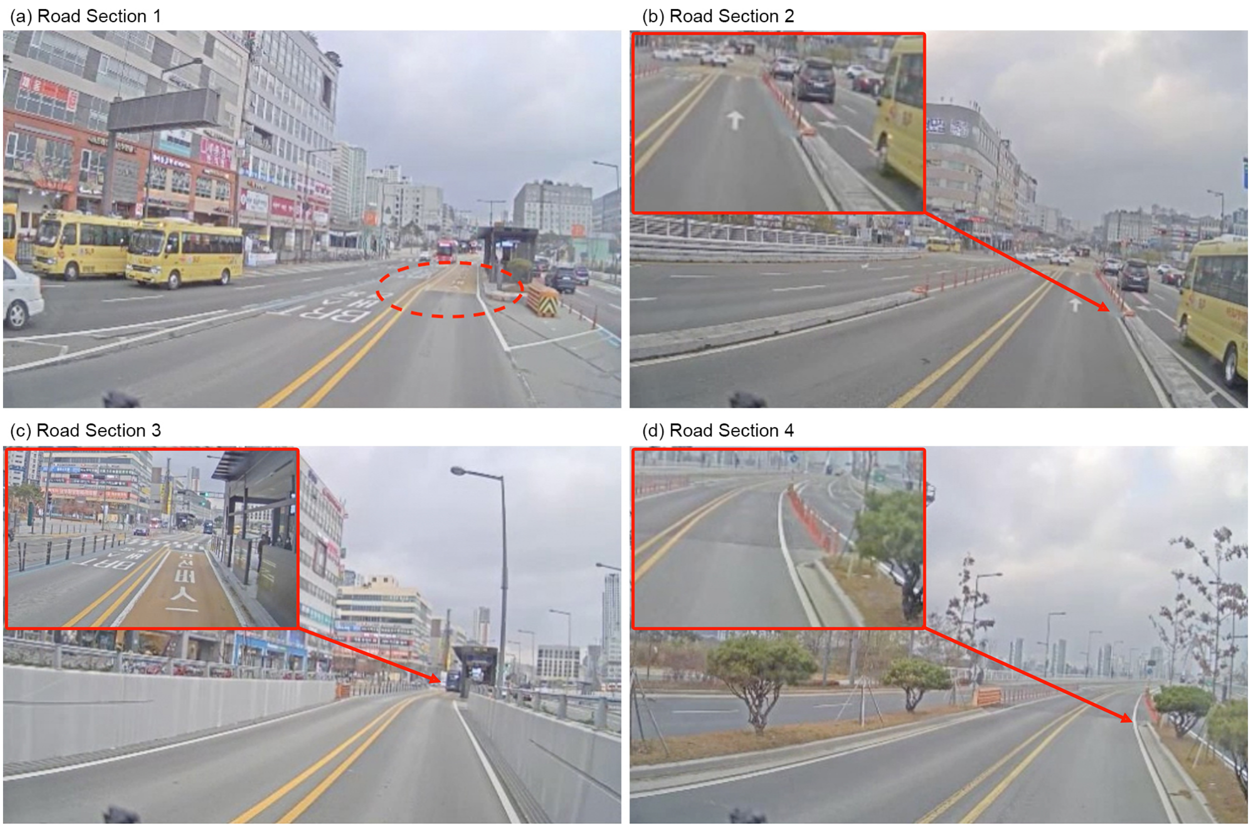

Figure 19: The Features of Road Sections with High Driving Risks in the Field Testing Site

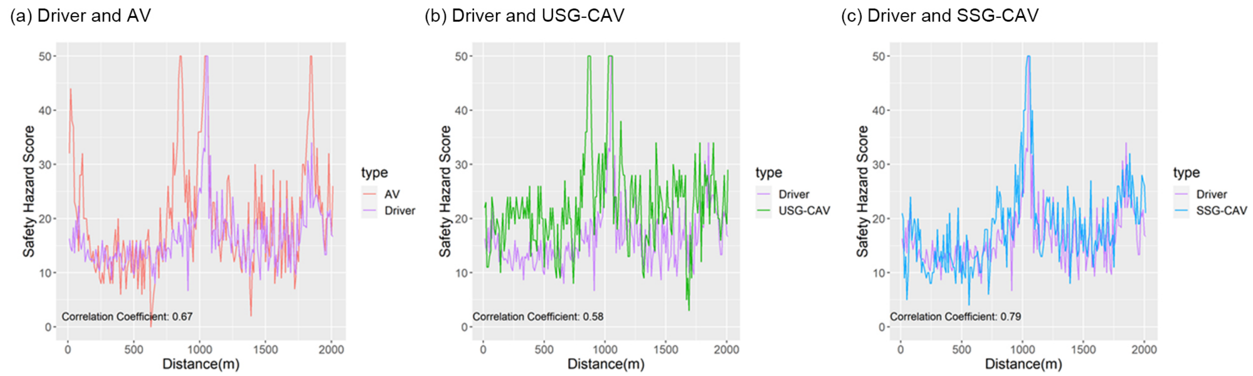

Figure 20: Spatial Trends in Safety Hazard Scores with respect to Two Different Driving Types

system can hardly have an advantage in terms of driving safety compared to the human-driven vehicle. On the other hand, one can observe that the correlation coefficient is 0.67, which is slightly greater than the correlation coefficient between Driver and USG-CAV. This describes that the Driver and AV have a positive linear relationship in safety hazard score, which implies that the spatial distribution of road sections with driving risks in the AV seems to be somewhat similar to that of Driver.

Unlike the case of Driver and AV, it can be observed that the Driver and USG-CAV show different patterns and amounts of safety hazard scores, as depicted in Figure 20 (b). The safety hazard scores of USG-CAV in almost every road section are much grater than those of Driver. The average safety hazard score of the USG-CAV was 22.493, which is the greatest one among the four driving types. Moreover, the correlation coefficient between Driver and USG-CAV is 0.58, which is lower than other ones, particularly in the case of Driver and AV. Such findings indicate that the USG-CAV cannot be substituted for the conventional AV system in terms of driving safety.

On the other hand, a remarkable improvement with respect to the safety hazard score can be observed in the SSG-CAV. As depicted in the case of Driver and SSG-CAV of Figure 20 (c), it is found that the safety hazard scores of SSG-CAV are much less than those of Driver in some road sections. Moreover, there are not significant performance gaps in the rest of road sections where the safety hazard scores of SSG-CAV are slighlty greater than those of Driver. The average safety hazard score of the SSG-CAV was 18.428, which is greater than that of Driver and less than those of AV and USG-CAV. Furthermore, since the correlation coefficient between Driver and SSG-CAV turns out to be 0.79, which is very close to 0.8, it provides sufficient evidence that the Driver and SSG-CAV shows a fairly strong positive relationship. The strong positive linear relationship in safety hazard score between the SSG-CAV and Driver indicates that the safety performance of the SSG-CAV is comparable to that of Driver. Hence, it is worth noting that the most effective alternative manners uprating the conventional AV system in terms of safety performance is to incorporate the SSG system into the AV system in the connected environment.

6. Conclusion

In this study, the framework for CA-BRT was proposed to facilitate the safe, comfortable, and efficient use of the connected and automated bus system to the BRT roads. The proposed C-ITS framework includes Traffic Management Center, Road Monitoring System, Communication System, and Connected and Automated Bus System. Particularly, the Traffic Management Center was deployed in real-world based on a cloud platform to properly manage computing loads induced by processing and storing various types of message in a situation where the number of operating buses was constantly changing. In addition, the SSG system was introduced to enhance the driving safety, ride comfort, and energy efficiency of the BRT bus based on information from in-vehicle sensors, road infrastructure, and legacy ITS. SSG system calculates the optimal guided speed based on deep reinforcement learning, which is computed in a cloud platform and transmitted to the ego vehicle through V2X communication. The provided guided speed for each road segment enables the ego vehicle to improve the ability to respond to various situations on the road considering driving risks given ODD constraints.

The proposed system was deployed in Sejong City, Republic of Korea, and several field tests were conducted for performance evaluation. The performance of the proposed system was compared with those of Driver and automated Vehicle (AV). They control the vehicle based solely on the information from in-vehicle sensors without any information from V2X communication. In comparison analysis, the proposed SSG system exhibited an improved vehicle performance, in terms of driving safety, ride comfort and energy consumption. Furthermore, in contrast to AV whose performance was mostly worse than Driver except for lateral severe deceleration and lateral hard acceleration, the performance of SSG system was similar to or better than that of Driver, particularly in terms of LPV and energy consumption. Therefore, we conclude that the results of the field-tests supports the effectiveness of SSG system which overcomes current limitations of AVs through proposed C-ITS framework.

The proposed framework for CA-BRT and SSG system showed an improved effect compared to AV. Despite the promising results of the proposed system, additional research on improvement efficiency in mixed traffic situations with drivers is needed for more practical use and more positive consequence. First, the speed guidance system for both connected and automated bus and driver-driven bus can be developed to maximize the positive influence on traffic operation and minimize the negative effect on drivers. In this study, we provide optimized sectional guided speeds only for the connected and automated vehicles through uni-cast communication. The uni-cast communication-based service is useful in that it provides optimized information for each vehicle by considering the each vehicle's status. However, its efficiency is limited because sectional guided speed is not provided to drivers. Unexpected movements of CAV induced by differences in provided information from system to driver and connected may lead to the inconvenience of driver. To overcome this limitation, speed guidance system for all vehicles operating on the road section is needed. In the future, therefore, a follow-up study will be conducted on traffic management system for both driver and CAV. Especially, by considering the increased number of service vehicle, more efficient way for communication method (e.g. broadcasting communication) and distributed computing method in cloud platform will be further considered in the future study. Second, it is necessary to develop more efficient way for utilizing information from the legacy ITSs such as the BIS, BMS, and ATMS. In this study, various data from the legacy ITS is actively used to achieve the maximum effect with the minimum installation cost for infrastructure. For example, congestion information near bus station and location of driver-driven bus is collected by using BIS, which is one of the most common legacy ITS in South Korea. However, current legacy ITS have some limitations to be used for CAVs. One example is the long data collection and transmission time interval of the legacy ITS. The legacy ITS is designed to collect and transmit the data at 30-second-interval, since the primary goal of legacy ITS is to support human manager's decisions in monitoring and managing road traffic system. In this study, the data with long time interval is processed to provide guided speed based on the information of the legacy ITS. In the future, we will further investigate on the solutions for whole data processing such as gathering, transmitting, and sharing. Finally, additional study can be conducted to reduce the real-to-virtual gap between vehicle's driving data and simulation used for reinforcement learning. In this study, the training and inference of the reinforcement learning algorithm use the simulation environment which is designed to be similar to the real-world situations. However, we found some real-to-virtual gaps, which results in situations that do not occur in the simulation environment including the degradation of driving stability owing to changes in the road environment. More sophisticated simulations can solve this problem by faithfully reproducing actual road and driving conditions; however, it will increase the time required for the simulation, which will lead to an increase in the time required for the generation of data needed in reinforcement learning. In future research, therefore, we will develop a reinforcement learning-based SSG system by combining and using the driving data that can deal with real-world road hazards and the results of the simulations focused on the operation efficiency. Also, training the reinforcement learning algorithm with transfer learning approach to reduce real-to-virtual can be another potential solution (Jin et al., 2022; Kortylewski et al., 2018).

CRediT authorship contribution statement

Seongjin Choi: Conceptualization, Methodology, Software, Investigation, Writing - Original Draft. **Donghoun Lee:** Conceptualization, Methodology, Validation, Formal analysis, Investigation, Software, Writing - Original Draft, Writing - Review & Editing. **Sari Kim:** Investigation, Visualization, Writing - Original Draft. **Sehyun Tak:** Conceptualization, Methodology, Validation, Formal analysis, Investigation, Resources, Data Curation, Supervision, Visualization, Writing - Original Draft, Writing - Review & Editing, Project administration, Funding acquisition .

Acknowledgements

This research was supported by the Ministry of Land, Infrastructure, and Transport (MOLIT, KOREA) (Project ID: RS-2022-00143579, project name: Development of Automated Driving System(Lv.4/4+)-based Car-Sharing Service Technologies (National R&D Project)).

References

Ainsalu, J., Arffman, V., Bellone, M., Ellner, M., Haapamäki, T., Haavisto, N., Josefson, E., Ismailogullari, A., Lee, B., Madland, O., et al., 2018. State of the art of automated buses. Sustainability 10, 3118.

Almannaa, M.H., Chen, H., Rakha, H.A., Loulizi, A., El-Shawarby, I., 2017. Reducing vehicle fuel consumption and delay at signalized intersections: Controlled-field evaluation of effectiveness of infrastructure-to-vehicle communication. Transportation Research Record 2621, 10–20.

Almannaa, M.H., Chen, H., Rakha, H.A., Loulizi, A., El-Shawarby, I., 2019. Field implementation and testing of an automated eco-cooperative adaptive cruise control system in the vicinity of signalized intersections. Transportation research part D: transport and environment 67, 244–262.

Amazon, a. Amazon eventbridge. URL: https://aws.amazon.com/eventbridge/?nc1=h_ls.

Amazon, b. Amazon kinesis. URL: https://aws.amazon.com/eventbridge/?nc1=h_ls.

Amazon, c. Amazon s3. URL: https://aws.amazon.com/s3/?nc2=type_a.

Amazon, d. Aws lambda. URL: https://aws.amazon.com/lambda/.

Asadi, B., Vahidi, A., 2010. Predictive cruise control: Utilizing upcoming traffic signal information for improving fuel economy and reducing trip time. IEEE transactions on control systems technology 19, 707–714.

Azad, M., Hoseinzadeh, N., Brakewood, C., Cherry, C.R., Han, L.D., 2019. Fully autonomous buses: A literature review and future research directions. Journal of Advanced Transportation 2019.

Bae, I., Moon, J., Seo, J., 2019. Toward a comfortable driving experience for a self-driving shuttle bus. Electronics 8, 943.

Bakhshi, A.K., Gaweesh, S.M., Ahmed, M.M., 2021. The safety performance of connected vehicles on slippery horizontal curves through enhancing truck drivers' situational awareness: A driving simulator experiment. Transportation research part F: traffic psychology and behaviour 79, 118–138.

Basso, L.J., Feres, F., Silva, H.E., 2019. The efficiency of bus rapid transit (brt) systems: A dynamic congestion approach. Transportation Research Part B: Methodological 127, 47–71.

Ben-Chaim, M., Shmerling, E., Kuperman, A., 2013. Analytic modeling of vehicle fuel consumption. Energies 6, 117–127.

BSI PAS 1883, 2020. Operational Design Domain (ODD) Taxonomy for an Automated Driving System (ADS) - Specification. Standard. The British Standards Institution (BSI).

Buechel, M., Knoll, A., 2018. Deep reinforcement learning for predictive longitudinal control of automated vehicles, in: 2018 21st International Conference on Intelligent Transportation Systems (ITSC), IEEE. pp. 2391–2397.

Campbell, M., Egerstedt, M., How, J.P., Murray, R.M., 2010. Autonomous driving in urban environments: approaches, lessons and challenges. Philosophical Transactions of the Royal Society A: Mathematical, Physical and Engineering Sciences 368, 4649–4672.

Cervero, R., 2013. Bus rapid transit (BRT): An efficient and competitive mode of public transport. Technical Report. Working paper.

Chen, H., Rakha, H.A., 2022. Developing and field testing a green light optimal speed advisory system for buses. Energies 15, 1491.

Chen, H., Rakha, H.A., Loulizi, A., El-Shawarby, I., Almannaa, M.H., 2016. Development and preliminary field testing of an in-vehicle eco-speed control system in the vicinity of signalized intersections. IFAC-PapersOnLine 49, 249–254.

Chu, Z., Wu, C., Sepehri, N., 2018. Automated steering controller design for vehicle lane keeping combining linear active disturbance rejection control and quantitative feedback theory. Proceedings of the Institution of Mechanical Engineers, Part I: Journal of Systems and Control Engineering 232, 937–948.

Colwell, I., Phan, B., Saleem, S., Salay, R., Czarnecki, K., 2018. An automated vehicle safety concept based on runtime restriction of the operational design domain, in: 2018 IEEE Intelligent Vehicles Symposium (IV), IEEE. pp. 1910–1917.

Das, A., Ghasemzadeh, A., Ahmed, M.M., 2019. Analyzing the effect of fog weather conditions on driver lane-keeping performance using the shrp2 naturalistic driving study data. Journal of safety research 68, 71–80.

Dion, F., Rakha, H., Zhang, Y., 2004. Evaluation of potential transit signal priority benefits along a fixed-time signalized arterial. Journal of transportation engineering 130, 294–303.

Dion, F., Rakha, H., Zhang, Y., 2005. Integration of transit signal priority within adaptive traffic signal control systems, in: 84th Annual Meeting of the Transportation Research Board, Washington, DC, Citeseer.

Du, Y., Chen, J., Zhao, C., Liu, C., Liao, F., Chan, C.Y., 2022. Comfortable and energy-efficient speed control of autonomous vehicles on rough pavements using deep reinforcement learning. Transportation Research Part C: Emerging Technologies 134, 103489.

Eboli, L., Mazzulla, G., Pungillo, G., 2016. Combining speed and acceleration to define car users' safe or unsafe driving behaviour. Transportation research part C: emerging technologies 68, 113–125.
Eckhoff, D., Halmos, B., German, R., 2013. Potentials and limitations of green light optimal speed advisory systems, in: 2013 IEEE Vehicular Networking Conference, IEEE. pp. 103–110.
Feng, Y.R., Meuleners, L., Stevenson, M., Heyworth, J., Murray, K., Fraser, M., Maher, S., 2021. Driving exposure, patterns and safety critical events for older drivers with and without mild cognitive impairment: findings from a naturalistic driving study. Accident Analysis & Prevention 151, 105965.
Fraade-Blanar, L., Blumenthal, M.S., Anderson, J.M., Kalra, N., 2018. Measuring automated vehicle safety: Forging a framework.
Fruehling, T., Hailemichael, A., Graves, C., Riehl, J., Nutt, E., Fischer, R., Saberi, A.K., 2019. Architectural safety perspectives & considerations regarding the ai-based av domain controller, in: 2019 IEEE International Conference on Connected Vehicles and Expo (ICCVE), IEEE. pp. 1–10.
Fujiwara, A., Chikaraishi, M., Khan, D., Ogawa, A., Suda, Y., Yamasaki, T., Nishino, T., Namba, S., 2022. Autonomous bus pilot project testing and demonstration using light rail transit track. International Journal of Intelligent Transportation Systems Research , 1–20.
Google Cloud Documentation, a. Dataflowe. URL: https://cloud.google.com/dataflow.
Google Cloud Documentation, b. Serverless. URL: https://cloud.google.com/serverless.
Google Cloud Documentation, c. What is cloud storage? URL: https://cloud.google.com/storage/docs/introduction.
Google Cloud Self-Paced Labs, . Google cloud pub/sub: Qwik start - console. URL: https://www.cloudskillsboost.google/focuses/3719?locale=en&parent=catalog.
Haarnoja, T., Zhou, A., Abbeel, P., Levine, S., 2018. Soft actor-critic: Off-policy maximum entropy deep reinforcement learning with a stochastic actor, in: International conference on machine learning, PMLR. pp. 1861–1870.
He, X., Liu, H.X., Liu, X., 2015. Optimal vehicle speed trajectory on a signalized arterial with consideration of queue. Transportation Research Part C: Emerging Technologies 61, 106–120.
Hobert, L., Festag, A., Llatser, I., Altomare, L., Visintainer, F., Kovacs, A., 2015. Enhancements of v2x communication in support of cooperative autonomous driving. IEEE communications magazine 53, 64–70.
IBM Cloud, a. Ibm cloud object storage. URL: https://www.ibm.com/cloud/object-storage.
IBM Cloud, b. Ibm db2 on cloud. URL: https://www.ibm.com/cloud/db2-on-cloud.
IBM Cloud Documentation, a. Ibm mq. URL: https://www.ibm.com/docs/en/cloud-private/3.1.1?topic=services-mq.
IBM Cloud Documentation, b. Introduction to ibm streams. URL: https://www.ibm.com/docs/en/streams/4.3.0?topic=welcome-introduction-streams.
IBM Cloud Education, . What is serverless? URL: https://www.ibm.com/cloud/learn/serverless.
ISO 34503, 2021. Road vehicles — Taxonomy for Operational Design Domain for Automated Driving Systems. Standard. International Organization for Standardization (ISO).
Jiang, R., Wu, Q., Zhu, Z., 2001. Full velocity difference model for a car-following theory. Physical Review E 64, 017101.
Jin, Z., Kim, J., Yeo, H., Choi, S., 2022. Transformer-based map-matching model with limited labeled data using transfer-learning approach. Transportation Research Part C: Emerging Technologies 140, 103668.
Jo, A., 2022. Robust hierarchical motion planning and control for automated bus (doctoral dissertation). Seoul National University .
Jo, A., Lee, H., Seo, D., Yi, K., 2022. Model-reference adaptive sliding mode control of longitudinal speed tracking for autonomous vehicles. Proceedings of the Institution of Mechanical Engineers, Part D: Journal of Automobile Engineering , 09544070221077743.
Johnsson, C., Laureshyn, A., Dágostino, C., 2021. A relative approach to the validation of surrogate measures of safety. Accident Analysis & Prevention 161, 106350.
Katsaros, K., Kernchen, R., Dianati, M., Rieck, D., 2011. Performance study of a green light optimized speed advisory (glosa) application using an integrated cooperative its simulation platform, in: 2011 7th International Wireless Communications and Mobile Computing Conference, IEEE. pp. 918–923.
Kesting, A., Treiber, M., Helbing, D., 2010. Enhanced intelligent driver model to access the impact of driving strategies on traffic capacity. Philosophical Transactions of the Royal Society A: Mathematical, Physical and Engineering Sciences 368, 4585–4605.
Kim, H., Lim, K., Kim, J., Son, W., 2020a. Operational design domain for testing of autonomous shuttle on arterial road. The Journal of The Korea Institute of Intelligent Transport Systems 19, 135–148.
Kim, H., Pyeon, H., Park, J.S., Hwang, J.Y., Lim, S., 2020b. Autonomous vehicle fuel economy optimization with deep reinforcement learning. Electronics 9, 1911.
Koopman, P., Fratrik, F., 2019. How many operational design domains, objects, and events?, in: SafeAI@AAAI.
Kortylewski, A., Schneider, A., Gerig, T., Egger, B., Morel-Forster, A., Vetter, T., 2018. Training deep face recognition systems with synthetic data. arXiv preprint arXiv:1802.05891 .
Laureshyn, A., 2010. Application of automated video analysis to road user behaviour. Lund University.
Le Vine, S., Zolfaghari, A., Polak, J., 2015. Autonomous cars: The tension between occupant experience and intersection capacity. Transportation Research Part C: Emerging Technologies 52, 1–14.
Lee, C.W., Nayeer, N., Garcia, D.E., Agrawal, A., Liu, B., 2020. Identifying the operational design domain for an automated driving system through assessed risk, in: 2020 IEEE Intelligent Vehicles Symposium (IV), IEEE. pp. 1317–1322.
Lee, D., Kim, S., Tak, S., Yeo, H., 2019a. Real-time feed-forward neural network-based forward collision warning system under cloud communication environment. IEEE Transactions on Intelligent Transportation Systems 20, 4390–4404. doi:10.1109/TITS.2018.2884570.
Lee, D., Tak, S., Choi, S., Yeo, H., 2019b. Development of risk predictive collision avoidance system and its impact on traffic and vehicular safety. Transportation research record 2673, 454–465.
Lee, D., Tak, S., Park, S., Yeo, H., 2017. Real-time associative memory–based rear-end collision warning system. Transportation Research Record 2621, 1–9.
Lee, D., Yeo, H., 2015. A study on the rear-end collision warning system by considering different perception-reaction time using multi-layer

perceptron neural network, in: 2015 IEEE Intelligent Vehicles Symposium (IV), IEEE. pp. 24–30.
Lee, D., Yeo, H., 2016. Real-time rear-end collision-warning system using a multilayer perceptron neural network. IEEE Transactions on Intelligent Transportation Systems 17, 3087–3097.
Lillicrap, T.P., Hunt, J.J., Pritzel, A., Heess, N., Erez, T., Tassa, Y., Silver, D., Wierstra, D., 2015. Continuous control with deep reinforcement learning. arXiv preprint arXiv:1509.02971 .
Litman, T., 2020. Autonomous vehicle implementation predictions: Implications for transport planning. Technical Report.
Liu, S., Liu, L., Tang, J., Yu, B., Wang, Y., Shi, W., 2019. Edge computing for autonomous driving: Opportunities and challenges. Proceedings of the IEEE 107, 1697–1716.
Lu, M., Turetken, O., Adali, O.E., Castells, J., Blokpoel, R., Grefen, P., 2018a. C-its (cooperative intelligent transport systems) deployment in europe: challenges and key findings, in: 25th ITS World Congress, Copenhagen, Denmark, pp. 17–21.
Lu, M., Turetken, O., Mitsakis, E., Blokpoel, R., Gilsing, R., Grefen, P., Kotsi, A., 2018b. Cooperative and connected intelligent transport systems for sustainable european road transport. Transport Research Arena 2018.
Luo, Y., Li, S., Zhang, S., Qin, Z., Li, K., 2017. Green light optimal speed advisory for hybrid electric vehicles. Mechanical Systems and Signal Processing 87, 30–44.
Microsoft Azure, . Serverless computing. URL: https://azure.microsoft.com/en-us/resources/cloud-computing-dictionary/what-is-serverless-computing/.
Microsoft Azure Documentation, a. Azure event hubs — a big data streaming platform and event ingestion service. URL: https://learn.microsoft.com/en-us/azure/event-hubs/event-hubs-about.
Microsoft Azure Documentation, b. Introduction to azure blob storage. URL: https://learn.microsoft.com/en-us/azure/storage/blobs/storage-blobs-introduction.
Microsoft Azure Documentation, c. Welcome to azure cosmos db. URL: https://learn.microsoft.com/en-us/azure/cosmos-db/introduction.
Microsoft Azure Documentation, d. Welcome to azure stream analytics. URL: https://learn.microsoft.com/en-us/azure/stream-analytics/stream-analytics-introduction.
Misener, J.A., Shladover, S.E., 2006. Path investigations in vehicle-roadside cooperation and safety: A foundation for safety and vehicle-infrastructure integration research, in: 2006 IEEE Intelligent Transportation Systems Conference, IEEE. pp. 9–16.
Mudge, R., Lutin, J.M., ITE, F., 2020. Automated bus rapid transit a new mode for high-quality, high-capacity transit corridors. Robotics Research .
Naranjo, J.E., Jiménez, F., Gómez, A., Valle, A., González, J., Cruz, A., 2020. Integration of c-its in autonomous driving, in: 2020 IEEE Intelligent Vehicles Symposium (IV), IEEE. pp. 27–32.
Nguyen, T., NguyenDinh, N., Lechner, B., Wong, Y.D., 2019. Insight into the lateral ride discomfort thresholds of young-adult bus passengers at multiple postures: Case of singapore. Case Studies on Transport Policy 7, 617–627.
Paddeu, D., Parkhurst, G., Shergold, I., 2020. Passenger comfort and trust on first-time use of a shared autonomous shuttle vehicle. Transportation Research Part C: Emerging Technologies 115, 102604.
Palacio, A., Tamburro, G., O'Neill, D., Simms, C.K., 2009. Non-collision injuries in urban buses—strategies for prevention. Accident Analysis & Prevention 41, 1–9.
Rakha, H., Van Aerde, M., 2015. Integration© release 2.40 for windows: User's guide—volume i: Fundamental model features. M. Van Aerde & Assoc., Ltd., Blacksburg, VA, USA, Tech. Rep .
Rakha, H.A., Gao, Y., et al., 2010. Calibration of steady-state car-following models using macroscopic loop detector data .
Rakha, H.A., Kamalanathsharma, R.K., Ahn, K., et al., 2012. Aeris: Eco-vehicle speed control at signalized intersections using i2v communication .
SAE J2735, 2020. V2X Communications Message Set Dictionary. Standard. Society of Automotive Engineers International.
SAE J3016, 2021. Taxonomy and Definitions for Terms Related to Driving Automation Systems for On-Road Motor Vehicles. Standard. Society of Automotive Engineers International.
Sallab, A.E., Abdou, M., Perot, E., Yogamani, S., 2017. Deep reinforcement learning framework for autonomous driving. Electronic Imaging 2017, 70–76.
Salonen, A.O., Haavisto, N., 2019. Towards autonomous transportation. passengers' experiences, perceptions and feelings in a driverless shuttle bus in finland. Sustainability 11, 588.
Schulman, J., Levine, S., Abbeel, P., Jordan, M., Moritz, P., 2015. Trust region policy optimization, in: International conference on machine learning, PMLR. pp. 1889–1897.
Schulman, J., Wolski, F., Dhariwal, P., Radford, A., Klimov, O., 2017. Proximal policy optimization algorithms. arXiv preprint arXiv:1707.06347 .
Seredynski, M., Dorronsoro, B., Khadraoui, D., 2013a. Comparison of green light optimal speed advisory approaches, in: 16th international IEEE conference on intelligent transportation systems (ITSC 2013), IEEE. pp. 2187–2192.
Seredynski, M., Laskaris, G., Viti, F., 2019. Analysis of cooperative bus priority at traffic signals. IEEE Transactions on Intelligent Transportation Systems 21, 1929–1940.
Seredynski, M., Mazurczyk, W., Khadraoui, D., 2013b. Multi-segment green light optimal speed advisory, in: 2013 IEEE International Symposium on Parallel & Distributed Processing, Workshops and Phd Forum, IEEE. pp. 459–465.
Seredynski, M., Ruiz, P., Szczypiorski, K., Khadraoui, D., 2014. Improving bus ride comfort using glosa-based dynamic speed optimisation, in: 2014 IEEE International Parallel & Distributed Processing Symposium Workshops, IEEE. pp. 457–463.
Simchon, L., Rabinovici, R., 2020. Real-time implementation of green light optimal speed advisory for electric vehicles. Vehicles 2, 35–54.
Sjoberg, K., Andres, P., Buburuzan, T., Brakemeier, A., 2017. Cooperative intelligent transport systems in europe: Current deployment status and outlook. IEEE Vehicular Technology Magazine 12, 89–97.
Sun, C., Deng, Z., Chu, W., Li, S., Cao, D., 2021. Acclimatizing the operational design domain for autonomous driving systems. IEEE Intelligent

Transportation Systems Magazine 14, 10–24.
Sun, C., Guanetti, J., Borrelli, F., Moura, S.J., 2020. Optimal eco-driving control of connected and autonomous vehicles through signalized intersections. IEEE Internet of Things Journal 7, 3759–3773.
Sun, C., Shen, X., Moura, S., 2018. Robust optimal eco-driving control with uncertain traffic signal timing, in: 2018 annual American control conference (ACC), IEEE. pp. 5548–5553.
Sunkari, S.R., Beasley, P.S., Urbanik, T., Fambro, D.B., 1995. Model to evaluate the impacts of bus priority on signalized intersections. Transportation Research Record , 117–123.
Tak, S., Choi, S., 2022. Safety monitoring system of cavs considering the trade-off between sampling interval and data reliability. Sensors 22, 3611.
Tak, S., Kim, S., Yeo, H., 2015. Development of a deceleration-based surrogate safety measure for rear-end collision risk. IEEE transactions on intelligent transportation systems 16, 2435–2445.
Tak, S., Kim, S., Yeo, H., 2016a. A study on the traffic predictive cruise control strategy with downstream traffic information. IEEE Transactions on Intelligent Transportation Systems 17, 1932–1943.
Tak, S., Kim, S., Yu, H., Lee, D., 2022. Analysis of relationship between road geometry and automated driving safety for automated vehicle-based mobility service. Sustainability 14, 2336.
Tak, S., Lee, J.D., Song, J., Kim, S., 2021. Development of ai-based vehicle detection and tracking system for c-its application. Journal of advanced transportation 2021.
Tak, S., Woo, S., Yeo, H., 2016b. Study on the framework of hybrid collision warning system using loop detectors and vehicle information. Transportation Research Part C: Emerging Technologies 73, 202–218.
Tang, T.Q., Yi, Z.Y., Zhang, J., Wang, T., Leng, J.Q., 2018. A speed guidance strategy for multiple signalized intersections based on car-following model. Physica A: Statistical Mechanics and its Applications 496, 399–409.
Tarko, A.P., 2018. Surrogate measures of safety, in: Safe mobility: challenges, methodology and solutions. Emerald Publishing Limited. volume 11, pp. 383–405.
Theofilatos, A., Yannis, G., Kopelias, P., Papadimitriou, F., 2016. Predicting road accidents: a rare-events modeling approach. Transportation research procedia 14, 3399–3405.
Thomas, E., 2001. Bus rapid transit, in: Presentation at the Institute of Transportation Engineers annual meeting, Chicago.
Thorn, E., Kimmel, S.C., Chaka, M., Hamilton, B.A., et al., 2018. A framework for automated driving system testable cases and scenarios. Technical Report. United States. Department of Transportation. National Highway Traffic Safety ....
Weng, J., Wang, Y., Huang, J., Zhang, L., 2013. Bus operation monitoring oriented public transit travel index system and calculation models. Advances in Mechanical Engineering 5, 389825.
Wu, X., He, X., Yu, G., Harmandayan, A., Wang, Y., 2015. Energy-optimal speed control for electric vehicles on signalized arterials. IEEE Transactions on Intelligent Transportation Systems 16, 2786–2796.
Xia, H., Boriboonsomsin, K., Schweizer, F., Winckler, A., Zhou, K., Zhang, W.B., Barth, M., 2012. Field operational testing of eco-approach technology at a fixed-time signalized intersection, in: 2012 15th International IEEE Conference on Intelligent Transportation Systems, IEEE. pp. 188–193.
Xin, Q., Fu, R., Yuan, W., Liu, Q., Yu, S., 2018. Predictive intelligent driver model for eco-driving using upcoming traffic signal information. Physica A: Statistical Mechanics and its Applications 508, 806–823.
Yang, H., Almutairi, F., Rakha, H., 2020. Eco-driving at signalized intersections: A multiple signal optimization approach. IEEE Transactions on Intelligent Transportation Systems 22, 2943–2955.
Zeng, X., Wang, J., 2018. Globally energy-optimal speed planning for road vehicles on a given route. Transportation Research Part C: Emerging Technologies 93, 148–160.
Zhang, Z., Zou, Y., Zhang, X., Zhang, T., 2020. Green light optimal speed advisory system designed for electric vehicles considering queuing effect and driver's speed tracking error. IEEE Access 8, 208796–208808.

A. C-ITS Message

A.1. Vehicle Detection Message (VDM)

Table 3
VDM-Object

Message Fields				Fields Description
		linkID		Link ID of road center line of HDMap in region of interet(ROI)
		timestamp		vehicle detection time (current)
(list)		objectInfo	ObjectID	Object ID
			VehicleType	Vehicle type
			VehicleTypeProb	Vehicle type probability
			ObjectStatus	Normal/Abnormal driving (abnormal if not moved for a certain period of time)
			Offset	Offset of event occurrence point for Link ID
			PosDistance	Distance between extracted longitude/latitude coordinate values and current HDMap Link
			PosLong	Longitude
			PosLat	Latitude
			Speed	Detection vehicle speed (km/h)
			Heading	Azimuth (degrees)
	(list)	objectPrediction	Timestamp	vehicle detection time (predicted)
			PosLong	Longitude
			PosLat	Latitude
			Speed	Speed (km/h)
			Heading	Azimuth (degrees)
			LinkID	Link ID of predicted position in the timestamp of detected object
			Offset	offset distance of predicted position in the timestamp of detected object from the Link starting point

Table 4
VDM-Link

Message Fields				Fields Description
	roadInfo	LinkID		Link ID of road center line of HDMap in ROI
		Timestamp		Currnet vehicle detection time (Unix timestamp in accuracy of milliseconds based on UTC time)
		AvgSpeed		Average vehicle speed on the link
		LinkTravelTime		Average link travel time (rolling horizon 1 sec)
		NumVehicle		Number of vehicles on the Link (current)
		ObjectStatus		Normal/Abnormal driving (abnormal if not moved for a certain period of time)
		(list)	ObjectID	ID of abnormal driving object
		(list)	Offset	Offset distance of event occurrence point from the Link starting point
		Queue		Delay occurrence (if driving at below certain speed)
		(list)	QueueID	Delay occurrence ID
			OffsetStart	Offset distance of starting point of the queue from the Link starting point
			OffsetEnd	Offset distance of end point of the queue from the Link starting point
(list)	roadPrediction	Timestamp		Vehicle detection time (predicted)
		NumVehicle		Number of vehicles on the Link (predicted)
		AvgSpeed		Average vehicle speed (predicted)

A.2. Pedestrian Detection Message (PDM)

Table 5
PDM-Object

Message Fields			Fields Description
linkID			Link ID of road center line of HDMap in ROI
timestamp			Pedestrian detection time (current)
(list)	objectInfo	ObjectID	Object ID
		PedestrianType	Pedestrian type
		ObjectStatus	Normal/Abnormal status of pedestrian
		Offset	Offset distance of event occurrence point from the Link starting point
		PosDistance	Vertical distance between detected object and the Link ID
		PosLong	Longitude
		PosLat	Latitude
		Speed	Detected pedestrian speed (km/h)
		Heading	Azimuth (degrees)
	(list) objectPrediction	Timestamp	Pedestrian detection time (predicted)
		PosLong	Longitude
		PosLat	Latitude
		Speed	Speed
		Heading	Azimuth (degrees)
		LinkID	Link ID of predicted position in the timestamp of detected object
		PosDistance	Vertical distance between detected object and the Link ID
		Offset	offset distance of predicted position in the timestamp of detected object from the Link starting point

Table 6
PDM-Link

Message Fields			Fields Description
roadInfo	LinkID		Link ID of road center line of HDMap in ROI
	Timestamp		Pedestrian detection time (current)
	OffsetStart		Offset distance of starting point of detection region from the Link starting point
	OffsetEnd		Offset distance of end point of detection region from the Link starting point
	(list)	AdjacentLinkID	Nearby Link ID of detection region Link ID
		OffsetStart	Offset distance of starting point of detection region from the nearby Link starting point
		OffsetEnd	Offset distance of end point of detection region from the nearby Link starting point
		NumPedestrianIn	Number of pedestrians crossing in the direction of nearby Link ID→Link ID
		AccyNumPedestrianIn	Accuracy of pedestrian movement direction
		AvgSpeedIn	Average speed of pedestrians crossing in the direction of nearby Link ID→Link ID
		NumPedestrianOut	Number of pedestrians crossing in the direction of Link ID→nearby Link ID
		AccyNumPedestrianOut	Accuracy of pedestrian movement direction
		AvgSpeedOut	Average speed of pedestrians crossing in the direction of Link ID→nearby Link ID
	ObjectStatus		Normal/Abnormal driving status
	(list)	ObjectID	ID of abnormal driving object
		Offset	Offset distance of event occurrence point from the Link starting point
(list) roadPrediction	Timestamp		Pedestrian detection time (predicted)
	NumPedestrian		Number of pedestrians for the Link (predicted)

A.3. Probe Vehicle Safety Data(PVSD)

Table 7
PVSD

Message Fields						Fields Description	
vehicleID					vehicleSize	Vehicle size	0 = unknown 1 = full-size 2 = mid-size 3 = compact
					capacityTotal	Max. no. of passengers	e.g., 24 = 24 passengers
					vehicleType	Vehicle type	0 = unknown 1 = electric 2 = diesel
					vehicleCAV	Automated driving type	0 = unknown 1 = connected autonomous vehicles 2 = connected vehicle 3 = manual driving
					vehicleNumber	Vehicle number (including temporary number)	
snapshot(list)	timeStamp				year	Snapshot creation time - based on UTC time in accuracy of milliseconds - DSRC.DDateTime used	
					month		
					day		
					hour		
					minute		
					second		Second (ms)
					offset		Time calibration
	currentBusDrivingInfo	cavCurrentProvidedInfo	routeID		lineNumber	Route number	ID distinguishing routes (paths), 10,000 is unavailable
					routeVersion	Path version	Sub ID of path-increases by 1 when path changes 10,000 is unavailable
			drivingMode			Driving mode - Automated driving/non-automated driving mode information	0 = unknown mode 1 = manual (non-automated) mode 2 = automated driving mode
			linkInfo	linkCodeInfo	layerCode	Layer information of HDMap	Link ID code system
					creationDate	Created date (3 character string)	year, month (M: hexadecimal, Jan. - Sept., A (Oct.), B (Nov.), C (Dec,)) E.g.) Created in Aug. 2021: 218 & in Nov. 2021: 21B
					classificationCode	Identification code	
					adminCode	Region code	
				uniqueNumber		Unique number	
				offsetOfVehicle		Vehicle position from road center line Link in HDMap	Integer type unit=0.01m Actual range of representable values is 0 - 262,142 262,143 indicates unavailable
			busTripStatus	drivingState		Current bus operation state - State information of driving preparation, driving (PIM based), turning back, testing (not PIM based driving)	0 = unknown mode 1 = operation stand-by (before departure, stand-by at garage or departure point) 2 = in operation (operation based on PIM path) 3 = operation terminated and turning back 4 = test driving (test driving unrelated to vehicle operation scenario or PIM) 5 = driving terminated
				vehicleManeuver		Vehicle movement state Vehicle maneuver aside from road maneuver - straight, right turn, left turn, U-turn	0 = unknown mode 1 = going straight 2 = making a right turn 3 = making a left turn 4 = making a U-turn
				emergencyAlert		Vehicle emergency situation notification - emergency stop (driver), accident over the vehicle	0 = no emergency or clear (normal driving state) 1 = emergency stop (driver input) 2 = accident (accident involving the vehicle, driver input)
				controlTransition		Whether the command to switch control right from automated driving to driver is reflected	0 = control right switching clear or normal driving (clear by command of a control center) 1 = control right switching command received (check if the command to switch to driver is received) 2 = control right switched (completed message of vehicle is transmitted to control center)
			driverControlState	acceleratorPositionSensorState		Accelerator pedal position (accelerator pedal switch pressed on/off)	False : deactivated, True : activated Similar (identical) to driverOverride information within chassis to be replaceable
				brakeSwitchPedal		Brake pedal switch state (brake pressed on/off)	False : deactivated, True : activated Similar (identical) to driverBraking information within chassis to be replaceable
		object	forwardVehic			Preceding vehicle	false = not present, true = present
			forwardVehicleDistance			Distance from the preceding vehicle (meter)	Integer type unit=0.01m Actual range of representable values is -1,000,000 - 1,000,001 1,000,001 indicates unavailable
			leftVehicle			Whether a vehicle is present to the left of Probe Vehicle	false = not present, true = present
			leftForwardVehicleDistance			Distance from the preceding vehicle on the left (meter)	Integer type unit=0.01m Actual range of representable values is -1,000,000 - 1,000,001 1,000,001 indicates unavailable
			rightVehicle			Whether a vehicle is present to the right of Probe Vehicle	false = not present, true = present
			rightForwardVehicleDistance			Distance from the preceding vehicle on the right (meter)	Integer type unit=0.01m Actual range of representable values is -1,000,000 - 1,000,001 1,000,001 indicates unavailable

Table 7 continued from previous page

Message Fields					Fields Description	
snapshot(list)(continued)	currentBusDrivingInfo	canErrorCode			CAN communication state	0 = unavailable 1 = active (normal) 2 = failed (abnormal)
		flags			Lane change flag	0=unavailable 1=lane change flag 2= flag after lane change 3=off path 4=keep path
	gps	precision		activeSatellites horizontalDOP verticalDOP	No. of incoming satellites Horizontal position error Vertical position error	
	vision	numOfObject			No. of detected obstacles	255 = unavailable
	lidar	numOfObject			No. of detected Box	65535 = unavailable
	radar	front	operation		Operation status	0=unavailable 1=object recognition communication error 2=sensor operation state (converting electrical signal to optical signal between a fiber-optic cable (xcvr:exa optical transceiver) and transmission equipment for data transmission) 3=whether sensor state is failed 4=whether sensor state is blocked 5=whether sensor is shut down due to overheat 6=partial sensor blockage 7=Sidelobe detection
			temperature		Sensor temperature	255 = unavailable
			fault	activeFault historyFault	Active Fault History fault	
		rear	(same fields as radar-front)			
	chassis	accel		latAccel longAccel yawRate	Lateral acceleration Longitudinal acceleration Yaw rate	units are 0.01 m/s^2, 2001=Unavailable (integer) units are 0.01 m/s^2, 2001=Unavailable (integer) units of 0.01 degrees per second (signed) (integer)
		steering			Steering angle	units of 1.5 degrees, a range of -189 to +189 degrees (integer) – +001 = +1.5 deg – -126 = -189 deg and beyond – +126 = +189 deg and beyond – +127 to be used for unavailable
		wheel	frontLeft frontRight rearLeft rearRight		Front-left wheel speed Front-right wheel speed Rear-left wheel speed Rear-right wheel speed	Units of 0.02 m/s, 8191=Unavailable (integer) Units of 0.02 m/s, 8191=Unavailable (integer) Units of 0.02 m/s, 8191=Unavailable (integer) Units of 0.02 m/s, 8191=Unavailable (integer)
		canAlive			CAN data state information - flag regarding normal output of CAN signal	false : abnormal true : normal
		driver	driverBraking		Whether a driver used the brake	false : brake not used true : brake used
			accEnable		Whether Adaptive Cruise Control is used	false : not used true : used
			driverOverride		Whether a driver operated the vehicle	false : driver did not operate any of brake, accelerator, or steering wheel true : driver operated at least one of brake, accelerator, or steering wheel
			gwayTsigLhsw		Left-turn signal	false : not used true : used
			gwayTsigRhsw		Right-turn signal	false : not used true : used

A.4. Automated Vehicle Safety Message(AVSM)

Table 8
AVSM

Message Fields						Fields Description	
timeStamp					year	Message created time - based on UTC time in accuracy of milliseconds - DSRC.DDateTime used	
					month		
					day		
					hour		
					minute		
					second		Second (ms)
					offset		Time calibration
vehicleID					vehicleSize	Vehicle size	0 = unknown 1 = full-size 2 = mid-size 3 = compact
					capacityTotal	Max. no. of passengers	e.g., 24 = 24 passengers
					vehicleType	Vehicle type	0 = unknown 1 = electric 2 = diesel
					vehicleCAV	Automated driving type	0 = unknown 1 = connected autonomous vehicles 2 = connected vehicle 3 = manual driving
					vehicleNumber	Vehicle number (including temporary number)	
snapshot(list)	timeStamp				year	Snapshot creation time - based on UTC time in accuracy of milliseconds - DSRC.DDateTime used	Year
					month		Month
					day		Date
					hour		Hour
					minute		Minute
					second		Second (ms)
					offset		Time calibration
	gps				gnssStatus	GPS signal reception status of GPS device installed within OBU	0 = Unavailable 1 = Void 2 = 2D_Fixed 3= 3D_Fixed
		ext	time		year	GPS time of ROS (Unix Epoch Time conversion) - based on UTC time in accuracy of milliseconds - DSRC.DDateTime used	Year
					month		Month
					day		Date
					hour		Hour
					minute		Minute
					second		Second (ms)
					offset		Time calibration
			angle		heading	Heading angle	Units of 0.0125 degrees, A range of 0 to 359.9875 degrees
					pitch	Pitch angle	Units of 0.01 degrees per second (32767 = Unavailable)
					roll	Roll angle	Units of 0.01 degrees per second (32767 = Unavailable)
			position		lat	ROS latitude	Units of 1/10 micro degree, Providing a range of $\pm$ 90 degrees (1 degree = 1,000,000 micro degree)
					long	ROS longitude	Units of 1/10 micro degree, Providing a range of $\pm$ 180 degrees (1 degree = 1,000,000 micro degree)
			velocity		east	Lateral speed	Units of 0.02 m/s, 8191=Unavailable (integer)
					north	Longitudinal speed	Units of 0.02 m/s, 8191=Unavailable (integer)
					up	Vertical speed	Units of 0.02 m/s, 8191=Unavailable (integer)
	vision	ext	lane	leftLane	type	Lane type	0 = unknown 1 = dashed 2 = solid 3 = undecided 4 = road-edge 5 = double-lane-mark (including dashed on one side) 6 = botts-dots 7 = invalid
					position	Lane position (distance)	Units : 0.01 meter
					laneCurvature	Lane curvature	Units : 0.01/m , 12001 = invalid
					laneHeading	Lane direction	Units of 0.0125 degrees, A range of 0 to 359.9875 degrees
					quality	Perceived accuracy level	0 = low-lv-0 (low quality. The lane measurements are not valid in low quality. The system will not give an LDW in that situation.) 1 = low-lv-1 2 = high-lv-2 3 = high-lv-3
				leftNextLane	(same fields as vision-ext-lane-leftLane)		
				rightLane	(same fields as vision-ext-lane-leftLane)		
				rightNextLane	(same fields as vision-ext-lane-leftLane)		

Table 8 continued from previous page

Message Fields						Fields Description	
snapshot(list) (continued)	vision (continued)	ext (continued)	obstacle (list)	brakeLight		Whether brake lights for obstacles are lit	false : unlit true : lit
				angleRate		Angular ratio from obstacle	Units 0.01 (50001 = Unavailable)
				accelX		X-axis acceleration of obstacle	LSB units are 0.01 m/s^2 (3,001 = Unavailable)
				angle		Angle from obstacle	Units 0.01 deg (36001 = Unavailable)
				posX		X-axis position of obstacle	Units of 0.01 Point (1,000,001 = Unavailable)
				posY		Y-axis position of obstacle	Units of 0.01 Point (1,000,001 = Unavailable)
				type		Obstacle information	0 = unknown 1 = vehicle 2 = truck(cargo vehicle) 3 = motorcycle 4 = pedestrian 5 = bicycle
				status		Obstacle state	0 = undefined, 1 = standing, 2 = stopped (moveable) 3 = moving 4 = oncomming, 5 = parked 6 = unused
				valid		Influence of obstacle	0 = unknown 1 = new valid 2 = older valid
				lane		Position of obstacle on lane	0 = not assigned, 1 = ego lane, 2 = next lane, or next next lane, 3 = invalid signal
				width		Obstacle width	Units 0.01 meter (10000001 = Unavailable)
				id		Obstacle ID	
				measured		Obstacle detection status	false : not detected true : detected
				longitudinalDistanceStd		Lateral distance	Units 0.01 meter (10000001 = Unavailable)
				inverseTtc		Inter-vehicle distance indicator	Units 0.01 meter (10000001 = Unavailable)
	lidar	numOfObject				No. of detected PointCloud (or Box)	65535 = unavailable
		track (list)	id			Tracked object ID	
			positionX			X-axis coordinate of estimated position of ego-vehicle coordinate system reference track	Units of 0.01 Point (1,000,001 = Unavailable)
			positionY			Y-axis coordinate of estimated position of ego-vehicle coordinate system reference track	Units of 0.01 Point (1,000,001 = Unavailable)
			yaw			Estimated heading direction of ego-vehicle coordinate system reference track	Units of 0.0125 degrees, A range of 0 to 359.9875 degrees
			yawRate			Estimated yaw rate of ego-vehicle coordinate system reference track	units of 0.01 degrees per second (signed)
			yawAccel			Estimated yaw acceleration of ego-vehicle coordinate system reference track	
			velX			X-axis moving speed	Units of 0.02 m/s (8191 = Unavailable)
			boundingBox1	x		First coordinate_x of four vertices of a track bounding box	Units 0.01 meter (10000001 = Unavailable)
				y		First coordinate_y of four vertices of a track bounding box	Units 0.01 meter (10000001 = Unavailable)
			boundingBox2	x		Second coordinate_x of four vertices of a track bounding box	Units 0.01 meter (10000001 = Unavailable)
				y		Second coordinate_y of four vertices of a track bounding box	Units 0.01 meter (10000001 = Unavailable)
			boundingBox3	x		Third coordinate_x of four vertices of a track bounding box	Units 0.01 meter (10000001 = Unavailable)
				y		Third coordinate_y of four vertices of a track bounding box	Units 0.01 meter (10000001 = Unavailable)
			boundingBox4	x		Fourth coordinate_x of four vertices of a track bounding box	Units 0.01 meter (10000001 = Unavailable)
				y		Fourth coordinate_y of four vertices of a track bounding box	Units 0.01 meter (10000001 = Unavailable)
			confidenceInd			Reliability of estimated track information	Units of 0.5, 0 ~100
	radar	front	ext	tracking	groupingMode	Grouping of detected object	0 = No grouping of stationary or moving targets 1 = Grouping moving targets only 2 = Grouping stationary targets only 3 = Grouping stationary and moving targets
					mrLrMode	Object detected range type: MR or LR	0 = reserved 1 = med-range-only 2 = long-range-only 3 = MR and LR
					pathIDAcc	ID of detected moving object when using ACC	
					pathIDAcc2	Second closest target ID	
					pathIDAcc3	Third closest target ID	
					pathIDAccStat	ID of detected static (not moving) object when using ACC	
					pathIDCmbbMove	Detection object with movement when using CMbB	
					pathIDCmbbStat	Detection object without movement when using CMbB	
					pathIDFcwMove	Detection object with movement when using FCW	
					pathIDFcwStat	Detection object without movement when using CMbB	
					foundTarget	Target detection status	false : 1 target not found true : 1 target found
					recommendUnconverge	Whether unsorting is recommended	false : Not recommended true : Recommended

Table 8 continued from previous page

Message Fields						Fields Description	
snapshot(list) (continued)	radar (continued)	front (continued)	ext (continued)	target (list)	groupingChanged	Boolean indicator that number of detections associated with the track have changed	false : no change true : change
					latRate	Lateral Rate	Units 0.01 (50001 = Unavailable)
					medRangeMode	Indicates which mode updated the fused track	0 = No MR / LR update 1 = med-range-update-only 2 = long-range-update-only 3 = Both MR / LR update
					oncoming	Oncoming Flag	false : not oncoming true : oncoming
					range	range	Units 0.01 meter (10000001 = Unavailable) - (+) = away from sensor set at 204.7 if >204.7
					rangeAccel	Range Acceleration	LSB units are 0.01 m/s^2 (3001 = Unavailable) - (+) = away from sensor set at 25.55 if >25.55 set at -25.6 if <-25.6
					rangeRate	Range Rate	Units 0.01 (50001 = Unavailable) - set at -81.92 if <-81.92
					rollingCount	rolling count	true : must, rolling count of all messages in this burst false : other
					status	track status	0 = no target 1 = new target 2 = new updated target 3 = updated target 4 = coasted target 5 = merged target 6 = invalid coasted target 7 = new coasted target
					width	track width	Units 0.1 meter
				align	speed	Calibrated vehicle speed	Units of 0.02 m/s, 8191=Unavailable (integer)
					yawRate	Calibrated yaw angle	units of 0.01 degrees per second (signed)
					updateCode	Automatic calibration information update status	Vertical alignment updated false : not updated true : updated
					autoAlignAngle	Automatic angle alignment	Units 0.01 deg (36001 = Unavailable)
				serialNum		Sensor S/N	
		rear	(same fields as radar-front)				
	chassis	driver			gwayHazardsw	Vehicle emergency light state	false : unlit true : lit
					gear	Vehicle gearshift state	0 = Neutral 1 = Park 2 = Forward gears 3 = Reverse gears 7 = not-equipped or unavailable value

A.5. Path Identification Message(PIM)

Table 9
PIM

Message Fields				Fields Description	
timeStamp			year month day hour minute	Message created time - based on UTC time in accuracy of milliseconds - DSRC.DDateTime used	
			second		Second (ms)
			offset		Time calibration
vehicleState	stateOfVehicle			Vehicle state information - Normal situation judgment	0 = normal 1 = breakdown 2 = emergency 3 = off path 4 = emergency replacement vehicle 5 = others
	stateChangeTime		year month day hour minute	Snapshot creation time - based on UTC time in accuracy of milliseconds - DSRC.DDateTime used	
			second		Second (ms)
			offset		Time calibration
vehicleNumber				Vehicle number (including temporary number)	
routeInformation	routeID		lineNumber	Route number	ID distinguishing routes (paths), 10,000 is unavailable
			routeVersion	Path version	Sub ID of path-increases by 1 when path changes 10,000 is unavailable
updateCodeRoute				Message update (path change) cause	0 = initial path/speed and path/speed not changed 1 = path/speed change due to demand for boarding 2 = path/speed change due to traffic conditions including delay, congestion, and slow driving 3 = path/speed change due to vehicle breakdown (diagnosis) 4 = path/speed change due to immobile obstacles including accident, fallen objects, and parking/stopping 5 = path/speed change due to moving obstacles including wrong-way driving, signal violation, and pedestrian 6 = others
route(list)	sequence			Order of vehicle recommended path	
	linkInformation	linkCodeInfo	layerCode	Layer information of HDMap	Link ID code system
			creationDate	Created date (refer to HDMap specifications)	
			classificationCode	Identification code	
			adminCode	Region code	
		uniqueNumber		Unique number	
		trafficSignal		Signal information provision status	false : not provided true : provided
		stationInfo	stationExist	Presence of bus stop	false : not present true : present
			stationID	Bus stop ID	
			offsetStart	Bus stop offset	Integer type unit=0.01m Actual range of representable values is 0 - 262,142 262,143 indicates unavailable
			stop	Whether a vehicle stops	false : not stopped true : stopped
			getIn	No. of passengers boarding	
			getOff	No. of passengers alighting	
	laneChangeInfo	laneChangeFlag		Lane change indication in the following Link	0 = no lane change 1 = attempts to change to left lane 2 = attempts to change to right lane
		offsetStart		Offset starting point of road center line Link in HDMap point where lane change should be started	Integer type unit=0.01m Actual range of representable values is 0 - 262,142 262,143 indicates unavailable

A.6. Vehicle Control Advisory Message(VCAM)

Table 10
VCAM

Message Fields			Fields Description	
timeStamp		year	Message created time - based on UTC time in accuracy of milliseconds - DSRC.DDateTime used	
		month		
		day		
		hour		
		minute		
		second		Second (ms)
		offset		Time calibration
vehicleState	stateOfVehicle		Vehicle state information - Normal situation judgment	0 = normal 1 = breakdown 2 = emergency 3 = off path 4 = emergency replacement vehicle 5 = others
	stateChangeTime	year	Snapshot creation time - based on UTC time in accuracy of milliseconds - DSRC.DDateTime used	
		month		
		day		
		hour		
		minute		
		second		Second (ms)
		offset		Time calibration
vehicleNumber			Vehicle number (including temporary number)	
routeInfo	routeID	lineNumber	Route number	ID distinguishing routes (paths), 10,000 is unavailable
		routeVersion	Path version	Sub ID of path-increases by 1 when path changes 10,000 is unavailable
	updateCodeSpeed		Message update (speed change) cause	0 = initial path/speed and path/speed not changed 1 = speed change due to demand for boarding 2 = speed change due to traffic conditions including delay, congestion, and slow driving 3 = speed change due to vehicle breakdown (diagnosis) 4 = speed change due to immobile obstacles including accident, fallen objects, and parking/stopping 5 = speed change due to moving obstacles including wrong-way driving, signal violation, and pedestrian 6 = others
	controlTransitionReason		Control right switching cause (reason)	0 = no control right switching 1 = control right switching command due to vehicle breakdown (sensor state diagnosis) 2 = control right switching command due to accidents 3 = control right switching command due to communication instability (communication failure) in a specific section 4 = control right switching command for automated driving prohibited zone (e.g., school zone) 5 = command to turn back by switching control right 6 = others

Table 10 continued from previous page

Message Fields					Fields Description	
speedAdvisory(list)	linkSequence				Order of vehicle recommended path	
	linkInfo	linkCodeInfo		layerCode	Layer information of HDMap	
				creationDate	Created date (refer to HDMap specifications)	
				classificationCode	Identification code	
				adminCode	Region code	
		uniqueNumber			Unique number	
		currentCommStatus	v2xSensitivity	curWaveRcpi	WAVE reception sensitivity	Current communication status of the Link (communication performance indicator)
				curLteRxSensitivity	LTE reception sensitivity	
				cur5gRxSensitivity	5G reception sensitivity	
			gpsPrecision	activeSatellites	No. of incoming satellites	Current GPS precision of the Link and number of incoming satellites
				horizontalDOP	Horizontal position error	
				verticalDOP	Vertical position error	
				gnssStatus	GPS signal reception status of GPS device installed within OBU	0 = Unavailable 1 = Void 2 = 2D_Fixed 3= 3D_Fixed
		reasonDeceleration	trafficSignal		Signal information provision status	false : not provided true : provided
			vehicleDetection	isDetection	Vehicle detection status	false : nearby vehicle not detected in path true : nearby vehicle detected in path
				collisionProb	Possibility of collision with detected vehicles	% (percent)
			pedestrianDetection	isDetection	Pedestrian detection status	false : nearby pedestrian not detected in path true : nearby pedestrian detected in path
				collisionProb	Possibility of collision with detected pedestrian	% (percent)
			stationExist		Presence of bus stop	false : not present true : present
			mergingSectionInfo	mergingSectionExist	Presence of a merging point	false : not present true : present
				collisionProb	Possibility of collision due to merging	% (percent)
			queueInfo	queue	Presence of delay	false : not present true : present (considered a delay if vehicle moves at below a certain speed)
				qOffsetStart	Offset starting point of a delay section for Link ID	Integer type unit=0.01m Actual range of representable values is 0 - 262,142 262,143 indicates unavailable
				qOffsetEnd	Offset end point of a delay section for Link ID	Integer type unit=0.01m Actual range of representable values is 0 - 262,142 262,143 indicates unavailable
			eventType		(Excluding collision possibility with pedestrian and at merging point) Events occurring within the lane	0 = normal 1 = delay, congestion 2 = slow driving 3 = block due to accident or fallen objects (fixed obstacle) 4 = block due to stopping or parking (fixed obstacle) 5 = dangerous situation due to wrong-way driving (moving obstacle) 6 = dangerous situation due to signal violation (moving obstacle) 7 = others
		controlTransitionExist			Command to switch driver's control right within Link	false : no driver's control right switching command (default) true : driver's control right switching command present
	offsetList(list)	offsetSequence			Offset order	
		offsetStart			Offset starting point of road center line Link in HDMap (two decimal points)	Integer type unit=0.01m Actual range of representable values is 0 - 262,142 262,143 indicates unavailable
		offsetEnd			Offset end point of road center line Link in HDMap (two decimal points)	Integer type unit=0.01m Actual range of representable values is 0 - 262,142 262,143 indicates unavailable
		advisorySpeed			Maximum recommended driving speed	Units of 0.02 m/s, 8191=Unavailable (integer)
		controlTransitionCommand			Driver control right command	0 = no control right switching command 1 = automated driving recommended (driver control command clear) 2 = command to switch from automated driving to driver

A.7. Signal Phase And Timing Message(SPaT)

Table 11
SPaT

Message Fields							Field Description	
timeStamp							MinuteOfTheYear - number of minutes elapsed since the start of the year	
name							Human readable name for intersection	
intersections	name						Human readable name for intersection	
	id	region					A globally unique regional assignment value	
		id					Intersection ID	
	revision						MsgCount	
	status						general status of the controller(s)	
	moy						MinuteOfTheYear - number of minutes elapsed since the start of the year	
	timeStamp						The mSec point in the current UTC minute that this message was constructed	Milliseconds / 100
	states (list)	movementName					movement by human readable name	
		signalGroup					A group id used to map to lists of lanes (and their descriptions) which this MovementState data applies to	
		state-time-speed	eventState				Movement phase status of current signal	0 = unavailable 1 = dark (The signal head is unlit) 2 = stop-Then-Proceed (Flashing red) 3 = stop-And-Remain (Red light) 4 = pre-Movement (Yellow and red lights flashing together) 5 = permissive-Movement-Allowed (Permissive green) 6 = protected-Movement-Allowed (Protected green) 7 = permissive-clearance (Permissive yellow) 8 = protected-clearance (Protected yellow) 9 = caution-Conflicting-Traffic (Flashing yellow"
			timing	minEndTime			The amount of time allocated for the display of a signal indication	Milliseconds / 100
		movementName					uniquely defines movement by name	
		signalGroup					A group id used to map to lists of lanes (and their descriptions) which this MovementState data applies to	
		state-time-speed	eventState				Signal phase state	
			timing	minEndTime			The amount of time allocated for the display of a signal indication	Milliseconds / 100
regional	regionId						Defined regions where unique additional content may be added and used in the message set	0 = noRegion 1 = addGrpA (USA) 2 = addGrpB (Japan) 3 = addGrpC (EU) 4 = addGrpD (KOREA)
	regExtValue	captain	name				Descriptive name of rigional fileds' contents	
			states (list)	signalGroup			A group id used to map to lists of lanes (and their descriptions) which this MovementState data applies to	
				next-event	eventState		Movement phase status of next signal	0 = unavailable 1 = dark (The signal head is unlit) 2 = stop-Then-Proceed (Flashing red) 3 = stop-And-Remain (Red light) 4 = pre-Movement (Yellow and red lights flashing together) 5 = permissive-Movement-Allowed (Permissive green) 6 = protected-Movement-Allowed (Protected green) 7 = permissive-clearance (Permissive yellow) 8 = protected-clearance (Protected yellow) 9 = caution-Conflicting-Traffic (Flashing yellow
					timing	startTime	Time remaining before this phase starts	Milliseconds / 100
						minEndTime	Phase duration	Milliseconds / 100
				event-after-next	eventState		Movement phase status of after next signal	0 = unavailable 1 = dark (The signal head is unlit) 2 = stop-Then-Proceed (Flashing red) 3 = stop-And-Remain (Red light) 4 = pre-Movement (Yellow and red lights flashing together) 5 = permissive-Movement-Allowed (Permissive green) 6 = protected-Movement-Allowed (Protected green) 7 = permissive-clearance (Permissive yellow) 8 = protected-clearance (Protected yellow) 9 = caution-Conflicting-Traffic (Flashing yellow
					timing	startTime	Time remaining before this phase starts	Milliseconds / 100
						minEndTime	Phase duration	Milliseconds / 100
				linkIDs (list)	linkCodeInfo	layerCode	Related links of this signal group	Layer information of HDMap
						creationDate		Created date (refer to HDMap specifications)
						classificationCode		Identification code
					linkID			Unique number

B. Simulation examples

Figure 21 shows the examples of the simulation output with different parameter setting.

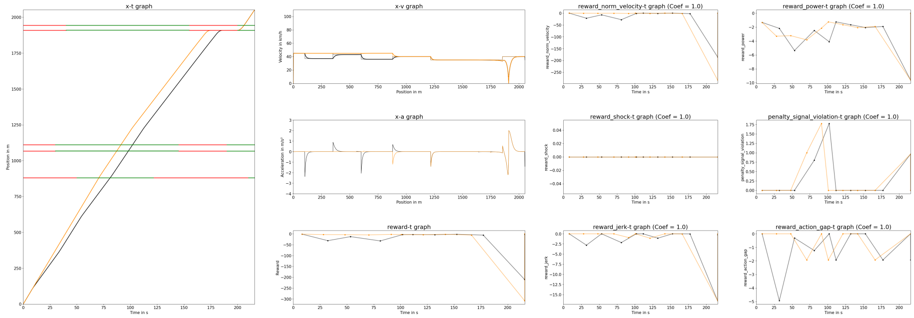

(a) $\alpha_{power} = 0.001$

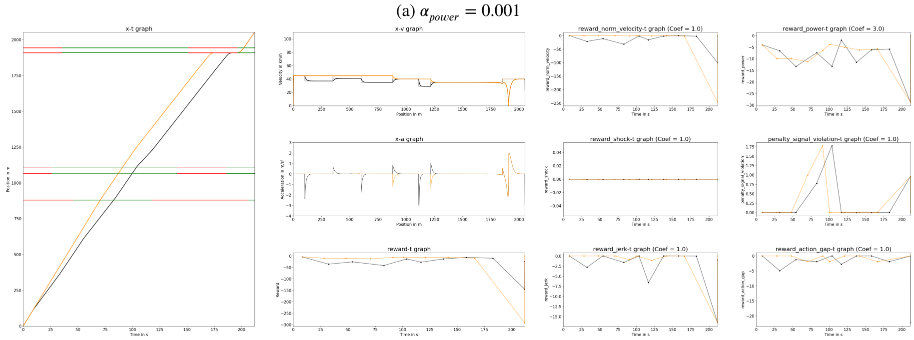

(b) $\alpha_{power} = 0.003$

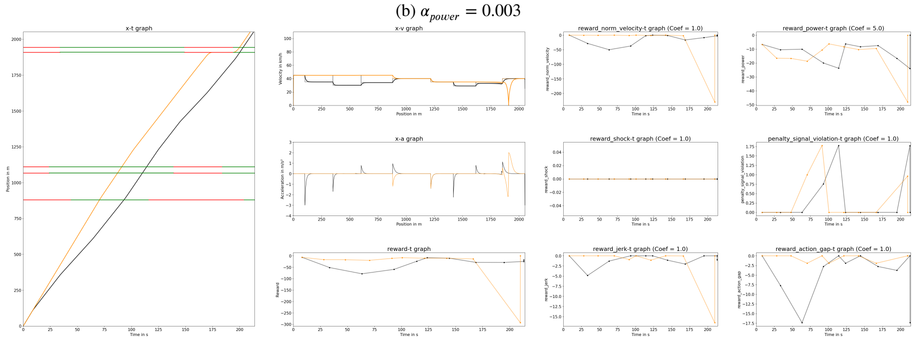

(c) $\alpha_{power} = 0.005$

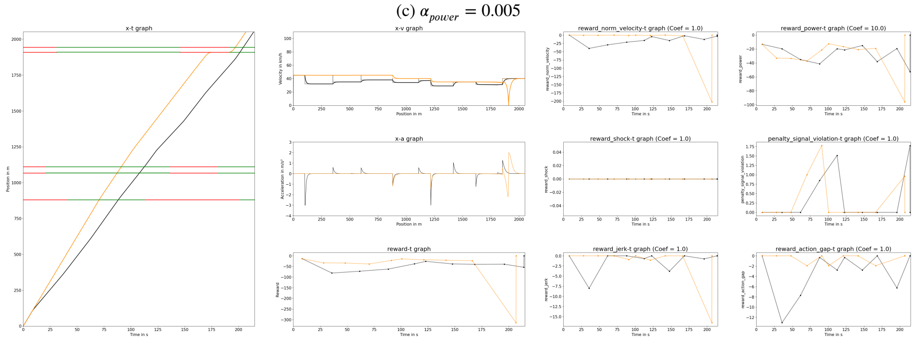

(d) $\alpha_{power} = 0.01$

Figure 21: Examples of simulation output